SOME ASPECTS OF
CREEP BEHAVIOUR OF 2.25Cr-1Mo STEEL

THESIS

Submitted in Partial Fulfilment of the
Requirements for the Degree of

DOCTOR OF PHILOSOPHY

In

ENGINEERING

By

SATYABRATA CHAUDHURI

Department of Metallurgical Engineering
INDIAN INSTITUTE OF TECHNOLOGY
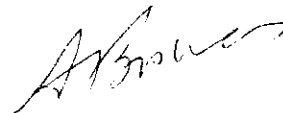KHARAGPUR 721 302, INDIA

1993.

CERTIFICATE

This is to certify that the thesis entitled "SOME ASPECTS OF CREEP BEHAVIOUR OF 2.25Cr-1Mo STEEL" being submitted by Sri Satyabrata Chaudhuri is a record of bonafide research work carried out by him in the National Metallurgical Laboratory, Jamshedpur, India and in the Department of Metallurgical Engineering, Indian Institute of Technology, Kharagpur, India, under our guidance and supervision. In our opinion the thesis has fulfilled the requirements according to the regulations of this Institute and has reached the standard necessary for submission.

The results incorporated in this thesis are original and have not been submitted to any other university or institute for the award of degree or diploma.

(R.N. GHOSH)
Deputy Director and Head
Computer Applications Division
National Metallurgical Laboratory
Jamshedpur, INDIA

(A. BISWAS)
Dept. of Metallurgical Engineering
Indian Institute of Technology
Kharagpur
INDIA
(At present on EOL)

In Memory
of
My Father

ACKNOWLEDGEMENT

SOME ASPECTS OF CREEP BEHAVIOUR OF 2.25Cr-1Mo STEEL

PREFACE

2.25Cr-1Mo steel is extensively used in high temperature components primarily because of its excellent creep resistance. This is evaluated mainly on the basis of uniaxial stress rupture tests at different stresses and temperatures. The data are represented in the form of a master rupture plot which describes applied stress as function of a combined parameter consisting of test temperature in $^{\circ}K$ and time to rupture in hours. Various forms of such parameters are commonly used to represent the data. This allows both interpolation and extrapolation to suit the requirement of a designer. However, the data represented on such a plot from various sources exhibit a wide scatter. In the present work an attempt has been made to identify the major factors responsible for this.

Analysis of stress rupture data clearly revealed that although different time-temperature parameters are used to represent the master rupture plot, there is only a marginal difference in their predictive powers. Larson-Miller Parameter being the simplest amongst them is often used in the design of high temperature components. Comparison of data from different sources revealed that minor variations in the composition within permissible level of the standard and the variation in section size of the product from which test specimens are made are the major source of scatter. A set of stress rupture tests were performed on specimens having identical chemical composition but different initial microstructures to show that the section size effect (normalised) is primarily due to variation in the initial microstructure.

Unlike stress rupture data, rupture ductility when plotted against similar time-temperature parameters does not show a definite trend. This is primarily because the extent of localized deformation (necking) varies in an unpredictable manner with test conditions. Based on an empirical formulation using a combined stress temperature parameter it is possible to predict long term rupture ductility. However, the approach being empirical, it has a limited predictive power since it does not take into consideration the mechanism of rupture. A new geometrical factor has, therefore, been introduced to represent the nature of rupture. This can be readily estimated from the reported rupture elongation and reduction in area. Using this a simple method of predicting rupture ductility has been suggested.

Modern design techniques increasingly look for a more exact description of the entire creep strain-time plot. Currently available empirical methods require estimation of a large number of material parameters. This is possible only if a large volume of creep strain time database is available. A physics based model which uses only the dominant mechanisms of deformation needs significantly less number of material parameters to describe the creep curves. A set of creep tests has been performed on specimens which have undergone both prior strain and thermal ageing. The results conclusively proved that the structural softening due to precipitate coarsening is the most dominant mechanism of creep in 2.25Cr-1Mo steel.

Constitutive laws representing evolution of creep strain and microstructural damage due to particle coarsening have been formulated in the form of a set of coupled differential equations. A computer programme has been developed to extract the material parameters of the above model directly from the creep curve. Stress-temperature dependence of these have been established to allow creep strain prediction for any arbitrary stress-temperature conditions. Comparison of the predicted strain time plots with available data indicate that a reasonably good mechanism based creep strain prediction is possible over a range of test conditions.

SOME ASPECTS OF CREEP BEHAVIOUR OF 2.25Cr-1Mo STEEL

ABSTRACT

Key Words : Creep, Cr-Mo steel, rupture strength, ductility, strain, particle coarsening, CRISPEN, microstructure, bainite, ferrite-carbide, ferrite-bainite, stress, temperature, mechanism, softening.

Creep and stress rupture properties of 2.25Cr-1Mo steel having different initial microstructures have been evaluated.   Bainitic structure has been found to give maximum rupture strength where as ferrite carbide structure provides maximum rupture ductility. Ferrite-bainite structure provides an optimum combination of strength and ductility.

Commercial grades of steels conforming to the same specification may have minor variations in chemical composition.   It has been shown that these variations can significantly alter the initial microstructure and thus influence stress rupture properties.   Section size of the product may also have similar effects on long term stress rupture properties.

Limitations of existing procedures for rupture ductility prediction have been re-examined.   An alternate procedure based on a stress-temperature function has been suggested.   Based on this approach rupture ductility prediction over a range of stress and temperature is possible within ± 20% of the actual data.   This approach, however, being empirical, does not take into consideration the nature of rupture. Concept of a geometric factor that determines the nature of rupture has been introduced to suggest an improved method of rupture ductility prediction.   Using this concept one can construct a rupture ductility diagram.   Such a diagram helps in identifying test conditions, under which specific mechanism of rupture is operative.   Reliable prediction of rupture ductility is possible within the domain of same mechanism.

Modern design practice demands a more exact description of the accumulation of creep strain. A computer based design aid called CRISPEN using established physical models of creep deformation has been developed jointly by NPL Teddington and Cambridge University (U.K.)for creep strain prediction of engineering alloys. This has been sucessfully used to predict the creep behaviour of a range of superalloys where strain softening is the most dominant mechanism of creep deformation. The present work examines how this approach could be modified to include the effect of softening due to time dependent particle coarsening, which is the most dominant mechanism of creep deformation in Cr-Mo steel. A computer program has been developed to analyse creep curves to extract the relevant constants. A large volume of existing database on 2.25Cr-1Mo steel has been used to validate the approach. The physical significance of the parameters used has been analysed to identify the nature of stress dependence of particle coarsening behaviour in these steels.

CONTENTS

LIST OF TABLES

I

LIST OF FIGURES

IV

VI

LIST OF SYMBOLS

σ	Stress
T	Temperature
t	Time
t_r	Rupture Time
ε	Strain at any instant 't'
$\overset{o}{\varepsilon}_m$ or $\overset{o}{\varepsilon}_i$	Minimum or initial creep rate
ε_f	Rupture strain
Q, Q_1	Activation Energy for self diffusion
n	Stress exponent
R	Universal gas constant
C	Larson-Miller Constant (in equation 2.15)
b	Sherby-Dorn Constant (in Equation 2.21)
t_o, T_o	Manson-Haferd constants (in Equation 2.34)
a_o, a_1, ..a_n	Regression Coefficients for Combined time-temperature parameters.
S	Average sum square error
l_o	Original (initial) length of the specimen
A_o	Original (initial) cross-sectional area of the specimen
l	Measured length at rupture
A	Measured cross-sectional area
EL	Elongation at rupture
RA	Reduction in area at rupture

P_1	Larson-Miller type parameter used in Goldhoff's model
$\dot{E}$	Average elongation rate
P_2	Combined temperature-average elongation rate parameter
M_o, M_1, M_2	Regression Coefficients [equation (3.11)]
m_o, m_1, m_3	Regression Coefficients [equation (3.12)]
σ_o	Friction or threshold stress
Q_l	Activation energy for lattice self diffusion
Q_p	Activation energy for pipe diffusion
α, ε_p	Stress-temperature dependent constant representing primary creep
β, a_2	Stress-temperature dependent constant representing tertiary creep
σ_i	Internal stress associated with dislocation density
H	Hardening Coefficient
R	Recovery Coefficient [equation(4.14)]
t_t	Time at which tertiary creep begins
θ_1, θ_2	Parameters defining primary or decaying component of creep curve
θ_3, θ_4	Parameters defining tertiary or accelerating component of creep curve
a_i,b_i,c_i,d_i	Regression Coefficients [Equation (4.18)]

$S_1, S_2, S_3 \ldots$	State variables for physical creep models
ω_1	Damage caused by microstructural changes in terms of dislocation density and particle size.
ω_2	Damage caused by loss of external section in constant load condition.
ω_3	Damage caused by loss of internal section due to cavitation or cracking at grain boundaries
ρ_i	Initial dislocation density
ρ	Dislocation density at time 't'
d_o	Initial inter particle spacing
d	Inter particle spacing at time 't'
C_1, C_2, C_3	Physical model parameters being functions of stress and temperature
C_F	Cooling time from AC_3 to 500^oC to avoid formation of proeutectoid ferrite
ε_n	Critical strain for necking to set in.
k	Geometrical factor representing nature of creep rupture
a, b	Physical model parameters representing extent of softening due to particle coarsening
K	Kinetics of particle coarsening
σ_{oi}	Initial threshold stress
C, Q_2	Temperature dependent constant of initial threshold stress
K_o, m, Q_1	Stress-temperature dependent constants of K

INTRODUCTION

SOME ASPECTS OF CREEP BEHAVIOUR OF 2.25Cr-1Mo STEEL

1.0 INTRODUCTION

Low alloy Cr-Mo steels are widely used for high temperature applications in power plants, oil refineries, chemical and petroleum industries for pipings, heat-exchangers, superheaters and pressure vessels because of their excellent creep and oxidation resistance. The presence of chromium in small amounts upto 0.5% acts as a carbide former and stabilizer. However, in large amounts upto 9% or more it improves corrosion and oxidation resistance of steels and influences hardenability.

The effect of chromium in ferritic creep resistant steels is complex. By itself, chromium gives some enhancement of creep strength, although increasing the chromium content in low carbon grades does not increase resistance to deformation at elevated temperatures[1]. When added in presence of molybdenum it generally leads to some reduction in creep strength[2]. In 0.5% Mo steel, the presence of chromium in amounts upto 2% does not increase the creep resistance but beyond 2% significant reduction in creep strength has been reported. For 1% Mo steel, the optimum creep strength occurs with about 2.25% Cr[3].

Molybdenum is an essential alloying element in ferritic steels where good creep resistance above 450°C is required. Even in small amounts (0.1 to 0.5%), molybdenum increases the resistance of these steels to deformation at elevated temperature. Much greater strength can be obtained by increasing the molybdenum level to about 1% but at the expense of greatly reduced rupture ductility[4]. This loss of ductility could be overcome by addition of chromium. In addition molybdenum is a carbide stabilizer and prevents graphitisation. For certain ranges of stress and temperature the dissolution of iron carbide and the concurrent precipitation of molybdenum carbide cause strain

1

hardening in these steels. Molybdenum in amounts upto 0.5% also minimises temper embrittlement. The optimum creep strength occurs at about 2.25% Cr. Therefore, amongst all grades of Cr-Mo steels this is the one which is most commonly used for a wide range of high temperature applications in both thermal and nuclear power plants. Becuase of its popularity it has become a standard reference material against which performance of other steels are measured.

The elevated temperature behaviour of this steel has been extensively studied under different heat-treated and service exposed conditions[5-44]. These are expected to produce a wide range of microstructures in the steel products depending on their chemical composition and section size. The influence of microstructure on rupture strength and ductility of this steel can be summarised as follows :

- Stress-rupture strength generally increases linearly with room temperature tensile strength upto about 565°C for times upto 10,000 hours.

- At a given strength level, tempered bainite results in higher creep strength than tempered martensite or ferrite-pearlite structures for temperatures upto 565°C and times upto 100,000 hours. For higher temperatures and times, the ferrite-pearlite structure is the strongest.

- Rupture ductility generally decreases with rupture time, reaches a minimum and then increases again. Test temperature, room temperature tensile strength, austenitizing temperature and impurity content increase the rate of decrease of ductility with time and cause the ductility minimum to occur at shorter times.

- Although fully bainitic microstructures have better creep strength under high stress, short-time conditions than those with a ferrite-bainite or ferrite-pearlite microstructure, degradation in strength occurs more rapidly at higher temperature than pearlitic structures. As a result,

2

ferrite-pearlite structure offers better low stress creep resistance.

The creep strength of Cr-Mo steels is mainly derived from a complex combination of solid solution and precipitation effects. In the early stages of creep, solid solution effects are the largest contributor to creep resistance. As the time progresses the precipitation of carbides (primarily Mo_2C) contributes more to the creep resistance. As the time progresses still further the strengthening effect of the carbides is reduced as a result of their coarsening.

The initial microstructure usually consists of bainite and ferrite containing Fe_3C carbides, ε-carbides and fine Mo_2C carbides. With increased ageing in service, or tempering in the laboratory, a series of transformation of carbide phases may take place[45]. This can be described by the following sequence

$$
\varepsilon\text{-Carbide} \longrightarrow Fe_3C \longrightarrow \boxed{\begin{array}{c} Fe_3C \\ + \\ Mo_2C \end{array}} \longrightarrow M_{23}C_6
$$

with $M_7C_3 \longrightarrow M_6C$ branching upward from the box.
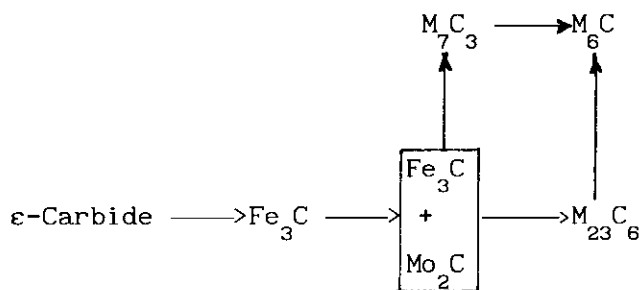
where M is mostly chromium.

Such an evolution of carbide structure and resulting coarsening of carbides, changes matrix composition leading to an overall decrease in creep strength. The time-temperature kinetics of carbide evolution in 2.25Cr-1Mo steel in both bainitic and martensitic conditions have been represented by Baker and Nutting[45] in the form of an isothermal diagram as shown in Fig.1.1. This is a useful tool for estimating service condition of steel components based on microstructural changes in terms of identification of carbides. Their morphology as well as composition of alloying elements in the matrix and carbide phases are primarily responsible for achieving an optimum creep resistance in

3

steels. The influence of alloying elements, heat-treatment parameters and service exposure on microstructural changes and mechanical properties of Cr-Mo steels have been extensively studied[46-58]. It has been reported that the creep resistance of such steels is determined by the stability of M_2C carbides. This can further be improved with the additions of V, Nb, Ti and B. This has been used in improving the creep strength of 2.25Cr-1Mo steel[28,59].
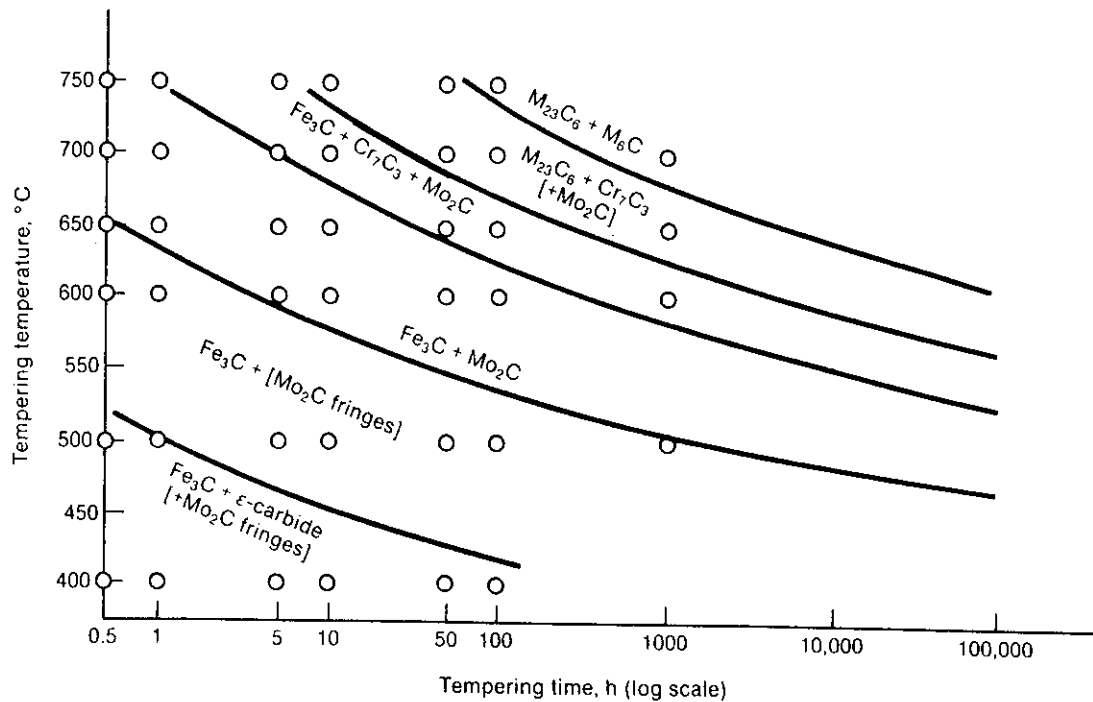
Fig.1.1 Isothermal diagram showing sequence of carbide formation in 2.25Cr-1Mo steel[45]

The performance of high temperature components are judged by their ability to withstand the operating stress and temperature without leading to failure or rupture. The design and manufacture of such components are based on standard codes[60,61]. It assumes that the components operate at a constant pressure and temperature for a period of at least 100,000 hours[60]. Paragraph A-150 of Section I, Power Boilers, of ASME Boiler and Pressure Vessel Code[61] states that the allowable stresses are to be no higher than the lowest of the following:

4

1. 1/4 of the specified minimum tensile strength at room temperature.

2. 1/4 of the tensile strength at elevated temperature.

3. 2/3 of the specified minimum yield strength at room temperature

4. 2/3 of the yield strength at elevated temperature.

5. Stress to produce a creep strain of 1% in 100,000 hours (or 0.01% in 1000 hours).

6. 2/3 of the average stress or 4/5 of the minimum stress to produce creep rupture in 100,000 hours as determined from extrapolated data, whichever is lower.

Fig.1.2 illustrates how these criteria are usually employed to establish the allowable stress for 2.25Cr-1Mo steel as a function of temperature. At temperatures beyond $482^{\circ}C$ ($900^{\circ}F$), it is the creep or rupture strength that determines the allowable stress. Therefore, in the evaluation of creep behaviour of these steels estimation of long term rupture strength has received considerable importance.

The evaluation of 2.25Cr-1Mo steel is mainly based on uniaxial stress rupture tests at different stresses and temperatures. The data so generated are analysed using combined time-temperature parameter viz. Larson-Miller Parameter to estimate long term rupture strength. Fig.1.3 gives a typical master rupture plot of this steel exhibiting wide scatter associated with stress rupture data[62]. However, with increasing use of Finite Element Method (FEM) in the design of high temperature components, assessment based on this approach where only one point is considered from the entire creep curve may not be sufficient.

5
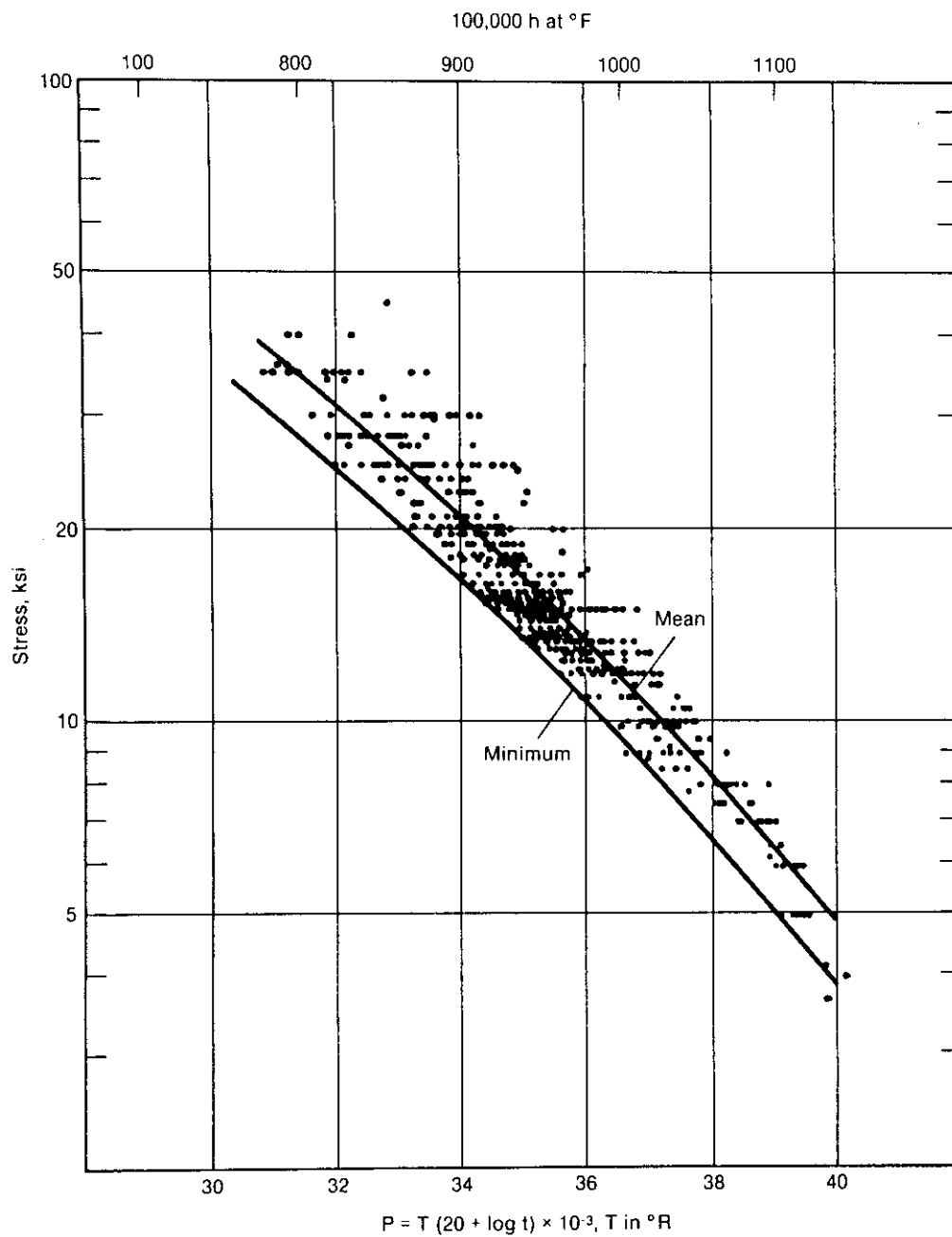
Fig.1.3 Master rupture plot of annealed 2.25Cr-1Mo steel exhibiting
wide scatter associated with stress rupture data[62]

(a) Such tests are easy to perform and are less expensive.

(b) Availability of a fairly large volume of stress rupture database for a wide range of engineering materials in comparison to their time dependent creep deformation database in the literature.

(c) Most design criteria of engineering components are based on creep rupture and not on the accumulation of creep strain.

Numerous time-temperature parametric models[63-67] are now available to predict long term creep rupture strength of engineering materials from short term data. Of these the three most frequently used parameters are

Larson-Miller Parameter[65] : $LMP = T(C + \log tr)$ (1.1)

Sherby-Dorn Parameter[66] : $SDP = \log tr - b/T$ (1.2)

Manson-Haferd Parameter[67] : $MHP = (\log tr - \log t_o)/(T - T_o)$ (1.3)

where C, b, T_o and t_o are constants, tr is rupture time in hours and T is temperature in ^oK. When rupture stress is plotted against such time-temperature parameters one obtains a common master rupture plot irrespective of the test temperature. A fifth degree polynomial in $\log \sigma$ is often used to represent such a rupture plot. This forms the basis for the estimation of rupture strength. The approach, being empirical, has only a limited extrapolation power beyond the domain of available experimental data. Besides the wide scatter in stress rupture data even for the same grade of steel as shown in Fig.1.3 adds to the degree of uncertainty in the predicted strength.

Unlike prediction of long term rupture strength, no appropriate methodology has yet been established to predict long term rupture ductility since analysis of rupture ductility data usually do not reveal any definite correlation with any of the commonly used time temperature parameters. This is primarily because the extent of localized

8

deformation (necking) varies in an unpredictable manner with test conditions. There is, therefore, a need to include a parameter which would describe the nature of rupture for more appropriate prediction of rupture ductility.

Increasing use of modern design techniques to conserve material and energy demand a more precise description of the entire portion of the creep curve to allow reliable interpolation or extrapolation. Among the various empirical creep strain prediction models[68-73] available in the literature, the use of θ - projection approach[70] and the Graham-Walles model[71] received considerable attention over the last two decades. Although these methods are being used to predict the creep curves of a number of engineering materials over a wide range of stress and temperature, they suffer from the limitation that a large number of parameters must be estimated. This is possible only if a large volume of experimental database is available. Besides, the approach being empirical, only a limited extrapolation is possible beyond the domain of available experimental data.

In contrast, the High Temperature Materials group of NPL, Teddington (UK) has proposed an approach to predict creep behaviour of engineering materials from the dominant mechanism of creep deformation using the principles of damage mechanics. In this approach the evolution laws for creep rate($\overset{o}{\varepsilon}$) and state variables ($\overset{o}{S}_1$, $\overset{o}{S}_2$) representing different forms of damages are expressed in the form of a set of coupled differential equations viz.:

$$\overset{o}{\varepsilon} = f\ (\sigma,\ T,\ S_1,\ S_2) \qquad\qquad (1.4)$$

$$\overset{o}{S}_1 = g\ (\sigma,\ T,\ S_1,\ S_2) \qquad\qquad (1.5)$$

$$\overset{o}{S}_2 = h\ (\sigma,\ T,\ S_1,\ S_2) \qquad\qquad (1.6)$$

where σ is the applied stress and T is the test temperature. Explicit forms of these functions (f, g and h) have been identified for a range

of engineering materials and a computer based design aid called CRISPEN has been developed to solve the above equations for Creep Strain Prediction of Engineering Materials under arbitrary stress – temperature conditions[74]. This package has been extensively used to predict successfully the creep behaviour of a range of superalloys where strain softening due to increasing dislocation density is the dominant mechanism. Unlike superalloys, in low alloy Cr-Mo steels the progressive weakening of the material by coarsening of precipitates is mainly responsible for its continuously increasing creep rate[75]. Based on the above observations, Dyson and McLean[76] formulated a set of constitutive equations to represent creep behaviour of materials where coarsening of precipitates is the dominant mechanism. However, appropriate methods to estimate the material parameters determining evolution of structural damage due to particle coarsening have not yet been established. This, therefore, restricts the applicability of CRISPEN to predict creep behaviour of low alloy Cr-Mo steel where coarsening of precipitates plays the dominant role.

In the context of the above, the present work was undertaken to study the following aspects of the creep behaviour of a 2.25Cr-1Mo steel.

(1) To compare effectiveness of the three parameters for predicting long term rupture strength.

(2) To study the influence of microstructures on stress rupture properties as well as on the shape of creep curve.

(3) To identify the major factors responsible for the wide scatter usually associated with stress rupture data.

(4) To identify the problems associated with prediction of creep rupture ductility and suggest a method of improving the same.

(5)   To establish experimentally the dominant mechanism of creep deformation in this material.

(6)   To develop an appropriate method for evaluation of material parameters and their stress-temperature dependence for predicting creep behaviour based on particle coarsening model.

(7)   To predict creep curves over a range of stress and temperature using the estimated material constants for the purpose of comparison with experimental as well as published creep data.

CREEP RUPTURE STRENGTH PREDICTION MODELS

2.0   CREEP RUPTURE STRENGTH PREDICTION MODELS

The performance of high temperature components in power plants, chemical industries and petroleum refineries are judged by their ability to withstand the operating stress and temperature without leading to failure or rupture. The design and manufacture of such components are based on relevant design codes[60] which would certify that the components would withstand design pressure and temperature for a period of at least 100,000 hours. The estimation of long term rupture strength required for such certification comes from a systematic analysis of stress rupture data of the respective materials. These could be conveniently generated in the laboratory by accelerated uniaxial stress rupture tests under constant load. The acceleration in such tests is achieved by performing tests at higher than normal operating stress/temperature conditions.

The experimentally generated stress rupture data are presented in the form of stress vs. rupture time plot at a constant temperature. A series of such curves at different temperatures[19], as shown in Fig.2.1, forms the basis of conventional design practice for high temperature components. It is rather unlikely that stress rupture data under all possible stress/temperature conditions will be available as the generation of such data is highly time consuming and expensive. Therefore, one must have a basis to interpolate or extrapolate the available database to obtain the desired information.

Over the years a number of procedures[63,65,67] has evolved to obtain a common master rupture plot from a series of stress rupture curves based on empirically established dependence of rupture stress on a combined time temperature parameter. Numerous parametric models[63-67,77-79] are now available to predict long term rupture strength of engineering materials. A list of a few such parametric models is given in Table-2.1. Although attempts have been made to justify the nature of these t - T functions on the basis of physics of deformation, these are essentially of empirical origin. The essential

12

Table - 2.1

A List Of Time-temperature Parameters Used for Creep-rupture Strength/Life Prediction

Name of the Model	Expression
Linear Parameters	
Larson-Miller	$T(C + \log tr)$
Sherby-Dorn	$\log tr - b/T$
Dorn	$tr[\exp\{-(\Delta H/RT)\}]$
Manson-Haferd	$(\log tr - \log t_o)/(T - T_o)$
Manson-Succop	$\log tr + CT$
Sud-Aviation	$\log tr + C\log T$
Non-Linear Parameters	
Manson-Brown	$(\log tr - \log t_o)/(T - T_o)^P$
Graham-Walles	$tr(T_o - T)^P$
Stress modified parameters	
Clauss	$\log tr + f_1(\sigma)f_2(T)$, where $f_1(\sigma)=a+b(\log\sigma)+C(\log\sigma)^2$ $f_2(T)=p+qT+rT^2$
Murry	$(\log tr - q\sigma)/(1/T-p)$
Chitty-Duval	$T - a\sigma^b \log tr$

14

2.1 Larson-Miller Parameter

This had its origin in the tempering studies of steel by Hollomon and Jaffe[80]. They noted that certain properties of quenched steel such as hardness varied with time and temperature during tempering treatment. This being a diffusional process it was possible to represent the change in hardness in the form of a master plot using a time - temperature parameter of the form T (20 + log tr), where T is the tempering temperature in $^{\circ}$K and tr is the time in hours.

Recognizing that the creep behaviour of metals and alloys has some similarity with tempering phenomena, Larson and Miller[65] felt that the time to rupture (tr) and the test temperature (T) for creep rupture might follow the same relationship as that used by Hollomon and Jaffe[80]. Selection of the parameter could also be justified from the nature of temperature dependence of minimum creep rate ($\overset{\circ}{\varepsilon}_m$). The time to rupture of any material is inversely proportional to its minimum creep rate ($\overset{\circ}{\varepsilon}_m$), whose temperature (T) dependence has been reported to be of the following form;

$$\overset{\circ}{\varepsilon}_m = A \exp[-Q/(RT)] \qquad (2.11)$$

where A is a material constant, Q is the activation energy and R is the universal gas constant. Consequently

$$tr \; \alpha \; (1/\overset{\circ}{\varepsilon}_m) = A' \exp[Q/(RT)] \qquad (2.12)$$

$$\text{or } \log tr = \log A' + Q/(2.3RT) \qquad (2.13)$$

$$\text{or } T (C + \log tr) = Q/(2.3R) \qquad (2.14)$$

where $\log A' = -C$. Assuming that the activation energy (Q) is a function of stress (σ), stress rupture data, therefore could be represented by a time-temperature function commonly known as Larson-Miller Parameter (LMP) as follows :

15

$$LMP = T(C+\log tr) = a_o + a_1 \log\sigma + a_2(\log\sigma)^2 + \ldots a_n(\log\sigma)^n \quad (2.15)$$

where C = Larson-Miller constant and a_o, a_1, a_2,.....a_n = Regression coefficients.

Several analytical and graphical procedures[63-65] have been used to estimate the constants in equation (2.15). However, with the easy availability of computers it is now convenient to estimate these by method of least squares. Chaudhuri et.al[81] developed a computer program to estimate the constant C and regression coefficients a_o, a_1, a_2,....a_n in equation (2.15) using such an approach. The algorithm of this program is given in Annexure-I. The database thus obtained could be used either for the estimation of long term rupture strength over a range of temperature or for life prediction under arbitrary stress/temperature conditions.

2.2 Sherby-Dorn Parameter

Sherby, Orr and Dorn[66] observed that during creep the activation energy(Q) remains constant for many materials irrespective of stress, temperature, strain and other metallurgical variables such as small alloying additions, grain size, substructure developed etc. In such cases, therefore, it would be more appropriate to assume log A' in equation (2.13) to be a function of applied stress σ, rather than Q. Thus one can explain the origin of Sherby-Dorn parameter (SDP) often used to express stress rupture data. The master plot in such cases is represented by

$$\log tr - (b/T) = a_o + a_1 \log\sigma + a_2(\log\sigma)^2 + \ldots + a_n(\log\sigma)^n$$
$$\ldots\ldots\ldots\ldots\ldots\ldots(2.21)$$

where b (=$Q/2.3R$), a_o, a_1, a_2.... a_n are constants.

Several graphical and analytical procedures[63,64,66] have evolved over the years for the estimation of the above constants from experimental data. However, with the availability of modern computational aids it is now more convenient to estimate these by method of least squares using the standard linear regression analysis

16

technique. The algorithm of the program developed by Chaudhuri et.al[81] is shown in Annexure-II. The database consisting of the above constants for a given material can form the basis for either estimation of long term rupture strength over a range of temperature or life prediction under arbitrary stress/temperature conditions.

2.3 Manson-Haferd Parameter

Manson-Haferd Parameter[67] unlike Larson-Miller and Sherby-Dorn parameters is based on the fact that plots of log tr vs. T at different stresses intersect at a fixed point given by To and log to for many materials. This parameter has been derived based on the assumption that the temperature (T) dependence of rupture time (tr) follows an exponential relation of the form

$$tr = A_1 \exp(A_2 T)$$
$$\text{or} \quad \log tr = \log A_1 + (A_2 T/2.3) \tag{2.31}$$

where A_1 is a constant and A_2 is a stress dependent function.

Since all the constant stress plots intersect at a point (To, log to),

$$\log to = \log A_1 + A_2 T_o/2.3 \tag{2.32}$$

On subtracting equation (2.32) from equation (2.31) and subsequent algebraic simplification one obtains

$$(\log tr - \log to)/(T - To) = A_2/2.3 \tag{2.33}$$

Assuming A_2 to be a polynomial function of log σ the master rupture plot could, therefore, be represented as

$$(\log tr - \log t_o)/(T - T_o) = a_o + a_1 \log\sigma + a_2 (\log\sigma)^2 + \ldots + a_n (\log\sigma)^n \tag{2.34}$$

where To, to, a_o, a_1, a_2, $\cdots$, a_n are constants.

The time temperature function in the left hand side of equation (2.34) is called the Manson Haferd Parameter. Several analytical and graphical techniques[63,64,67] have evolved over the years for the estimation of the constants in equation (2.34). With the introduction of an additional constant the procedure is a little more complex than that in the case of Larson-Miller and Sherby-Dorn parameters. However, with the availability of modern computational aids it is quite convenient to estimate these using method of least squares based on non linear regression analysis. It has been reported that sometimes with limited data with large scatter solution may not converge. In such cases linear regression technique could be adopted for a set of predefined values of T_0, the set giving minimum error being chosen for subsequent analysis.

Chaudhuri et.al[81] developed a computer program to estimate the optimum values of the Manson-Haferd constants T_0 and log t_0 and other regression coefficients using the entire set of data. The algorithm based on which the program has been developed is shown in Annexure-III. Creation of a database consisting of the above constants forms the basis for either estimation of long term rupture strength over a range of temperature or life prediction at any arbitrary stress and temperature. Chattopadhya et.al[82] have further consolidated the above programs[81] for rupture data analysis in the form of a software package for creep life prediction called CLIP. This is a menu driven program with on line help and having facilities for creation and storage of data file, analysis of data for prediction of long term strength and graphic display. It also has a simulation module to predict life under arbitrary stress/temperature conditions.

18

CREEP RUPTURE DUCTILITY PREDICTION MODELS

3.0 RUPTURE DUCTILITY PREDICTION MODELS

In the design of high temperature components considerable attention
has been paid for estimation of creep and rupture strength of
engineering materials. Since creep rupture ductility often varies
inversely with rupture strength, over a range of stress and temperature
both the properties must be optimised for a given application. Rupture
ductility is, therefore, an important yet neglected parameter
determining integrity of high temperature components. Gross and uniform
deformation of components is usually the exception rather than the rule.
Localised defects and stress concentrations often play decisive role in
failure. Under such conditions, the growth of a crack or a defect is
governed by rupture ductility. Besides, ductility may drop below a
critical level under service conditions rendering the component notch
sensitive. Many investigators suggested that the critical level of
smooth bar stress rupture ductility of about 10% reduction in area in a
Cr-Mo-V steel may be desirable for avoidance of notch
sensitivity[83,84]. It is, therefore, felt that the prediction of long
term creep rupture ductility of materials based on short term data is
essential for high temperature applications.

3.1 Goldhoff's Model

Under service conditions, the drop of stress rupture ductilities of
high temperature materials to critical levels corresponding to the onset
of notch sensitive behaviour generally occurs after long exposure.
Goldhoff[85] was the first to attempt prediction of long term
ductilities of materials based on short term test data.. The important
steps involved in his approach are as follows :

(1) Collection of short term test data in terms of rupture time (tr) in
     hours and the average elongation rate ($\dot{E}$) in % per hour over a
     range of stress (σ) and temperature (T). The average elongation
     rate ($\dot{E}$) is obtained by dividing the total elongation at rupture by
     the rupture time.

(2) Analysis of the above test data using a Larson-Miller type parameter. The equations used in this analysis are

$$\sigma = M_o + M_1 P_1 + M_2 P_1^2 + M_3 P_1^3 + \ldots\ldots \qquad (3.11)$$

where $P_1 = (T + 460)(20 + \log tr)$ and M_o, M_1, M_2, M_3 ... = Regression coefficients.

$$\sigma = m_o + m_1 P_2 + m_2 P_2^2 + m_3 P_2^3 + \ldots \qquad (3.12)$$

where $P_2 = (T + 460)(25 - \log \dot{E})$, and m_o, m_1, m_2, m_3 = Regressions coefficients; T = Temperature in $^\circ F$.

The regression coefficients M_o, M_1, M_2, M_3,.... are estimated by analysing stress rupture data using equation (3.11). Similar procedure is followed to estimate the regression coefficients of equation (3.12). Having estimated all the regression coefficients of equations (3.11) and (3.12), it would be possible to determine the rupture elongation at any given temperature and time to rupture. The stress is first estimated from equation (3.11) for any given temperature and time to rupture and thereafter, $\dot{E}$ is estimated from equation (3.12). Rupture elongation at a given temperature and time to rupture is thus determined by multiplying the estimated $\dot{E}$ with the time to rupture.

3.2 Viswanathan and Fardo's Model

Several functional relationships amongst elongation, reduction in area, temperature and stress were explored by Viswanathan and Fardo[86]. They used the stress temperature dependence of ductility data (%RA) on 1.25Cr-0.5Mo steel[87] as shown in Fig.3.21. They found poor correlations while analysing the entire set of data in Fig.3.21. The correlations were thereafter improved when the analysis was confined to the regions where % elongation and % RA decrease with decreasing stress. An excellent correlation was, obtained between the average elongation rate ($\dot{E}$) and time to rupture (tr) over the entire data set and could be described as

20

$ln(\overset{\bullet}{E}) = 4.202 - 1.18 \space ln(tr)$ (3.21)

This model clearly indicates that the relationship between $\overset{\bullet}{E}$ and tr is independent of stress and temperature.

An analysis of rupture ductility database[34] using Goldhoff's model as well as Viswanathan and Fardo's model has been attempted in the present work. The usefulness of these methods in the prediction of long term rupture ductility of 2.25Cr-1Mo have been critically examined.
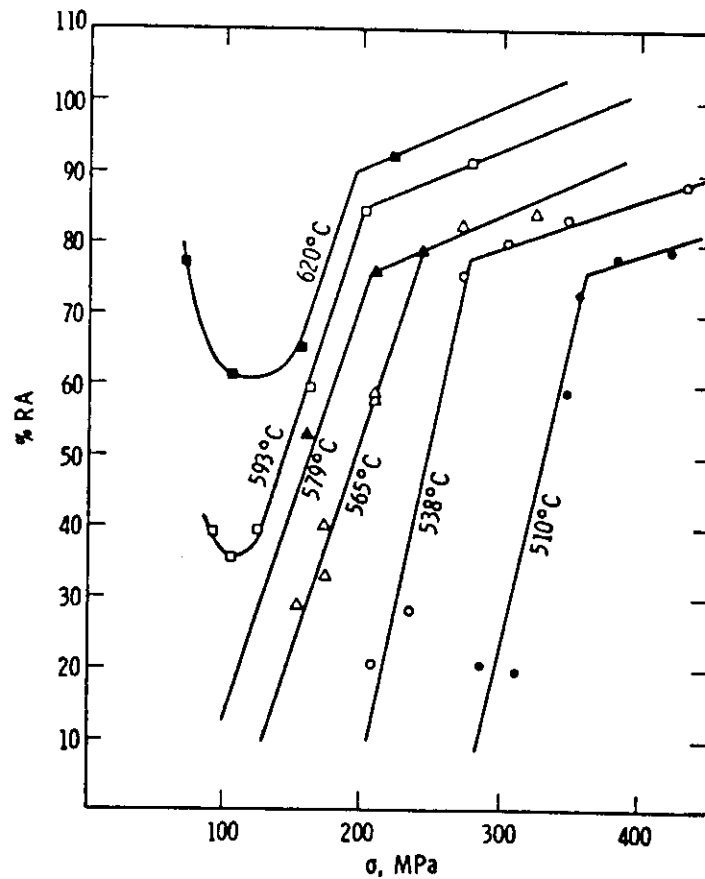
Fig.3.21   Variation of rupture ductility (%RA) with stress and temperature for 1.25Cr-0.5Mo steels[87]

CREEP STRAIN PREDICTION MODELS

4.0 CREEP STRAIN PREDICTION MODELS

Creep curves of pure metals or single phase alloys in general consist of three easily identifiable stages namely primary, secondary and tertiary creep[88]. The secondary stage maintains a constant creep rate signifying that a steady state is achieved through a balance of recovery and work-hardening[89]. Moreover this rate is often adequately described by a power law expression[88] predicted by recovery controlled creep model [89,90]

$$\overset{o}{\varepsilon}_m = A\,\sigma^n\,\exp(-Q/RT) \tag{4.0a}$$

where $\overset{o}{\varepsilon}_m$ = minimum creep rate, A = constant, n = stress exponent, σ = applied stress, Q = activation energy for self diffusion and T = temperature in degree Absolute.

The creep behaviour of complex engineering alloys deviates from this general pattern in two main respects. Firstly, a well established steady state creep regime is rarely observed; rather, after a small primary creep strain, the creep rate progressively increases from a minimum value ($\overset{o}{\varepsilon}_m$) until fracture occurs. Secondly when the minimum creep rates are analysed in terms of equation(4.0a) unrealistic values of n and Q are obtained.

The concept of friction stress (σ_o) pioneered by Wilshire and co-workers[91-93] has proved to be useful in rationalising the minimum creep rate data of engineering alloys with the ideas of recovery creep through Bailey-Norton equation

$$\overset{o}{\varepsilon}_m = A_1(\sigma-\sigma_o)^{n1}\exp(-Q_1/RT) \tag{4.0b}$$

Using values of σ_o determined by analysing transient creep following stress reduction, the above equation (4.0b) yields values of n1 = 4 and Q1 nearly equal to activation energy of self diffusion for a wide range of materials[94]. The magnitude of σ_o has been reported to change not

only with stress[95] and temperature[96] but also to vary through out creep life[97-99]. By arguing that time dependent coarsening of microstructure reduces σ_0 and thus, through equation(4.0b), increases creep rate, Burt et.al.[97], Stevens et.al[98], Williams et.al[99] have provided a plausible explanation of the extensive tertiary creep regime in engineering alloys. Singh et.al[100] studied the creep behaviour of Cr-Mo-V steel having a wide range of microstructures. Their analysis at $550^{\circ}C$ revealed that the friction stress depends on microstructure and beyond a critical value (threshold) "runaway" creep takes place. The magnitude of this threshold may also change as a result of long term exposure (10^{5} hours at $540^{\circ}C$/150 MPa).

Although the power law representation of minimum creep rate is extensively used to analyse most creep data, in certain cases the expressions such as

$$\overset{o}{\varepsilon}_m = A \exp[B\sigma] \exp[-Q/RT] \qquad\qquad (4.0c)$$

$$\overset{o}{\varepsilon}_m = A [Sinh\sigma]^n \exp[-Q/RT] \qquad\qquad (4.0d)$$

better describe the creep behaviour. These expressions are consistent with physical models which assume glide to be diffusion controlled and consider creep in terms of reaction rate theory rather than of recovery control[88].

A number of mechanisms justifying stress and temperature dependence of minimum creep rate have been proposed[101]. Table 4.1[102] gives a summary of these. The one which is dominant depends on test conditions to which the material is exposed and on its properties. Deformation mechanism maps popularised by Ashby[103] provide a simple method of representing the fields of dominant mechanism of creep as a function of stress and temperature. Fig.4.1 gives a typical creep mechanism map for Cr-Mo-V steel[103,104]. Therefore, while developing a model of creep deformation it must always be realised that it can only be appropriate within a certain range of operating conditions.

Table - 4.1

Mechanisms of Thermal Creep

Stress region	Mechanism	Stress Dependence	Activation Energy for the creep process
High	Power law breakdown	$\exp(B\sigma)$	Of the order of activation energy for lattice self-diffusion Q_1
Intermediate			
(a)Low temperature	Recovery by low temperature climb	σ^7	activation energy for pipe diffusion, Q_p ($= 0.6Q_1$)
(b)High temperature	Recovery by high temperature climb	σ^5	Q_1
	Viscous glide (in solid solution)	σ^3	Q_1
Low	Harper-Dorn Creep	σ	Q_1
	Nabarro-Herring Creep	σ	Q_1
	Coble Creep	σ	Q_{gb}, Activation energy for grain boundary diffusion

Fig.4.1 : Typical Creep Mechanism Map for 1%Cr-Mo-V Steel[104]

Development of creep strain prediction models has been influenced by the computational facilities that are available to both research workers who develop the model and to the engineers and material technologists who use them for a wide range of applications. The vastly increased speeds of computers resulting from the parallel processing capability has made use of finite element design technique quite economical. However, their growing use demands a more exact description of creep behaviour of engineering materials. In fact lack of accurate material property data and constitutive models describing evolution of damage currently limit full exploitation of such design potential[105]. The assumption of a steady state creep behaviour for complex alloys leads to over estimate in performance. The level of sophistication of analytical design using FEM depends on ability to accurately represent the full shape of creep curve under varying stress and temperature conditions. This is one of the most active areas of research in the field of creep of engineering materials. The models currently available fall under two general categories each having particular benefits.

a) Empirical models look for mathematical patterns in the data that are available and assume that this description can be extended to arbitrary conditions for which data are not available. These models are usually framed in terms of specific expressions describing evolution of creep strain as function of time. Development is essentially through a process of hypothesis and validation. It is an inductive process.

b) Physical models build on an understanding of mechanisms that are known to control the accumulation of creep strain. They are developed by deductive process from a series of facts that are known to be true and describe the phenomena in terms of microstructural aspects of the materials.

4.1 Empirical Models

Several models have been developed with varying degrees of success. Examples of models describing the primary and steady state creep of simple metals have been given by amongst others, Andrade[106], Garofalo[107], Webster et.al[108]. For example ignoring elastic strains, the following expressions have been widely used :

$$\varepsilon = \alpha t^{1/3} + \overset{o}{\varepsilon}_m t \qquad\qquad (4.11)$$

$$\varepsilon = \varepsilon_p [1 - \exp(-c\overset{o}{\varepsilon}_m t)] + \overset{o}{e}_m t \qquad\qquad (4.12)$$

The equation (4.12) is a direct consequence of recovery controlled creep model[109]. It envisages that the evolution of dislocations during creep gives rise to an internal stress (σ_i) that resists creep, strain rate being governed by

$$\overset{o}{\varepsilon} = A (\sigma - \sigma_i)^n \qquad\qquad (4.13)$$

The rate of change of σ_i has a positive contribution due to new dislocations being created with increasing strain and a negative contribution associated with dislocations being destroyed by recovery which increases with increasing σ_i

$$\overset{o}{\sigma}_i = H\overset{o}{\varepsilon} - R\sigma_i \qquad\qquad (4.14)$$

The constants H and R are the hardening and recovery coefficients respectively. Ion et.al.[110] have shown that the equations (4.13) and (4.14) integrate to give equation (4.12). Even when efforts have been made to develop equations describing the strain time behaviour during creep, attentions have usually been directed towards primary and secondary stages. Yet the creep failure is invariably preceded by tertiary stage. Indeed in many commercial creep resistant alloys tertiary stage dominates the creep curve shape in tests of long duration. When attempts have been made to develop constitutive equations capable of representing the strain time behaviour through out the creep test, in general, the tertiary stage has been included simply

by adding a further accelerating function to the expression used to describe primary and secondary creep. Thus equation (4.11) transforms to

$$\varepsilon = \alpha t^{1/3} + \overset{o}{\varepsilon}_m t + \beta t^3 \qquad (4.15)$$

This would allow representation of any creep curve for a given stress and temperature in terms of three parameters α, $\overset{o}{\varepsilon}_m$ and β.

Similarly equation (4.12) could be extended to include the tertiary term as

$$\varepsilon = \varepsilon_p [1 - \exp(-c \overset{o}{\varepsilon}_m t)] + \overset{o}{\varepsilon}_m t + a_2 \exp\{b_2(t - t_t)\} \qquad (4.16)$$

where a_2, b_2 define the shape of tertiary stage of the creep curve which begins at a time t_t. Graphical evaluation of the parameters of above equation (4.16) for several pure metals and simple alloys show that b_2 is directly related to minimum creep rate. This indicates that the processes controlling creep rate are the same through out the creep life. Unfortunately the estimation of time to onset of tertiary stage, t_t, is subjective. Moreover in tests carried out at constant stress and temperature, the commencement of tertiary stage may be attributed to localised deformation (necking), development of grain boundary cavities and cracks or to a progressive loss of creep strength due to particle coarsening. These processes seem incompatible with the idea that the tertiary stage begins only after a specified time t_t in any test[111].

An alternative view pioneered by Wilshire is to consider creep behaviour merely as a consequence of two competing events. These are (1) a primary creep process that decays through out the entire creep life and (2) a tertiary creep process that accelerates from the commencement of the test. With this approach, a minimum rather than a steady state or secondary stage is attained. Representation of a normal creep curve[70,112] is, therefore, of the form

$$\varepsilon = \theta_1 (1 - e^{-\theta_2 t}) + \theta_3 (e^{\theta_4 t} - 1) \qquad (4.17)$$

28

where θ_1, θ_2 define primary or decaying components and θ_3, θ_4 define tertiary or accelerating components of the curve. Computer programs are available to extract parameters θ_1, θ_2, θ_3 and θ_4 from experimental strain-time curves. In order to allow interpolation or extrapolation of data over different stress and temperature conditions it is necessary to describe the parameter θ_i as a function of stress (σ) and temperature (T). The form commonly used is given by

$$\log \theta_i = a_i + b_i T + c_i \sigma + d_i \sigma T \qquad (4.18)$$

Clearly a set of 16 constants will be required to characterize creep curve for any engineering materials over a range of stress and temperature.

4.2 Physical Models

Physics based model tries to identify underlying atomistic processes responsible for creep. These are viscous flow, diffusion, time dependent dislocation motion, grain boundary sliding, void growth, microstructural changes and so forth. There has been some success in mechanism based prediction of creep behaviour of pure metals and single phase alloys. These have been derived from the classic papers by Hart[113,114] on the implications of dislocation structure and the associated hardening of solid solution alloys in determining the deformation characteristics. The approach which has been progressed in several centres, but most notably by Miller[115,116] expresses the deformation rate in terms of current state variables (S_1, S_2, S_3, ...) that are clearly related to the known physical processes of deformation.

Equations describing the strain rate and rate of evolution of state variables S_1, S_2, S_3 etc. are expressed in a phenomenological (empirical) form consistent with the underlying physics.

$$\overset{o}{\varepsilon} = f\ (\sigma,\ T,\ S_1,\ S_2 .....)$$
$$\overset{o}{S_1} = g\ (\sigma,\ T,\ S_1,\ S_2 ....) \qquad (4.21)$$
$$\overset{o}{S_2} = h\ (\sigma,\ T,\ S_1,\ S_2 ...)$$

The strain histories are computed by numerical integration of the above equations (4.21). A series of complex numerical procedures has been developed to do these effectively; the notable amongst these being the MATMOD equation (Materials Model) developed by Miller[116,117]. The current status of the activities is reviewed in a recent multiauthor publication[116]. Table 4.21 gives a summary of the physical mechanism represented within the MATMOD equations.

The representation of creep behaviour of complex engineering alloys however, should include tertiary creep effect[118]. This could be best described in terms of a set of damage parameters ω_1, ω_2, ω_3,..... The foundation of continuum damage mechanics by Kachanov[119] and subsequent development by Rabotnov[120], Leckie and Hayhurst[121] and Lemaitre and Chaboche[122] have been largely empirical but have used a similar set of formalism to that given in eqn. set (4.21).

$$\overset{o}{\varepsilon} = f\ (\sigma,\ T,\ \omega_1,\ \omega_2\ldots.)$$
$$\overset{o}{\omega}_1 = g\ (\sigma,\ T,\ \omega_1,\ \omega_2,\ldots) \qquad\qquad (4.22)$$
$$\overset{o}{\omega}_2 = h\ (\sigma,\ T,\ \omega_1,\ \omega_2\ldots.)$$

Recent work at NPL and Cambridge University[123,124] has reformulated the specific forms of equation set (4.22) to reflect the actual damage mechanisms that are known to lead to tertiary creep in certain engineering alloys such as Ni-base superalloys and ferritic steels. A review of the appropriate mechanisms and their influence on $\overset{o}{\varepsilon}$ has been given by Ashby and Dyson[123]. Ion et.al.[110] and Barbosa et.al.[124] describe how this formalism can be incorporated into a software package designated CRISPEN which operates on IBM compatible personal computer to

- analyse creep curves in order to evaluate parameters of equation set (4.22); and

- simulate creep performance for arbitrary loading conditions including changing stresses and temperatures by interpolation/extrapolation from the available database of model parameters.

Table - 4.21

Internal Physical Mechanisms Represented within the MATMOD Equations

Macroscopic behaviour	Internal Physical basis	MATMOD variables
Temperature dependence	Diffusion (lattice, pipe)	θ', D_{eff}
Non-interactive solute strengthening	Cottrell atmospheres (substitutional solutes)	$F_{sol.1}$
Interactive solute strengthening	Vacancy-interstitial pairs	$F_{sol.2}$
Directional work-hardening	Dislocation pileups, bowed segments, curved subgrain boundaries	R
Directional recovery	Climb, Cross-slip	R(Recovery term)
Isotropic work - hardening	Forest dislocations, subgrain boundaries	F_{def}
Isotropic thermal recovery	Dislocation annihilation	F_{def} (thermal recovery term)
Isotropic strain softening	Glide of 'concave' dislocations	F_{def} (dynamic recovery term)

The most novel aspect of this approach has been to replace the empirical continuum damage mechanics based equations with explicit forms that are fully consistent with current understanding of deformation and fracture mechanisms that occur in advanced high temperature engineering materials.

Dyson and McLean[125] have recently reviewed the current status on CRISPEN approach. This represents the full nonlinear strain evolution in terms of state variables that account for changing macro and micro structural features in a material during deformation. Ashby and Dyson[126] identified three broad categories of damages that can make significant contribution to tertiary creep in high temperature alloys. They are

1. changes in materials microstructure, (e.g. dislocation density, size of particles) that reduce the strength of the material (ω_1).

2. loss of external section due to geometrical changes that leads to a change in stress in constant load condition (ω_2)

3. loss of internal load bearing section due to cavitation or cracking which commonly occurs at grain boundaries (ω_3)

The damage parameters ω_1, ω_2 and ω_3 can be defined in a number of ways. The effect of ω_1 on $\overset{o}{\varepsilon}$ can be represented either as a linear or as an exponential function of creep strain when it is due to an increase in mobile dislocation density. In case coarsening of precipitates is responsible for loss of strength, ω_1 should be defined in terms of initial and current threshold stress. When damage ω_2 is defined as a linear function of strain and ω_3 is defined as a fraction of cross-sectional area damaged due to cavitation or cracking, it can be shown that the creep rate is an exponential function of ω_2 and ω_3[127,128]. The exact form of the expression representing the damage and its relationship with strain rate has been summarised by Dyson[129]; a simple version of the same is given in Table 4.22.

Table - 4.22

Expressions for Strain and Damage Accumulation Rate

Damage Mechanism	Damage Parameter(ω)	$\overset{o}{\varepsilon}$	$\overset{o}{\omega}$
Strain Softening[110]			
Linear	$\rho/\rho_i - 1$	$\overset{o}{\varepsilon}_i(1+\omega)$	$C\overset{o}{\varepsilon}$
Exponential	$\ln(\rho/\rho_i)$	$\overset{o}{\varepsilon}_i \exp(\omega)$	$C\overset{o}{\varepsilon}$
Time Softening[130] (particle coarsening)	$(\sigma_{oi}-\sigma_o)/(\sigma-\sigma_{oi})$	$\overset{o}{\varepsilon}_i(1+\omega)^n$	$a(1-b\omega)^4$
Loss of External Section (Uniform strain under constant load)[130]	$(n/3\varepsilon_f)\ln(A_o/A)$	$\overset{o}{\varepsilon}_i \exp(\omega)$	$(n/3\varepsilon_f)\overset{o}{\varepsilon}$
Loss of Internal Section (Cavitation)[131]	$n \ln(A_o/A)$	$\overset{o}{\varepsilon}_i \exp(\omega)$	$n \overset{o}{\varepsilon}$

NB : A_o = initial area, A = Area at time 't', σ = applied stress, σ_o = threshold stress, σ_{oi} = initial threshold stress, ρ_i = initial dislocation density, ρ = dislocation density at time 't', ε_f = rupture strain, C, a,b are constants.

In general the tertiary creep behaviour is determined by the combined effects of various types of damage and it can be difficult to seperate the precise contribution of each. The situation may be simpler in certain forms of creep test. The constant stress condition which is achieved by compensating the loss of specimen cross-sectional area with decreasing load should remove ω_2 from consideration. Similarly while

modelling creep behaviour of single crystals it is not necessary to consider ω_3 as there is no grain boundary where cavities could nucleate. This, therefore, provides a very flexible system of representing creep behaviour of engineering materials. The simplest set takes all types of damage as influencing the creep rate through exponential function.

$$\overset{o}{\varepsilon} = \overset{o}{\varepsilon}i(1-S) \ \exp(\omega_1 + \omega_2 + \omega_3)$$
$$\overset{o}{S} = H\overset{o}{\varepsilon}_i(1-S) - RS$$
$$\overset{o}{\omega}_1 = C_1\overset{o}{\varepsilon}$$
$$\overset{o}{\omega}_2 = C_2\overset{o}{\varepsilon} \tag{4.23}$$
$$\overset{o}{\omega}_3 = C_3\overset{o}{\varepsilon}$$

The model parameters $(\overset{o}{\varepsilon}_i,$ H, R, C_1, C_2, $C_3)$ will in general be functions of stress and temperature.

For simple uniaxial creep in tension the equation set (4.23) can be expressed in terms of a single composite damage $\omega = \omega_1 + \omega_2 + \omega_3$

$$\overset{o}{\varepsilon} = \overset{o}{\varepsilon}_i(1-S) \ \exp(\omega)$$
$$\overset{o}{S} = H\overset{o}{\varepsilon}_i(1 - S) - RS \tag{4.24}$$
$$\overset{o}{\omega} = C\overset{o}{\varepsilon}$$

where $C = C_1 + C_2 + C_3$, $C_2 = n$, $C_3 = n/\varepsilon_f$ for materials exhibiting power law creep with a stress exponent n and fracture strain ε_f. The four parameters $(\overset{o}{\varepsilon}_i,$ C, H, R) thus define the creep deformation and creep curves are generated by numerical integration of equation set (4.24).

The intrinsic softening observed in Ni base superalloys due to accumulation of mobile dislocations can best be described by a damage parameter that increases linearly with strain and modifies the creep rate by a linear function. When the loss of external and internal section influence creep rate through exponential function, the appropriate sets of equations can be written as

$$\dot{\varepsilon} = \dot{\varepsilon}_i(1-S)(1+\omega_1)\exp(\omega_2+\omega_3)$$
$$\dot{S} = H\dot{\varepsilon}_i(1-S)-RS$$
$$\dot{\omega}_1 = C_1\dot{\varepsilon} \tag{4.25}$$
$$\dot{\omega}_2 = C_2\dot{\varepsilon}$$
$$\dot{\omega}_3 = C_3\dot{\varepsilon}$$

Replacing $\omega_2 + \omega_3$ by ω the equation set (4.25) reduces to

$$\dot{\varepsilon} = \dot{\varepsilon}_i(1-S)(1+\omega_1)\exp(\omega)$$
$$\dot{S} = H\dot{\varepsilon}_i(1-S)-RS$$
$$\dot{\omega}_1 = C_1\dot{\varepsilon} \tag{4.26}$$
$$\dot{\omega} = \dot{\omega}_2+\dot{\omega}_3 = (C_2 + C_3)\dot{\varepsilon} = C'\dot{\varepsilon}$$

Here the entire behaviour can be described by five parameters ($\dot{\varepsilon}_i$, H, R, C_1, C').

Unlike superalloys the loss of strength in ferritic steels is primarily due to coarsening of precipitates. It would, therefore, be more appropriate to use the form given in Table 4.22. Loss of internal and external section may continue to influence creep rate through exponential functions. In this case the appropriate set of equations can be written as

$$\dot{\varepsilon} = \dot{\varepsilon}_i(1-S)(1+\omega_1)^n\exp(\omega_2+\omega_3)$$
$$\dot{S} = H\dot{\varepsilon}_i(1-S)-RS$$
$$\dot{\omega}_1 = a(1-b\omega_1)^4 \tag{4.27a}$$
$$\dot{\omega}_2 = C_2\dot{\varepsilon}$$
$$\dot{\omega}_3 = C_3\dot{\varepsilon}$$

In cases when the effects of primary creep and cavitation are insignificant S and ω_3 may be ignored. The above equation set (4.27a), therefore, reduces to

$$\dot{\varepsilon} = \dot{\varepsilon}_i(1+\omega_1)^n\exp(\omega_2)$$
$$\dot{\omega}_1 = a(1-b\omega_1)^4 \tag{4.27b}$$
$$\dot{\omega}_2 = n\dot{\varepsilon}$$

The CRISPEN provides a simple procedure for analysing creep curves of engineering materials using equation sets (4.23) and (4.25). This has been shown to predict quite well creep behaviour of a range of superalloys such as In 738LC, SRR99 etc. Although it provides a frame work for numerical integration of equation set (4.27a), it does not include a satisfactory procedure for estimating the materials parameters determining the effects of particle coarsening on creep behaviour. Therefore so far as the usefulness of the above approach in representing the creep bahaviour of materials susceptible to time softening has not been evaluated. The present work attempts to do this. Annexure V gives the details of the steps involved in this attempt.

Winstone[71] has recently compared the creep strain predictions by empirical and physical models for SRR99. Each creep curve was analysed to give appropriate sets of model parameters which were expressed as functions of stress and temperature. Using these analytical expressions for the parameters' lives for each of the test conditions were calculated and compared with measured values. These comparisons as shown in Figs 4.21 and 4.22 indicate that there is little to choose between various models for representing constant stress/load creep data. However, the more demanding test is the prediction of strain accumulation during more complex loading conditions.

As materials become increasingly complex and anisotropic it is important that the computational approaches are sufficiently flexible to accomodate characteristics of the material. The fact that CRISPEN based approach satisfies above requirements is evident from the way it has been used to account for creep in single crystal superalloys[132,133] and metal-matrix composites[134].
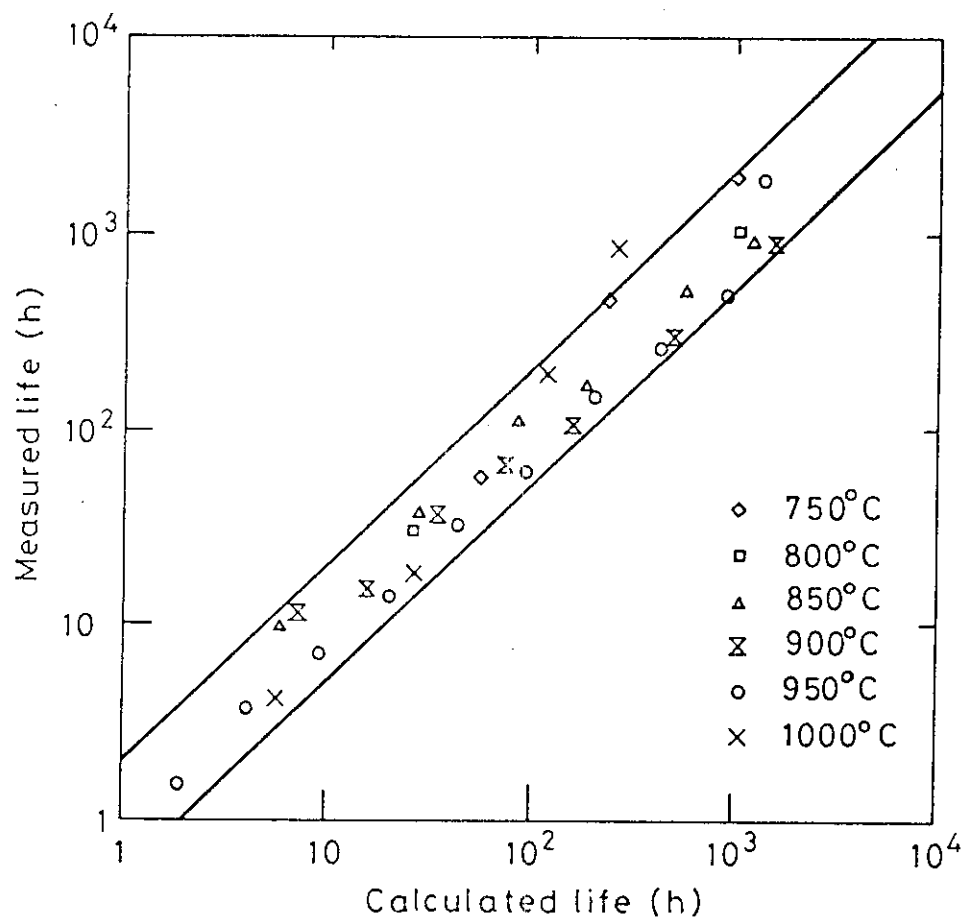
Fig.4.21 Comparison of Calculated and Experimental Rupture Time of SRR99 using θ-Projection Concept.
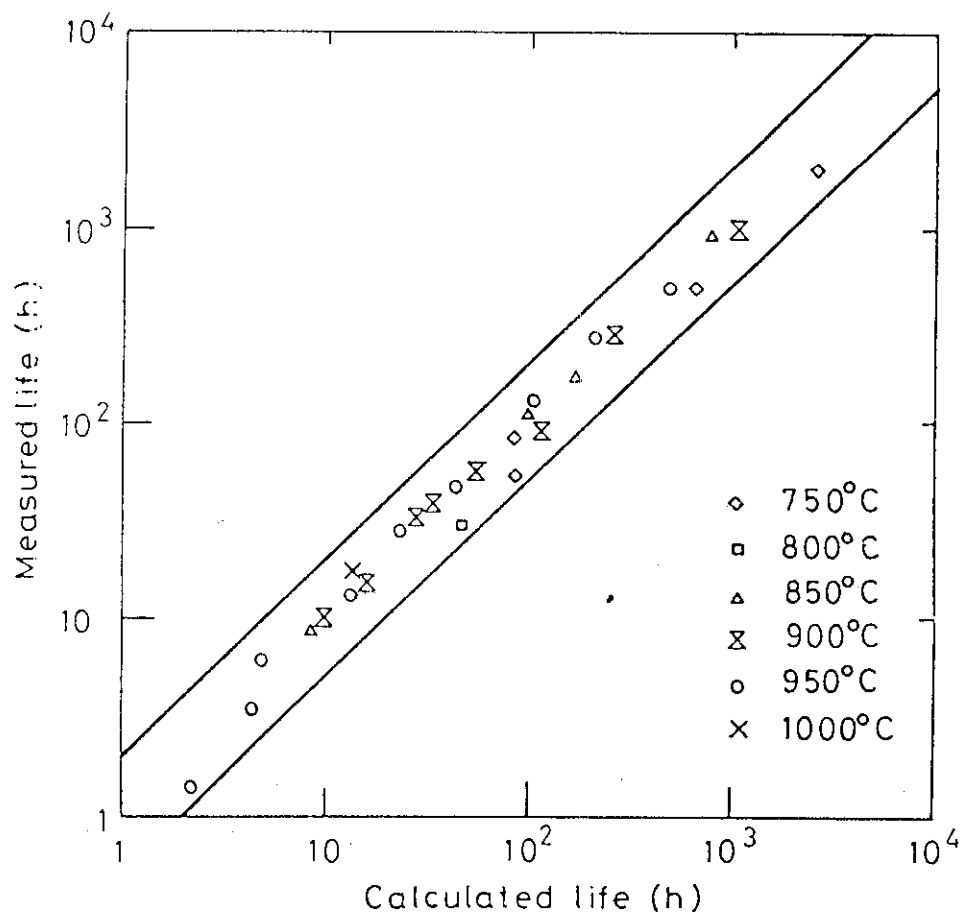
Fig.4.22 Comparison of Calculated and Experimental Rupture Time of
SRR99 using Physical Model.

38

EXPERIMENTAL

5.0 EXPERIMENTAL

Specimens were made from forged test bars of 25 mm square section corresponding to a commercial grade of steel (ASTM A213 T22). The chemical composition of the steel along with the permisible range as per specification are given in Table 5.1

Table 5.1
Chemical Composition of Steel and its ASTM Specification

Steel	Element wt%						
	C	Mn	Si	Cr	Mo	S	P
Present steel	0.14	0.46	0.28	2.33	0.98	0.010	0.030
ASTM Spec. A213 T22	0.15 max.	0.30- 0.60	0.50 max.	1.90- 2.60	0.87- 1.13	0.05 max.	0.03 max.

Creep tests were conducted on this steel to study the effect of initial microstructures on its creep behaviour and to identify the dominant mechanisms of creep deformation.

5.1 Microstructures

Three different microstructures have been considered in this study. These are (a) dispersion of ferritic grains in tempered bainitic matrix; (b) fully tempered bainite and (c) dispersed carbides in ferritic matrix. These microstructures are presented in the Chapter on "Results and Discussion".

5.2 Heat Treatments

The microstructures as described above were developed on the test bars by selecting the following heat-treatment cycles.

39

a)   Normalizing at 920°C for 1 hour followed by tempering at 730°C for 3 hours.

b)   Normalising at 990°C for 1 hour, followed by forced air cooling and tempering at 730°C for 3 hours.

c)   Normalizing and tempering cycles as in (b) followed by further ageing at 650°C for 190 hours.

5.3   Creep and Rupture Tests

Constant load creep tests were performed in air on specimens having above microstructures in Mayes creep testing machines at different temperatures.   The specimens for creep tests were made from the heat-treated bars.   In order to measure creep strain till rupture it was necessary to modify standard test specimen.   A schematic diagram of the modified specimen used for creep tests is shown in Fig.5.31.   The initial stress levels at each of the temperatures in the range of 500°C to 600°C were so selected as to obtain rupture within a reasonable span of time.   During the entire span of creep tests the temperatures were maintained within +/- 2°C.   The creep strain was monitored till rupture using LVDT gauge with an accuracy of +/- 0.001%.   Creep tests were also performed on the thermally aged and pre-strained specimens to establish whether strain or time softening is the more dominant mechanism of deformation.
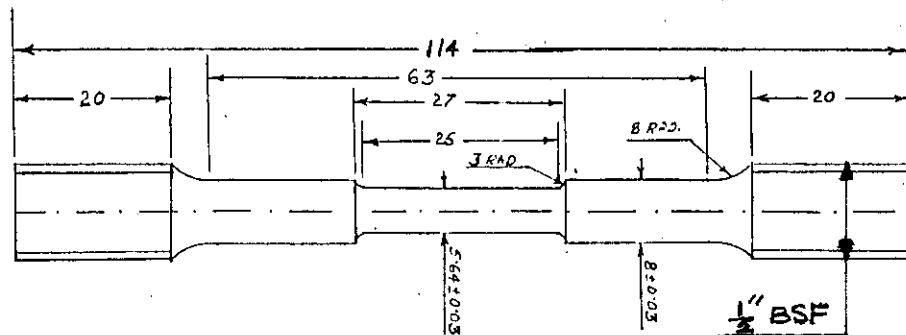
All dimensions are in mm

Fig.5.31   Schematic Diagram of Modified Specimen used for Creep Tests

RESULTS AND DISCUSSION

6.0 RESULTS AND DISCUSSION

Creep and stress rupture data on 2.25Cr-1Mo steel collected from published literature as well as those obtained from the experiments conducted in this work were analysed. The analysis revealed that even though different time temperature parameters were used to predict long term rupture strength from short term data, there is only a marginal difference in their predictive power. Therefore, the designers who often use the simplest of these viz. Larson-Miller Parameter are quite justified.

Rupture data collected from different sources for the same grade of steel (ASTM A213 T22) showed significant difference in their stress rupture properties. A detailed analysis was undertaken to identify the factors responsible for such scatter. Experiments were also conducted to show that the extent of these scatter could be associated with the variations in microstructures.

Rupture ductility data have also been analysed using the methods currently available. Although on the basis of empirical formulation it is possible to predict long term ductility from short term data, this approach cannot be extensively used because it does not take into account the nature of rupture. In this context the problem of reliable ductility prediction has been studied.

Experimental creep strain-time plots under different test conditions were analysed to identify the dominant mechanism of creep. The material constants describing the nature of creep curves were extracted from a fairly large database. These were subsequently used to predict creep behaviour under arbitrary stress temperature conditions.

The details of the above aspects have been presented in this Chapter.

6.1 Parameter Effectiveness

The predictive power of various time-temperature parameters viz. Larson-Miller, Sherby-Dorn and Manson-Haferd Parameters for estimating long term properties from stress rupture data is often judged by the following parameter (S) representing average sum square error between experimental (t_{exp}) and predicted (t_{pred}) rupture times;

$$S = (1/n) \ \Sigma(t_{exp} - t_{pred})^2 \qquad (6.11)$$

where n is the number of tests.

Data reported by NRIM on one particular cast of 2.25Cr-1Mo steel[44] have been used to compare their effectiveness. The chemical composition and manufacturing details of this steel are given in Tables 6.1 and 6.2 respectively.

Using the above parametric methods the rupture data were analysed. A 3rd order polynomial was chosen to represent the master rupture plot as selection of higher order polynomials did not show any marked improvement in predictive power. The master rupture plots along with the best fit curves are shown in Figs.6.11 - 6.13. The material constants thus obtained were used to estimate long term rupture strength viz. 30,000 hr and 100,000 hr over a range of temperatures $(500°C-575°C)$. The results are given in Tables 6.3 and 6.4 respectively. The master rupture plots indicate that the extent of scatter in rupture data is similar irrespective of the parameter used. Comparison of sum square error(S) given in the Table 6.3 indicates only a nominal difference between Manson-Haferd and Larson-Miller Parameters although it is the lowest for the former. The error, however, is rather high in the case of Sherby-Dorn Parameter. It has already been shown in the Chapter on "Creep Rupture Strength Prediction Models" that origin of this parameter is based on the assumption that activation energy is independent of stress and temperature. The fact that use of SDP is not giving as accurate prediction as with the other two parameters clearly

42

indicates that activation energy is indeed a function of temperature and stress. In other words the mechanism of creep deformation changes with the test condition.

The results also indicate that the difference in the estimated and experimental rupture times are insignificant particularly in the light of the level of accuracy expected in reporting rupture strength of engineering materials. The use of Larson-Miller Parameter, simplest of all time- temperature functions by most designers is thus well justified.

In the above analysis the optimum value of Larson-Miller constant C was obtained by the method of least squares. However, the designers often use 20 as the value of C, for the estimation of long term rupture strength for similar grades of steel. The values of 30,000 hr and 100,000 hr rupture strength with C as 20 were also estimated using the same set of rupture data. A comparison of the predictions obtained with C as 20 with those with optimum C for 30,000 hr and 100,000 hr rupture strength are given in Tables 6.3 and 6.4 respectively. A comparison of the sum square error(S) in these two cases shows only a nominal difference. Long term rupture strengths estimated by these methods are, therefore, nearly equal. Besides, the nature of master rupture plot with C as 20 (Fig.6.14) is similar to those obtained with the optimum value of C (Fig.6.11). Therefore, in subsequent analysis Larson-Miller Parameter with C as 20 only has been used. This has an additional advantage as it facilitates easy graphical comparison of the extent of scatter in stress rupture data, since the time-temperature functions represented along the X-axis are identical.

6.2 Influence of Microstructure

The mechanical behaviour of steel is a strong function of its microstructure. The creep rupture strength cannot, therefore, be an exception. In order to evaluate the influence of microstructure on stress rupture behaviour of 2.25Cr-1Mo steel specimens were prepared from the forged test bars of 25 mm square section collected from a

single cast but having undergone different heat-treatment cycles of normalising and tempering. Even though such steels are cooled in air as in a normalising heat-treatment, because of the presence of alloying elements ferrite-bainite structure develops in these steels. Subsequent tempering at 730°C for 3 hours ensures structural stability during service. A representative microstructure (type A) consisting of dispersed ferritic grains in tempered bainitic matrix is shown in Table 6.5. Creep and stress rupture tests were performed on a set of specimens having such a microstructure.

The second set of specimens was prepared from the same forged test bar after normalising at 990°C for 1 hour, followed by forced air cooling. This develops a fully bainitic structure which was subsequently tempered at 730°C for 3 hours to impart microstructural stability. A representative microstructure (type B) of such a specimen is shown in Table 6.5.

The third set of specimens was prepared from the normalized and tempered bars as in the second set with an additional thermal ageing treatment at 650°C for 190 hours. Such a heat-treatment is expected to produce a relatively coarse dispersion of carbide in the prior bainitic regions. A representative microstructure (type C) of such a specimen is shown in Table 6.5. A summary of various heat treatment procedures used to develop three different microstructures are also given in Table 6.5.

Creep tests in air were performed on each of the above sets of specimen over a range of stress and temperature to generate creep and stress rupture data under the above microstructural conditions. The rupture data so obtained have subsequently been analysed using Larson-Miller Parameter with C as 20. The respective stress rupture data along with the best fit curve under different microstructural conditions are presented in Fig.6.21. The results clearly reveal that the extent of scatter in the master rupture plot for the steel having the same initial microstructure is very small. However, a large variation in the stress rupture properties could be obtained by altering the microstructure.

Long term rupture strength under different microstructural conditions of this steel have been estimated in the temperature range of 500°C to 575°C. The 30,000 hour and 100,000 hour rupture strengths are given in Tables 6.6 and 6.7 respectively. The results clearly reveal that 100% tempered bainitic structure (Type B) gives the maximum rupture strength with the lowest rupture ductility where as a dispersion of coarse carbides in a ferritic matrix (Type C) gives the minimum rupture strength but the highest ductility in the same steel. This loss of rupture strength is due to coarsening of carbides as a result of a prolonged thermal exposure. This shows that the steel is susceptible to time dependent structural softening. The percentage loss of rupture strength due to such softening has been estimated and the values are given in Tables 6.6 and 6.7. A uniform dispersion of ferrite-bainite structure (Type A) has been found to give an optimum combination of rupture strength and ductility. Therefore, steels having such microstructures are used in high temperature engineering components.

Having established that microstructural variation controls the long term rupture properties of Cr-Mo steel, it is worthwhile to examine its influence on the entire shape of creep strain-time plot. Typical creep strain time plots of this steel at 550°C and 150/170 MPa stress under different microstructural conditions discussed above are shown in Fig.6.22(a) and Fig.6.22(b) respectively. These plots clearly exhibit the dominance of tertiary creep behaviour under all microstructural conditions. However, the extent of tertiary creep is more in steel containing bainitic matrix in comparison to other microstructures. The creep strain-time plots at 600°C, and 80/100 MPa, shown in Fig.6.23(a) and Fig.6.23(b) respectively, also exhibit the similar features.

In short amongst the three different microstructures considered in the work bainitic structure offers maximum resistance to creep deformation, whereas ferrite-carbide structure has the least resistance to creep deformation.

The Microstructure that develops in a low alloy Cr-Mo steel is a function of its chemical composition, austenitic grain size and the cooling rate. Although now with the recent developments in modern steel making practice[135] it is possible to control the chemical composition within a much smaller band most specifications for creep resistant steels (e.g. ASTM A213 T22) allow a fairly wide range of variation in the compositions (Table 5.1). These variations in chemical composition could influence the type of microstructure that develops in the steel and consequently determine its stress rupture properties. Likewise even though most Cr-Mo steel products are cooled in air after hot working to develop a normalized microstructure, cooling rate would vary depending on the section size of the product. This too, therefore, is likely to control the microstructure of the final product and consequently affect the high temperature properties. It would, therefore, be interesting to examine the influence of section size and minor variations in chemical composition on the rupture strength of this steel.

6.3 Influence of Chemical Composition

Most specifications on Cr-Mo steel allow a minor variation in chemical composition. Allowable range of composition for ASTM A213 T22 grade is given in Table 5.1. In order to examine the influence of the variation in chemical composition on stress rupture properties, data on a set of steels[39] conforming to the same specification but having different compositions were collected from literature. While selecting the data care was taken to see that samples were made from steel products having identical section size and heat treatment cycle. This would ensure that if at all there is a variation in the initial microstructure of the specimens it would be solely due to the variation in their chemical composition.

Microstructure that develops in a steel could be predicted on the basis of its time-temperature-transformation diagram. A typical diagram for a 2.25Cr-1Mo[136] steel is given in Fig. 6.30(a). In most commercial applications these steels are used in either annealed or normalized and tempered condition. On account of low carbon content and

high amount of carbide forming elements present, formation of pearlite is suppressed. Under normal rate of cooling as encountered in practice a ferrite-bainite microstructure is expected. The amount of bainite may vary depending on cooling rate from 15 to 100%. Given the transformation diagram it is possible to estimate the percentage of bainite in a given steel product from its cooling rate. However, it is impossible to expect that such diagrams will be available for all possible range of chemical compositions given in the specifications. It is, therefore, necessary to use a simpler parameter which could give us an idea about the likely microstructure in a given steel product of this grade. Critical cooling rate which is just sufficient to avoid formation of proeutectoid ferrite in this steel could be one such parameter. This can be estimated from chemical composition using empirical relations given in literature[137-139]. The expression used in this case is as follows :

$$\log C_F = \Sigma \; b_j X_j - 1.931 \qquad\qquad (6.31)$$

where X_j denotes wt% alloying element and b_j = partial regression coefficient (1/wt%) for respective elements. Values of b_j for common alloying elements are given in Table 6.8. C_F represents cooling time from AC_3 to $500^{\circ}C$ measured along the cooling curve which is just sufficient to avoid formation of proeutectoid ferrite [Fig.6.30(b)]. The estimated values of time to suppress ferritic transformation for a range of steels are given in Table 6.9. This shows that a minor variation in the chemical composition could change the critical time at least by a factor of 2. It is evident from Fig.6.30(a) that such a change in the critical time could significantly alter distribution of bainite in the steel product from 15 to 100%. Therefore, it is expected that the stress rupture data for all the steels given in Table 6.9 should lie between the master rupture plot for 100% Bainite and Ferrite-Bainite structure obtained in the present work. Fig.6.31 shows that it is indeed so. Therefore, it may be concluded that the variation in the stress rupture behaviour of these steels due to minor variation in composition is primarily due to the variation in their respective initial microstructures.

47

6.4 Influence of Initial Section Size

Cooling rate of any steel product during normalizing heat treatment depends on its section size. While the rate of heat extraction is a function of the surface area, the amount of heat to be removed depends on its volume. Therefore, surface area to volume ratio could give an idea about the likely cooling rate for a selected steel product. In the case of steel tubes this is inversely proportional to its thickness. Therefore, it is likely to determine the microstructure in any steel product. Stress rupture data on samples collected from steel tubes of various section size with nominal composition conforming to ASTM A213 T22 grade were examined. Table 6.10 gives the chemical composition for a range of section thickness of these steels. It is nearly impossible to get stress rupture data on steels having exactly the same composition but having different product thickness. Therefore, in order to estimate the effect of compositional variation on microstructures, critical cooling rate to avoid formation of proeutectoid ferrite has also been estimated and reported in Table 6.10. It is seen that although the critical cooling rates vary within a factor of 2 variation in section size (thickness) is much more. Therefore, it is expected that the stress rupture properties will vary within a relatively wider range. Fig.6.41 gives the stress rupture data for the steels given in Table 6.10. Master rupture plots for 100% Bainite, Ferrite-Bainite and Ferrite-Carbide structure obtained in the present work were also superimposed on this figure. The results clearly reveal that the stress rupture data lie even below the master rupture plot for Ferrite-Bainite structure. It can, therefore, be concluded that in this case the range of microstructural variation is more than that solely due to variation in chemical composition. This clearly shows that product section size has a significant effect on the stress-rupture properties of Cr-Mo steel.

48

6.5 Rupture Ductility Prediction

Rupture ductility of Cr-Mo steels under different test conditions are reported in terms of percent elongation (EL) and percent reduction in area (RA). These are calculated from the change in gauge length and the change of cross sectional area at rupture. Like long term rupture strength prediction, several attempts have been made to predict long term rupture ductility. However, such predictions do not show satisfactory correlation with the actual result. For integrity assessment of high temperature engineering components, rupture ductility prediction is of considerable importance. Presence of localised defects and stress concentration often play critical roles during creep leading to rupture. In such situations growth of cracks and defects would be governed by the creep rupture ductility of the material[140]. Since in many cases it varies inversely with rupture strength, both the properties must be optimised for a given application.

Rupture ductility data reported by NRIM on two different casts of 2.25Cr-1Mo steel[44] were analysed based on Larson-Miller Parameter. Elongation and reduction in area when plotted against LMP, as shown in Figs.6.51-6.52 respectively, exhibit very high scatter without revealing any definite trend. In such a case rupture ductility prediction becomes a difficult assignment. The factor responsible for this is the extent of localised deformation or necking. Strain at which necking sets in, varies in an unpredictable manner with the test conditions. Besides, minor variation in chemical composition and cooling rate which determines microstructural features in a product form may also contribute to the extent of scatter.

% Elongation at rupture reported by Wolf[34] on 2.25Cr-1Mo steel having the same microstructure have also been analysed based on LMP. The results are shown in Fig.6.53. At a given temperature the data show a definite trend with a peak. The location of the peak shifts with increasing temperature to higher values of the parameter. The same set of data, when represented in the form of % Elongation vs. stress plot (Fig.6.54), a similar trend is obtained. However, in this case the

location of the peaks shifts to lower values of stress with increasing temperature. A close examination will reveal that the shape of the plots is a mirror image of the set given in Fig.6.53. This is primarily because LMP is inversely related to applied stress (vide Fig.6.53). Therefore, when % EL is plotted against LMP one obtains a plot as an inverse function of stress only. Consequently predictions made whether on the basis of Fig.6.53 or Fig.6.54 should indeed be identical. Besides, the ductility has been considered as a function of stress only. A representation of rupture ductility as a function of both stress and temperature on the other hand is likely to give a better prediction. Based on these observations an attempt has been made to develop a temperature modified stress parameter (P) for better ductility prediction; the form being $(\log \sigma + A/T)$, where A is a constant. Elongation (%El) has been expressed as

$$\%EL = f\ (P) = a_0 + a_1 P + a_2 P^2 \tag{6.51}$$

Substituting the expression of P in equation (6.51) and subsequent algebraic simplification one obtains the following equation

$$\%EL = C_1 + C_2 \log \sigma + C_3/T + C_4 (\log \sigma)^2 + C_5 (\log \sigma/T) + C_6 (1/T)^2 \tag{6.52}$$

where C_1, C_2, C_3, C_4, C_5 and C_6 are constants.

This represents %EL as a function of the independent variables $\log \sigma$ and $1/T$. The six constants can be estimated by least square analysis of a set of ($\log \sigma$, $1/T$, %EL) data using PLOT software. These can subsequently be used for rupture ductility prediction over a range of stress and temperature. Data reported by Wolf have been analysed using this approach. The estimated values have also been compared with the reported data in Fig.6.55. The results clearly indicate that the ductility prediction based on this approach is possible within +/- 20% of the actual value.

50

The same procedure was adopted for the analysis of rupture ductility data under three different microstructural conditions. The results shown in Figs.6.56(a-c) indicate a fairly good agreement between the predicted and the experimental results under all microstructural conditions. However, this approach has a limited applicability since it is empirical in nature and does not take into account the nature of creep rupture which depends on the test conditions.

The same rupture ductility data have also been analysed based on Goldhoff's as well as Viswanathan and Fardo's models[85,86]. Ductility prediction according to Goldhoff's model (equations 3.11 and 3.12) is based on the estimated values of rupture time and average elongation rates[85]. The former is estimated from the master rupture plot of stress vs Larson-Miller Parameter with constant C as 20 {Fig.6.57(a)} whereas the latter is obtained from Fig.6.57(b) where rupture stress is plotted against a temperature-strain rate function with the constant C as 25. To assist numerical evaluation in either cases a third degree polynomial function was used to represent the master plot and the coefficients were evaluated by method of least squares. For a given stress/temperature condition the time to rupture can be computed from the polynomial function representing the curve in Fig.6.57(a) where as the average elongation rate could similarly be estimated from the curve in Fig.6.57(b). Thus the rupture ductility is given by the product $(t_r \dot{E})$. Although prediction of average elongation rate and rupture time agree fairly well with the experimental values [Fig.6.57(c)], prediction of rupture ductility is not at all satisfactory [Fig.6.57(d)].

Analysis of rupture ductility data based on Viswanathan's model[86] assumes that average elongation rate $(\dot{E})$ is given by

$$\log (\dot{E}) = a_0 + a_1 \log (t_r) \qquad\qquad (6.53)$$

where tr is the rupture time in hours and a_0 and a_1 are constants which could be evaluated by least squares from experimental data. Fig.6.58(a) gives Elongation rate as a function of rupture time for a 2.25Cr-1Mo steel. Using this, elongation rate under any test condition can be

51

predicted from the time to rupture. Subsequently rupture ductility is obtained from the product (tr$\dot{\varepsilon}$). Fig.6.58(b) gives a comparison of the experimental and the predicted ductility data. This hardly shows a satisfactory trend. A relationship of the type given in eqn. 6.53 is based on the assumption that the specimen fails only at a fixed value of strain. Therefore, irrespective of the test conditions estimated rupture ductility has been found to be around 40% only. This estimate has been arrived at from the average line shown in Fig.6.58(a). If the same were estimated from a lower bound line given in the same figure estimated ductility is of the order of 20%. A similar calculation based on the upper bound gives 85% as the predicted average ductility. This shows that the prediction could vary widely depending on the exact location of the line between the two limits and therefore it is not at all satisfactory.

Localised deformation (necking) has a significant contribution to the total creep strain at rupture. Extent of this could vary with the test conditions. Cr-Mo steels are susceptible to embrittlement due to segregation of trace elements[141-143] like P, As, Sn etc. at grain boundary. Under such conditions it may fail at a very low strain without appreciable necking. Usually this takes place at certain intermediate values of the time temperature parameter. Existance of such a regime makes ductility prediction even more uncertain. This problem has been more critically examined in the following section.

6.6 Localized Deformation

Rupture ductility expressed in terms of percent elongation or reduction in area is composed of two distinct parts viz. uniform deformation and localised deformation. The extent of uniform deformation beyond which necking sets in may change with test conditions. In such a situation reliable prediction of rupture ductility becomes a difficult task. Hart[144] as well as Burke et.al.[145] analysed the conditions under which necking sets in during creep. Under Newtonian viscous flow, the stress exponent being unity no localized deformation is expected. Since most engineering materials

52

have significantly higher creep stress exponent(n), necking may set in quite early though for detectable level of necking typically a creep strain of about 5% to 10% may be necessary. Analysis of Burke et.al.[145] showed that the true creep strain (ε_n) at which necking first influences creep rate is given by :

$$\varepsilon_n = 2/(n-1) \qquad\qquad (6.60)$$

This indicates that with increasing stress exponent the critical strain for necking to set in decreases. In case of 2.25Cr-1Mo steel[40,41,146] where n in the high stress regime is reported to be around 12, necking sets in when ε_n in equation (6.60) is about 0.18 which is rather high. Therefore, a better analytical procedure for describing localised deformation during creep is required.

6.61 Rupture Ductility Diagram

Rupture ductility at a given stress and temperature is represented in terms of elongation (EL) and reduction in area (RA). These are estimated from the measured length (l) and cross-sectional area (A) of the specimen at rupture using the following equations :

$$EL = (l/l_o) - 1 \qquad\qquad (6.61a)$$
$$RA = 1 - A/A_o \qquad\qquad (6.61b)$$

where A_o, l_o represent the original cross-section and length of the specimen respectively.

Whilst the product $A_o l_o$ represents the initial volume of the test specimen, the product Al may have a totally different physical significance depending on the mechanism of creep deformation. This is evident from the schematic representation of the nature of creep deformation given in Fig.6.61(a). Under ideal Newtonian flow deformation is uniform all along the gauge length. This implies that the product Al would still represent the volume of the test piece.

53

Since deformation is not accompanied by any change in volume, the ratio $(A.1)/(A_o 1_o)$ will be unity.

On the other hand if such a deformation is accompanied by nucleation and growth of voids as is found in a number of high temperature materials, the product A.1 could exceed the original volume by the volume of cavities. In such a situation the ratio $(A.1)/(A_o 1_o)$ would be greater than unity.

Creep rupture is usually preceded by a localised deformation as shown in Fig.6.61(a). Since in this case, A denotes the cross section area of the specimen at the necked region, the product (A.1) would represent only a part of original volume $A_o 1_o$. Consequently the ratio $(A.1)/(A_o 1_o)$ would be less than unity. Indeed its magnitude could give an indication of the severity of necking. The ratio hereafter designated as k is a simple indicator of the nature of creep rupture. Magnitude of k will depend on the material as well as test condition. It is thus possible to derive the following relationship between reduction in area RA and elongation EL using equations (6.61a) and (6.61b)

$$RA = 1 - k/(1 + EL) \hspace{3cm} (6.61c)$$

Using this equation (6.61c) a rupture ductility diagram can be constructed by plotting RA against EL for different values of k {Fig.6.61(b)}. The curve corresponding to k = 1 represents ideal Newtonian deformation. This divides the diagram into two distinct regions dominated by varying degrees of either necking (k < 1) or cavitation (k > 1).

In order to assess the applicability of such a diagram in predicting the nature of creep rupture, ductility data on this steel reported by NRIM[44] have been superimposed. The results, shown in Fig.6.61(c), clearly indicate that the mechanism of rupture varies widely from the regime of cavitation to extensive necking with k approaching 0.1. Because of such a wide variation, rupture ductility

54

plots of Cr-Mo steels in terms of elongation (EL) and reduction in area (RA) as a function of LMP usually do not reveal any definite correlation. Since the mechanism of rupture is strongly dependent on test conditions, rupture ductility prediction for such steels is a difficult task.

In contrast the rupture ductility data on superalloys reported by NRIM[147] when plotted on the ductility diagram (Fig.6.61(d))lie within a narrow field on either side of the plot corresponding to Newtonian flow. This indicates that the failure in this alloy could be either due to only a limited amount of localised deformation or cavitation depending on the test parameter. Indeed cavitation has been reported to be the dominant mode of failure in this alloy and necking is not extensive[127].

In case of Zr-Nb alloy[148] rupture ductility data, shown in Fig.6.61(e), were found to lie in the necking regime extending from k = 0.9 to k = 0.4. Since the mechanism of rupture in case of superalloys and Zr-Nb alloys do not vary extensively with test conditions, rupture ductility plots for such materials in terms of either %EL or %RA vs LMP often exhibit a definite correlation.

Examination of the fractured surface of creep exposed specimen of 2.25Cr-1Mo steel under Scanning Electron Microscope (Fig.6.62) indicates predominantly intergranular fracture. The fact that k is around 0.94 would indicate that. This is a characteristic of most intergranular rupture where necking is not extensive. In contrast to this, Fig.6.63 shows that for lower value of k (= 0.23) the mechanism of creep rupture is predominantly transgranular, the necking or localised deformation being highly prominent.

The construction of ductility diagram is based on the assumption that both necking and cavitation may not take place simultaneously. In reality, however, both the mechanisms may be operative at values of k close to unity. Therefore, construction of diagram in this regime i.e. at values of k close to unity may require further refinement. In most

55

situations, however, rupture ductility data lie well within the regime of necking. As long as the nature of creep rupture defined in terms of k remains the same, reliable prediction of rupture ductility is possible. Such a diagram helps us in identifying conditions under which this is likely to be so and explains why in certain alloys the prediction of rupture ductility becomes difficult.

6.7 Dominant Mechanism of Creep Deformation

Unlike pure metals or stable single phase alloys, a Cr-Mo steel usually exhibits continuously increasing creep rate over most part of its life. A schematic representation of the creep curve of a pure metal as well as an experimentally obtained creep curve of 2.25Cr-1Mo steel at 550°C, 150 MPa having an initial microstructure, consisting of tempered bainite is shown in Fig.6.71. Microstructures of this steel before and after creep exposure are shown in Figs.6.72(a.b). These clearly indicate that the carbides in the steel coarsen significantly during creep. Softening due to coarsening of carbides may, therefore, appear to be responsible for the continuously increasing creep rate. However, in the case of superalloys in spite of particle coarsening, strain softening due to increased mobile dislocation density was identified as the dominant mechanism for tertiary creep[76,149,150]. Therefore, it was necessary to conduct experiments to study the effect of prior thermal exposure and pre-strain on the shape of its creep curve to establish whether time softening or strain softening is the dominant mechanism of creep deformation.

The influence of thermal exposure on the shape of creep curve of the steel having bainitic structure is shown in Fig.6.73. The rate of accumulation of creep strain after thermal exposure when the microstructure transforms to ferrite and carbide, is significantly higher. Influence of prestraining on the shape of the creep curve as well as its comparison with the former are shown in Figs.6.74 and 6.75 respectively. Besides, influence of pre-strain on the shape of creep curve of the thermally exposed steel having ferrite-carbide structure have also been studied and presented in Fig.6.76. Irrespective of

whether the initial structure of the steel is bainite or ferrite-carbide prior straining has been found to improve the reistance to creep deformation to some extent. There is certainly no contribution from pre-strain towards the overall softening effect observed in this steel. These observations clearly reveal that of the two, carbide coarsening has a greater influence in controlling the creep behaviour of this steel.

This concept has infact been effectively utilized in the development of newer grades of creep resistant steels. Increase of Cr content in steel beyond 2.25% was earlier known to have a harmful effect on its long term rupture strength[3]. This is primarily because carbides present in these coarsen rapidly. If these could be replaced by more stable forms of carbides having greater resistance to time dependent growth, creep properties are likely to improve significantly. Therefore Cr-Mo steels containing small amount of V/Nb have vastly improved rupture strength. Table 6.11 gives a comparison of the rupture strengths of a few grades of such steels[151-152]. This shows that the strength of 9Cr-Mo steel without Nb is lower than that of 2.25Cr-Mo steel particularly at higher temperature of $600^{\circ}C$ and above, whereas with Nb its strength becomes significantly higher. All these go to show that the time dependent particle coarsening determines the creep properties of Cr-Mo steel.

6.8 Mechanism Based Creep Strain Prediction

Having established time softening to be the dominant mechanism of tertiary creep in 2.25Cr-1Mo steel it is now possible to develop a model based approach for creep strain prediction. The creep behaviour of the steel could be represented by a set of coupled differential equations 4.27(b). This means a set of four material parameters viz. initial or minimum creep rate ($\overset{o}{\varepsilon}_i$); parameters 'a' and 'b' representing the extent of time softening and stress exponent (n), are required to characterize the complete shape of a creep curve. While standard methods for estimation of the parameters $\overset{o}{\varepsilon}_i$ and n are available in the literature there is no mention as to how 'a' and 'b' could be estimated. A new

method was therefore developed to estimate these parameters directly from creep curves.

6.81 Estimation of Model Parameters

The time dependent damage accumulation on the basis of equation set 4.27(b) can be estimated from the creep curve by the following expression

$$\omega_1 = \{ (\overset{o}{\varepsilon}/\overset{o}{\varepsilon}_i)^{1/n} \exp(-\varepsilon) \} - 1 \qquad (6.81)$$

The values thus obtained can be further numerically differentiated to generate $\overset{o}{\omega}_1{}^{1/4}$ vs ω_1 plot. A linear relation would indicate that the time softening model is applicable and the parameters a, b representing the extent of softening are estimated from the intercept and the slope. Having estimated the parameters, it is now possible to generate creep strain-time plot by numerical solution of the three coupled differential equations given in equation set 4.27(b). A computer programme has been developed using standard numerical methods, to analyse creep curves of materials whose behaviour is described by the particle coarsening model. The important steps describing the algorithm of this program are given in Annexure-IV. Fig.6.81 presents a set of creep curves having different predetermined set of model parameters (a,b) given in Table 6.12. Values estimated by the programme described above have also been included in Table 6.12. The close match is a clear indication that the method developed can indeed estimate the material parameters (a,b). This, therefore, opens up a possibility of transforming creep curves into a database of model parameters from which predictions could be made for arbitrary loading conditions.

6.82 Analysis of Creep Curves

Creep curves of 2.25Cr-1Mo steel over a range of stress/temperatures[34] were analysed using this method. Each individual creep curves were converted into strain rate vs strain plot

and the initial creep rate was estimated. Subsequently its stress temperature dependence was established (Fig.6.83). It was found to be given by

$$\overset{o}{\varepsilon}_{1} = \overset{o}{\varepsilon}_{oi} \ \sigma^{n} \ \exp \ (-Q/RT) \qquad\qquad (6.82a)$$

where $\overset{o}{\varepsilon}_{oi}$ is a reference creep rate, n stress exponent, Q activation energy. The constants ($\overset{o}{\varepsilon}_{oi}$, n, Q) were estimated using the data plotted in Fig.6.83 by multiple regression analysis. These are reported in Table 6.13. As in Fig.6.82 $\overset{o}{\omega}_{1}^{1/4}$ vs ω_{1} plots were obtained for a set of stress/temperature. Linear nature of the plot indicates that those creep curves could be described by time softening model. Parameters a & b were obtained from the intercept and slope of this plot.

In order to establish stress-temperature dependence of the parameters controlling the extent of time softening it is necessary to look into their physical significance. This has been examined by Dyson and McLean[76]. Using Lifshitz-Slyozov description of particle coarsening[153] it has been shown that a and b are given by

$$a = (K\sigma_{oi}^{4})/\{3B^{3}(\sigma - \sigma_{oi})\} \qquad\qquad (6.82b)$$
$$b = (\sigma - \sigma_{oi})/\sigma_{oi} \qquad\qquad (6.82c)$$

where B is a constant relating threshold stress (σ_{o}) to inter-particle spacing (d) and K is the rate constant for particle coarsening having following relations with current particle spacing (d) and initial spacing (d_{o})

$$\sigma_{o} = B/d \qquad\qquad (6.83a)$$

$$d^{3} = d_{o}^{3} + Kt \qquad\qquad (6.83b)$$

Algebraic simplification of equations (6.82b,c) and (6.83a) gives the following relation for the product of the parameters a and b

$$ab = K/3d_{o}^{3} \qquad\qquad (6.84)$$

59

Since σ_{oi} which represents the initial value of the threshold stress (σ_o) is given by (B/d_o) where d_o is the initial average interparticle spacing. This could be estimated from the plot b vs σ (Fig.6.84). From the nature of the expression for b, it is apparent that the plots at different temperatures would intersect at b = -1. The slopes of the plots at different temperatures is a measure of the initial threshold stress σ_{oi} which has been found to follow the following relation

$$\sigma_{oi} = C \exp (-Q_2/RT) \qquad (6.82)$$

where C and Q_2 are constants. The estimated values of initial threshold stress (σ_{oi}) at different temperatures were obtained using the data plotted in Fig.6.84. These were subsequently analysed to estimate the constants C and Q_2. The estimated constants, thus obtained, are reported in Table 13. Figure 6.86 which gives a plot of log σ_{oi} vs 1/T indicates that such a representation is indeed applicable.

The linear nature of the plot log (ab) vs log σ at different temperatures in Fig.6.85 indicate that K should have the following stress and temperature dependence

$$K = K_o\sigma^m\exp(-Q_1/RT) \qquad (6.85)$$

where m and K_o are constants and Q_1 is the activation energy for stress induced particle coarsening. The constants ($K_o/3d_o^3$, m, Q_1) can thus be obtained using the data plotted in Fig.6.85 by multiple linear regression analysis. It is possible to estimate K_o from the average initial interparticle spacing (d_o) since it is inversely related to the initial threshold stress (σ_{oi}). The estimated values of these constants (K_o, m, Q_1), thus obtained, are reported in Table 6.13.

Askins et.al.[154] have monitored by interrupted creep testing at different stresses and temperatures, carbide particle coarsening that takes place in 1Cr-0.5Mo steel. It has been suggested that the parameter K representing the kinetics of carbide coarsening can be described by

$$K = K_o \exp(pT) \qquad\qquad (6.86)$$

where K_o and p being reported as constants. Apparently no effect of stress on coarsening has been reported. Table 6.14 gives a comparison of the magnitude of K reported by Askins et.al. and those estimated from the analysis of the creep curves as described in this work. The two estimates are quite close keeping in view the wide scatter that is normally associated with size and distribution of carbides in Cr-Mo steel.

Estimation of microstructural parameters determining creep of Cr-Mo steel has been the major limitation for the use of particle coarsening model in the life assessment of high temperature components. Conventional approaches as that adopted by Askin et.al[154] would involve large volumes of experiments involving interrupted creep tests. Present analysis provides an alternative approach which relates the kinetics of particle growth to directly measurable engineering parameters such as creep strain. Thus it permits use of appropriate physics based model for describing creep of Cr-Mo steel. A part of this work has recently been published[155].

Having estimated the eight material constants reported in Table 6.13 it is now possible to predict creep behaviour of 2.25Cr-1Mo steel based on carbide coarsening model at any arbitrary stress/temperature conditions.

6.9 Creep Strain Prediction

Creep curves of this steel have been predicted over a range of stress and temperature using the material constants given in Table 6.13. These have been compared with the experimental plots available in literature, as well as those obtained in this work.

Creep curve predictions at $500^{\circ}C$ have been compared with the experimental results reported by Wolf[34] in Figs.6.91(a,b). These

reveal that although the nature of the predicted plots is very similar to the experimental plots magnitude of predicted strain compare fairly well with experimental values only up to 5% strain.

Comparison of theoretical predictions with experimental plots at 550°C {Fig.6.92(a)} and 600°C {Figs.6.93(a,b)} over a wide range of stress also revealed similar trend. The shape of the creep curves have been modelled in terms of four material parameters. Keeping in view that these are estimated from their stress-temperature dependence given in Figs.6.83-6.86 and the extent of scatter which is associated with creep curves, predictions are fairly satisfactory.

The above comparison has been made with the set of strain-time plots from which the material database has been extracted. Therefore, one may argue that it is not surprising that the predictions should be satisfactory. Fig.6.92(b) presents a theoretical creep curve for a specific test condition. Experimental data from a different source[18] have been superimposed on the same for comparison. The experimental values are indeed very close to the theoretical predictions. Satisfactory prediction in this situation is certainly of greater significance. Figs.6.94(a,b) and Figs.6.95(a,b) present typical comparison of theoretical creep curves with the set of experimental plots at 550°C and 600°C respectively obtained under different microstructural conditions. Here as well the predictions are found to be satisfactory. All these conclusively demonstrate that like superalloy, model based creep strain prediction is possible even in case of Cr-Mo steels.

A broader comparison between the measured and predicted time to achieve 5% strain, as shown in Fig.6.96(a), indicates that the agreement is quite satisfactory within the scatter of creep data. However, when the comparison was made for the predicted values of time to achieve 10% strain, as shown in Fig.6.96(b), it was found that the predicted time is longer than the actual time. Onset of localised deformation or necking could be responsible for this deviation. This has not been taken into consideration in this creep strain prediction model. Calculation of

uniform strain from measurement of diameter of the uniformly deformed region of a rupture sample indicate that the necking begins in this steel beyond a strain of 5%. As far as design applications are concerned necking means unstable deformation. Therefore, prediction of strain beyond necking may not be of great relevance.

CONCLUSIONS

7.0 CONCLUSIONS

1. Effectiveness of Larson-Miller and Manson-Haferd time-temperature parameters in predicting rupture properties of Cr-Mo steels are nearly identical.

2. Relatively low predictive power of Sherby-Dorn parameter is an indication of changing creep mechanism with test conditions.

3. Prediction of long term rupture strength using Larson-Miller constant as 20 compares fairly well with those predicted with the optimum value of the constant.

4. Stress rupture property is a strong function of the initial microstructure of steel. Bainitic structure has the highest rupture strength, ferrite-carbide structure has the lowest rupture strength, whereas ferrite-bainite structure has the optimum combination of rupture strength and ductility.

5. Minor variations in chemical composition within permissible range of specifications significantly alter initial microstructure and, therefore, affect stress rupture properties.

6. Varying thickness of steel products determines the cooling rate through the critical range of transformation and therefore controls initial microstructure before creep test. Consequently this too, affects stress rupture properties.

7. Ductility prediction using Larson-Miller type parameter attempts to relate it with applied stress only. Therefore, it cannot predict rupture ductility over a wide range of temperatures.

8. Fairly accurate rupture ductility predictions could be made using a stress-temperature parameter under all microstructural conditions.

9. More precise ductility prediction is possible within a narrow range of a geometrical factor k determining the nature of the rupture.

10. Coarsening of carbides is the most dominant mechanism of creep deformation in Cr-Mo steel. A mechanism based creep strain prediction model has been developed for Cr-Mo steel. This can predict fairly well creep strain up to 5% under different stress temperature conditions.

11. Parameters determining kinetics of carbide coarsening can be extracted from an analysis of the creep curve.

12. Kinetics of particle coarsening depends on applied stress. The present work has helped establish a definite functional relationship.

REFERENCES

REFERENCES

1. J.D. Baird and A. Jamieson, JISI, Vol.210, (1972), p.847

2. A. Krisch, Jernkontorets Ann, Vol.155, (1971), p.323-331

3. G.V. Smith, Properties of Metals at Elevated Temperatures, McGraw-Hills, (1950), p.231

4. J.D. Baird, Jernkontorets Ann, Vol.151, (1971), p.311-321

5. M.K. Booker and others, Analysis of elevated-temperature tensile and creep properties of normalised and tempered 2.25Cr-1Mo steel, Oak Ridge National Laboratory, Advanced Materials for Pressure Vessel Service with Hydrogen at High Temperature and Pressures (Proc. Conf.), ASME, Orlando, Fla; (1982), P.273-286.

6. R.L. Klueh, Creep-Rupture strength of annealed 2.25Cr-1Mo steel, Scripta Metall, 19(7), (1985) P.789-793

7. Y. Nishizaka and others, Changes in microstructures and mechanical properties of Cr-Mo reactor vessel steels during long term service, J. Pressure Vessel Technology, Trans.ASME, 107(3), (1985), P.285-294

8. N.G. Needham and T. Gladman, Intergranular Creep Cavitation in 2.25Cr-1Mo Steels, Advances in Physical Metallurgy and Applications of Steel (Proc. Conf.), The Metals Society, England, (1981), P.309-317

9. J.A. Todd and D.W. Chung, Development of 2.25Cr-1Mo steel for coal conversion vessels, Special Steels and Hard Materials (Proc. Conf.), South Africa, (1982), P.207-212

10. T. Wada, Changes in microstructures and tensile strength of Cr-Mo steels after long-term service exposure. Unusual Techniques and New applications of Metallography, (Proc.Conf.), Vol.4, ASM, USA, (1982)

11. A.M. Abdel-Latif and others, Effects of microstructural degradation on creep life prediction of 2.25Cr-1Mo steel, Advances in Fracture Research (Fracture 81), (Proc.Conf.), Vol.4, France, (1981), p.1613-1620.

12. R.L. Klueh and J.L. Grifith, Mechanical Properties of tube sheet forging, J. Mater. Energ. Syst, 3(3), (1981) p.26-38.

13. R.L. Klueh, Creep of decarburised and aged 2.25Cr-1Mo steel, J. Nucl. Mater, 96(1-2), (1981), P.205-207

14. P.R. Taylor and R.F. Johnson, Analysis of long term creep rupture and elevated temperature yield or proof stress data, JISI, (Sept, 1971), P.714

15. M.K. Booker and others, Mechanical Property Correlation for 2.25Cr-1Mo Steel in Support of Nuclear Reactor System Design, Int. J. Pressure Vesssels Piping, Vol.5, (1977)

16. A. Plumtree and G. Shen, Prediction of Long-term Creep and Rupture Life, ISIJ International, Vol.30, No.10, (1990), p.812-816

17. R. Viswanathan, Strength and Ductility of 2.25Cr-1Mo Steels in Creep at Elevated Temperatures, Metals Technology, (June,1974), p.284-294

18. K. Maruyama, H. Kushima and T. Watanabe, Prediction of Long Term Creep Curve and Rupture Life of 2.25Cr-1Mo stel, ISIJ International, Vol.30, No.10, (1990), p.817-822

19. M. Nakashiro, S. Kihara, F. Kishimoto and T. Fujimore, Evaluation of Long-term Creep Strength of 2.25Cr-1Mo Heat Transfer Tube in Actual Service Stress Level Range, ISIJ International, Vol.30, No.10, (1990), p.823-828

20. D. Lonsdale and P.E.J. Flewitt, Effect of small changes in impurity element content on creep life of 2.25Cr-1Mo steel, Mater. Sci. Eng, 41(1), (1979), p.127-136

21. A. Plumtree and J.Y. Guinemar, Prediction of boiler tube life before and after service exposure, Advances in Life Prediction Methods (Proc. Conf.), ASME, New York, (1983), p.357-361.

22. R.A. Selva, Life Assessment of boilers operating in creep conditions, chart. Mech. Eng., 31(3), (1984), p.42-46.

23. K.R. Williams, Creep life prediction of microsturcturally unstable ferritic steels. Advances in Life Prediction Methods (Proc. Conf.), ASME, New York, (1983), p.363-375.

24. Data sheets on the elevated temperature properties of 2.25Cr-1Mo steel for boiler and heat exchanger seamless tubes, NRIM Creep Data Sheets, No.3B, (1986)

25. T. Iwadate and others, Prediction of remaining life of high temperature/pressure reactors made of Cr-Mo steels, J. Pressure Vessel Technology, Vol.107(3), (1985), p.230-238.

26. M. Kitagawa and others, Damage assessment of 2.25Cr-1Mo heavy section component in fossil-fired power plant (in Japanese), Ishikawajima-Harima Eng.Rev., 28(5), (1988), p.299-305

27. L.A. James and K.W. Carlson, Prediction of creep deformation and failure for 0.5Cr-0.5Mo-0.25V and 2.25Cr-1Mo steels, J. Pressure Vessel Technology (Trans ASME), Vol.107(3), (1985), p.279-284

28. R.L. Klueh and R.W. Swindeman, Microstructure and mechanical properties of a modified 2.25Cr-1Mo steel, Metall. Trans.A, 17A(6), (1986), p.1027-1034.

29. I. Kozasu and others, Alloy modifications in 2.25Cr-1Mo and 3Cr-1Mo steels for high temperature and high pressure hydrogen service, Research on Chrome-Moly Steels (Proc.Conf), ASME, (1984), p.53-75

30. C. Leymonie, Residual life of components in Cr-Mo and Cr-Mo-V steels after maintenance for long periods at high temperature (in French), Mem. Elud. Sci. Metall, 83(1), (1986), p.5-14

31. Data sheets on the elevated temperature properties of quenched and tempered 2.25Cr-1Mo steel plates for pressure vessels, NRIM Creep Data Sheets, 36A, (1991)

32. J.D. Parker, Prediction of the service behaviour of 2.25Cr-1Mo steel components in electricity generating plant, Strength of Metals and Alloys (Proc. Conf.), Montreal, (1985), p.749-754

33. V.M. Radhakrishnan, Relationship between minimum creep rate and rupture time in Cr-Mo steels, J. Mater Eng. Perform, 1(1), 1992, p.123-128.

34. H. Wolf, Kriechen Der Legierungen NiCr22Co12Mo und 10CrMo910 bei Konstanter und Zyklischer Beanspruchung, D. Ing. Thesis, Erlangen University, Erlangen, (1990)

35. K. Laha, K. Bhanu Sankara Rao and S.L. Mannan, Creep Behaviour of Post-weld Heat-treated 2.25Cr-1Mo Ferritic Steel, Base Weld Metal and Weldments, Mater.Sci. Engr. A129, (1990), p.183-185

36. M.C. Murphy and G.D. Branch, Metallurgical Changes in 2.25Cr-1Mo Steels during Creep-rupture Test, JISI, 209, (1971), p.546-561

37. Data Sheets on the elevated temperature properties of quenched and tempered 2.25Cr-1Mo steel plates for pressure vessels, NRIM Creep Data Sheet No.36, (1985)

38. Data Sheets on the elevated temperature properties of normalised and tempered 2.25Cr-1Mo steel plates for pressure vessels, NRIM Creep Data Sheet No.11A, (1980)

39. BSCC High Temperature Data, The Iron and Steel Institute, London, (1972-73)

40. S. Chaudhuri, N. Roy and R.N. Ghosh, Influence of Microstructures on Creep Behaviour of 2.25Cr-1Mo steel. NML Report No.11420131, (October, 1990)

41. S. Chaudhuri, R. Singh and R.N. Ghosh, Stress Rupture Properties of Indigenously Produced 2.25Cr-1Mo Steel, NML Report No.1205, (September, 1985)

42. G.V. Smith, Elevated Temperature Strength and Ductility of quenched and tempered 2.25Cr-1Mo steel, in Current Evaluation of 2.25Cr-1Mo steel in Pressure Vessels and Piping, ASME, (1972)

43. Elevated Temperature Properties of Ferritic Steels, Metals Handbook, Vol.1, 10th edition, (1990), p.617

44. Data sheets on the elevated temperature properties 2.25Cr-1Mo steel, for boiler and Heat exchanger Seamless tubes, NRIM Creep Data Sheets, No.3A, (1976)

45. R.G. Baker and J. Nutting, The Tempering of 2.25Cr-1Mo steel after quenching and normalising, JISI, (July,1959) p.257-269

46. N. Gope and others, Influence of Long Term Aging at 520°C and 550°C and the superimposed creep stress on the microstructure of 1.25Cr-0.5Mo steels, Metall. Trans A, 23A(1), (1992), p.221-235

47. I. Masumoto and others, Electron microscopic examination of a service embrittled 2.25Cr-1Mo steel, Trans.Jpn.Weld Soc, 17(2), (1986), p.138-144

48. B.J. Shaw, Study of carbides formed in low alloy chromium-molybdenum steels, Met. Prop. Counc. MPC, 21, (1984), p.117-128

49. R.A. Stevens and D. Lonsdale, Isolation, identification and quantification by X-ray diffraction of carbide phases in a 2.25Cr-1Mo steel, J. Mater. Sci., 20(10), (1985), p.3631-3638

50. T. Utsunomiya and others, The transformation and carbide precipitation of 2Cr and 9Cr steel (in Japanese) Tetsu to Hagane, 73(11), (1987), p.1582-1589

51 M. Dirand and L. Afquir, Crystal structure of carbide precipitates in low alloy steels at different tempering stages (in French), Acta. Metall, 31(7), (1983), p.1089-1107

52. R.L. Klueh, Heat-treatment of 2.25Cr-1Mo steel for brceder reactor steam generators, Nucl. Technology 57(1), (1982), p.114-124

53. R. Peiri and others, Influence of alloying elements on the transformation and precipitation processes during cooling of creep resistant tube steels after austenitising. I – chromium – Molybdenum steels (in German), Arch. Eisenhuttenwes, 51(8), (1980), p.355-360

54. T. Wada and G.T. Eldis, Transformation characteristics of 2.25Cr-1Mo steel, Application of 2.25Cr-1Mo steel for thick-wall pressure vessels (Proc. conf), ASTM, Denver, (1980), p.343-362

55. G.P. Wazadlo and others, Decarburization and thermal ageing – their effect upon 2.25Cr-1Mo steel mechanical properties, Second International Conference on Liquid Metal Technology (Proc. Conf.) (1980)

56. K.J. Kurzydlowski and W. Zielinski, M_2C-M_6C carbide transformation in low alloy Cr-Mo ferritic steels, Met. Sci, 18(4) (1984), p.223-224

57. A.B. Muhammad and others, Effects of types of carbides on temper embrittlement in commercial 2.25Cr-1Mo steel, Advances in Physical Metallurgy and Applications of Stels (Proc. Conf.), The Metals Society, England, (1981), p.340-368

58. A.M. Abdel-Latif, J.M. Corbett and D.M.R. Taplin, Analysis of carbides formed during accelerated ageing of 2.25Cr-1Mo steel, Metal science, Vol.16, (February, 1982), p.90-96

59. G.S. Sangdahl and M. Semchyshen, Ed., Application of 2.25Cr-1Mo steel for Thick-Wall Pressure Vessels, STP755, ASTM, (1982)

60. British Standard : 1113, (1969)

61. ASME Boiler and Pressure Vessel Code, Section I, ASME, New York

62. G.V. Smith, Ed. Supplemental Report on the Elevated Temperature Properties of Chromium Molybdenum Steels, Metal Properties Council, ASTM Data Series,DS 6S1, ASTM, (1971)

63. J.B. Conway, Stress Rupture Parameters; Origin, Calculation on Use, Gordon and Beach, New York, (1968)

64. S.S. Manson and C.R. Ensign, A quarter Century of Progress in the development of correlation and extrapolation methods for creep rupture data, ASME, J. Engg. Mat. Technology, Vol.101, (1979), p.315-325

65. F.R. Larson and J. Miller, Trans, ASME, Vol.74, (1952), p.765

66. R.L. Orr, O.D. Sherby and J.E. Dorn, Correlation of rupture data for metals at elevated temperature, Trans. ASM, Vol.46, (1954), p.113

67. S.S. Manson and A.N. Haferd, A Linear time-temperature relation for extrapolation of creep and stress rupture data, NASA TN 2890, (March, 1952)

68. E.N. La and C. Andrade, Proc. Royal Soc (London), Vol.A84, (1910), p.1

69. P.G. McVetty, Mech. Engg, Vol.56, (1934), p.49

70. R.W. Evans, J.D. Parker and B. Wilshire, An extrapolative procedure for long term creep strain and creep life prediction, Recent advances in creep and fracture of engineering materials and structures, Pineridge Press, (1982), p.135-184

71. M.R. Winstone, Modelling creep behaviour of single crystals, Symposium Proc. on single crystals for turbine blades, (June, 1988), MTU/SMCT Muchen.

72. C.E. Pugh, Constitutive Equations for Creep Analysis of Liquid Moderated Fast Breeder Reactor (LMFBR) components, in S.Y. Zamrik and R.I. Jetters, editors, Advances in Design for Elevated Temperature Environment, ASME, New York, (1975), p.1-16

73. F.K.G. Odquist, Mathematical Theory of creep and creep rupture, Carendon Press, Oxford, England, (1974)

74. B.F. Dyson and M. McLean, ISIJ International, Vol.30, (1990), p.802

75. K.R. Williams and B.J. Cane, Mater. Sci. Engng., Vol.38, (1974), p.199

76. B.F. Dyson and M. McLean, Acta. Metall, 31, (1983), p.17

77. R.W. Evans and B. Wilshire, Creep of Metals and Alloys, The Inst. of Metals, (1985), p.63

78. Harry Krauss, Creep analysis, John Willey, New York, (1980)

79. Metals Handbook, Vol.8, 9th edition, p.334

80. J.H. Hollomon and L.D. Jaffe, Trans. AIME, 162, (1945), 223

81. S. Chaudhuri, R. Singh, S. Lalita and R.N. Ghosh, Development of Computer softwares for evaluation of rupture strength and residual life of boiler tubes/steam pipes in thermal power plants. NML Report No.09600403, (Feb., 1988)

82. L. Chattopadhya, R. Singh and R.N. Ghosh, CLIP : A menu driven software for creep life prediction,NML Report No.03421139, (May, 1991)

83. R.M. Goldhoff, Stress Concentration and Size Effects in a Cr-Mo-V steel at Elevated Temperatures, Joint International Conference on Creep, Institute of Mechanical Engineers, London, (1963)

84. R. Viswanathan and C.G. Beck, Effect of Aluminium on the Stress Rupture Properties of Cr-Mo-V Steels, Met. Trans A, Vol.6A, (Nov.1975), p.1997-2003

85. R.M. Goldhoff, A Method for Extrapolating Rupture Ductility, in Elevated Temperature Testing Problems, STP400, ASTM, Philadelphia, (1971), p.82-90

86. R. Viswanathan and R.D. Fardo, Parametric Techniques for Extrapolating Rupture Ductility, in Ductility and Toughness Considerations in Elevated Temperature Service, G.V. Smith, Ed., MPC8, ASME, New York, (1978)

87. R. Viswanathan, The Effect of Stress and Temperature on the Creep and Rupture Behaviour of 1.25%Cr-0.5%Mo Steel, Met. Trans.A, Vol.8A, (1977), p.877-883

88. O. Sherby and P. Burke, Prog. Mater. Sci., 13, 325, (1967)

89. D. McLean, Rep. Prog. Physics, 29, 1 (1966)

90. R. Lagneborg, Int. Metall. Rev., 17, 130 (1972)

91. P.L. Threadgil and B. Wilshire, Proc. Conf. on Creep Strength of Steels, p.8, The Metals Society, London, (1974)

92. P.W. Davis, G. Nelmes, K.R. Williams and B. Wilshire, Metals Science, 7, 87 (1973)

93. J.D. Parker and B. Wilshire, Metals Sci., 9, 248, (1975)

94. W.J. Evans and G.F. Harrison, Metals Sci., 10, (1976), p.307

95. W.J. Evans and G.F. Harrison, Metals Sci., 13, (1979), p.641

96. K.R. Williams and B. Wilshire, Metals Sci., 7, (1973) p.176

97. H. Burt, J.P. Dennison and B. Wilshire, Metals Sci, 13, 295, (1979)

98. R.A. Stevens and P.F.J. Flewitt, Acta. Metall, 29, 867, (1981)

99. K.R. Williams and B.J. Cane, Mater. Sci.Engng. 38, 199, (1979)

100. R. Singh and S. Banerjee, Resisting Stress of a Low Alloy Ferritic Steel after Creep Exposure in Service, Acta. Metall, Vol.40, No.10, p.2607-2616, (1992)

101. T.G. Langdon and F.A. Mohamed, Mater. Sci. and Engng., 32 (1978), 103

102. I.S. Batra and P. Dasgupta, Trans. I.I.M., Vol.41, No.5, 433, (Oct. 1988)

103. H.F. Frost and M.F. Ashby, Deformation Mechanism Maps, Permagon Press, Oxford, (1982)

104. CEGB-Universities Collaborative Project on 1%Cr-Mo-V Steel, (1974)

105. B.F. Dyson, Proc. of the "Ashby Symposium" Chicago, (Sept.,1988)

106. E.N. da C. Andrade, Proc. Royal. Soc. A84, (1910)

107. P. Garofalo, "Fundamentals of Creep and Creep-Rupture in Metals", Macmillan, New York, (1965)

108. G.A. Webster, A.P.D. Cox and J.E. Dorn, Metal. Sci. J.3, 221 (1969)

109. R.N. Ghosh and M. McLean, Scripta Metall, 23, 1301 (1989)

110. J.C. Ion, A. Barbosa, M.F. Ashby, B.F. Dyson and M. McLean, "The modelling of creep for engineering design I", NPL Report DMA(A) 115, April, (1986)

111. R.W. Evans and B. Wilshire, Creep of Metals and Alloys" The Institute of Metals, Londonn, (1985), p.192

112. R.W. Evans, I. Beden and B. Wilshire, Proc. 2nd Int. Conf. on Creep and Fracture of Engineering Materials and Structures, (Eds. B. Wilshire and D.R.J. Owen), Pineridge Press, Swansea, 1984, p.1277

113. E.W. Hart, Acta Metall, 18, 599 (1970)

114. E.W. Hart, J. Engng. Mater. Tech., 98, 193, (1976)

115. A.K. Miller, J. Engng. Mater. Tech. 98H, 97 (1976)

116. A.K. Miller, The MATMOD Equations, in Unified Constitutive Equations for Creep and Plasticity (ed. A.K. Miller) p.139, Elsevier, Amsterdam (1987)

117. A.K. Miller and A.A.Ziaai-Moayyed, ASTM STP-765, (1982), p.202

118. R.N. Ghosh and M. McLean, High Temperature Deformation in Engineering Alloys - Modelling for Strain or Load Control, Acta. Metall. Mater, Vol.40, No.11, (1992), p.3075-3083

119. L.M. Kachanov, Izv Akad. Nauk S.S.R 8, 26 (1958)

120. Yu. N. Rabotnov, Proc.XII IVTAM Congress, Stanford (edt. by H. Hetenyi and W.G. Vincenti), p.342, Stringer, Berlin (1969)

121. F.A. Leckie and Hayhurst, Acta. Metall, 25, 1059, 1977

122. J. Lemaitre and J.L. Chaboche, Mecanique des Materiaux Solides, Dunod, Paris (1985), English edn, Cambridge University Press (1988)

123. M.F. Ashby and B.F. Dyson, in Advances in Fracture Research (edited by D.M.R. Taplin et. al) p.30, Pergamon Press, Oxford (1984)

124. A. Barbosa, N.G. Taylor, M.F. Ashby, B.F. Dyson and M. McLean, Proc. 6th Int. Symp. on Superalloys (edited by D. Duhl et.al) p.683 Metall. Soc. A.I.M.E, New York (1988)

125. B.F. Dyson and M. McLean, J. Iron & Steel Inst of Japan, 30, 802 (1990)

126. M.F. Ashby and B.F. Dyson, Proc. 6th Int. Conf. on Fracture (ICF6), New Delhi, p.3, Pergamon Press, Oxford (1984)

127. B.F. Dyson and T.B. Gibbons, Acta Metall, 35, 2355, (1987)

128. B.F. Dyson, Rev.Phys. Appl, 23, 605, (1988)

129. B.F. Dyson, Proceeding of the "Ashby Symposium", Chicago, Sept., (1988)

130. M.F. Ashby and B.F. Dyson, Advances in Fracture Research, Vol.1 (Pergamon Press, 1984) Eds.S.R. Valluri, et.al.3

131. B.F. Dyson and F.A. Leckie, Mat. Sci. and Engg., A103, (1988), 111

132. R.N.Ghosh, R.V. Curtis and M. McLean, Acta.Metall Mater, 38, (1990), p.1977

133. M. McLean, R.N.Ghosh, R.V. Curtis, U. Basu-Conlin and M.R. Winstone in "Superalloy 1992", The Metallurgical Society, Warrendale, PA, (1992), p.609

134. S. Gota and M.McLean, Role of interfaces in creep of fibre-reinforced metal-matrix composities - I continuous fibres (p.153); - II short fibres (p.165), Acta. Metall. Mater, Vol.39, No.2 (1991)

135. M. Cristinacce, Development in production of engineering steels - the advantages for gear manufacturers from secondary steel making, Materials and Design, Vol.13, No.1, (1992), p.33

136. Ausscheidungsatlas der Stähle (Herausgeber: Arbeitskreis Elektronenmikroskopie des Werkstoffausschusses des Vereins Deutscher Eisenhüttenleute), Düsseldorf, (1983), p.95

137. R. Cooper, The Prediction of Steel Hardenability Using Multiple Regression Analysis, Heat Treatment of Metals, (1983.1), p.15

138. W. Hewitt, Hardenability - its Prediction from Chemical Composition, Heat Treatment of Metals, (1981.2), p.33

139. T. Kunitake and H. Ohtani, Calculating the Continuous Cooling Transformation Characteristics of Steel from its Chemical Composition, The Sumitomo Search, No.2, (Nov, 1969), p.18

140. R. Viswanathan, Damage Mechanisms and Life Assessment of High Temperature Components, ASM International, Metals Park, Ohio, (1989), p.76

141. M.B.D Ellis and others, Effects of impurity segregation on sustained load cracking of a 2.25Cr-1Mo steel, Strength of Metals and Alloys (ICSMA 7), Vol.2, (Proc. Conf.), Pergamon Press, Montreal, (1985), p.1087-1092

142. U. Frauzoni and others, Effects of residual impurities on creep embrittlement in a 2.25Cr-1Mo steel, Boll.Tech. Finsider, 404, (1985), p.98-101

143. S. Sato and others, Effects of chemical composition and heat treatment on creep embrittlement of Mo steel and Cr-Mo steels, Advanced Materials for Pressure Vessel Service with hydrogen at high temperatures and pressures, (Proc. Conf.) Orlando, Fla, ASME, (1982), p.259-272

144. E.W. Hart, Acta. Metall, 15, (1967), p.351

145. M.A. Burke and W.D. Nix, Acta. Metall, 23, (1975), p.793

146. B.J. Cane, The Process Controlling Creep and Creep Fracture of 2.25Cr-1Mo Steel, CEGB Report RD/LR 1979, CEGBRL, Leatherhead, England, (1979)

147. NRIM Data Sheets on Ni base superalloys, No.34A, (1989)

148. S. Chaudhuri, R. Singh, T.K. Sinha and S. Banerjee, Evaluation of Creep and Stress rupture properties of Zr-2.5%Nb pressure tube alloy, NML Report No.11612042, (Feb, 1992)

149. R.A. Stevens and P.F.J. Flewitt, Mater, Sci. Engg., 37, (1979), p.237

150. H.R. Tipler and M.S. Peck, Final Report on COST 50 Programme, U.K. 17, Division of Materials Applications, National Physical Laboratory, Teddington, U.K., DMA(A) 33, (1981)

151. V.K. Sikka, Development of Modified 9Cr-1Mo Steel for Elevated Temperature Service, in Topical Conference on Ferritic Alloys for Use in Nuclear Energy Technologies (Proceedings of a Conference in Snowbird, UT), Metallurgical Society of AIME, Warrendale, PA, (1984), p.323

152. Atlas of Creep and Stress Rupture Curves (Ed. H.E. Boyer), A.S.M. International, (1988)

153. I.M. Lifshitz and I. Slyozov, J. Phy. Chem. Solids, 19, (1961), p.35

154. M.C. Askins et.al., Remaining Life of Boiler Pressure Parts - Base Materials Model, Report RP 2253-1, Vol.3, EPRI, Palo Atto, Calif. (1988)

155. S. Chaudhuri, N. Roy and R.N. Ghosh, Modelling High Temperature Creep of Cr-Mo Steel, Acta.Metall. Mater, Vol.41, No.1, (1993), p.273-278.

SOME ASPECTS OF CREEP BEHAVIOUR OF
2.25Cr-1 Mo STEEL

APPENDIX - A

Creep and Rupture Data used in the Thesis

Submitted by :

Satyabrata Chaudhuri

1993

Department of Metallurgical Engineering
Indian Institute of Technology
Kharagpur 721 302
INDIA

TABLES

Table - 6.1

Chemical Composition of Steel Reported by NRIM
and Its Specification[44]

Type of Steel	Element, wt%						
	C	Mn	Si	Cr	Mo	S	P
NRIM Steel	0.10	0.43	0.23	2.46	0.94	0.009	0.011
Specification STBA 24 JIS G3462	<0.15	0.30-0.60	<0.5	1.90-2.60	0.87-1.13	<0.030	<0.030

Table -6.2

Manufacturing Details of Steel in Table - 6.1

Type of Melting	Size of ingot, tons	Deoxidation Process	Production Form and Dimensions, mm	Processing and Thermal History
Basic Electric Arc	5.8	Si-killed	Tube 50.8 OD,8.0 WT; 5000L	Rotary Pierced and cold drawn 930°C, 20 Mins; 720°C, 130 mins, AC.

NB : OD = Outer Diameter, WT = Wall Thickness, L = Length
    AC = Air Cooled.

Table - 6.3

Estimated 30,000 hr-Rupture Strength [MPa] of Steel [Table-6.1] Using
Larson-Miller, Sherby-Dorn and Manson-Haferd Parameters

Type of Parameter	Sum Square Error(s)	Temperature$^{\circ}$C			
		500	525	550	575
Larson-Miller	0.1707×10^{-1}	140	113	91	71
Sherby-Dorn	0.4634×10^{-1}	142	111	85	63
Manson-Haferd	0.1309×10^{-1}	140	111	89	69
Larson-Miller with C as 20	0.1765×10^{-1}	141	114	92	72

Table - 6.4

Estimated 100,000 hr-Rupture Strength[MPa] of Steel[Table-6.1] Using
Larson-Miller, Sherby-Dorn and Manson-Haferd Parameters.

Type of Parameter	Sum Square Error(s)	Temperature$^{\circ}$C			
		500	525	550	575
Larson-Miller	0.1707×10^{-1}	121	97	77	58
Sherby-Dorn	0.4634×10^{-1}	119	90	66	47
Manson-Haferd	0.1309×10^{-1}	117	92	72	53
Larson-Miller with C as 20	0.1765×10^{-1}	123	98	78	59

Table - 6.5
Microstructures Developed in 2.25Cr-1Mo Steel Following
Different Heat Treatments

Type of Microstructure	Heat Treatments	Microstructural Features
A	Normalising: 920 C for 1 hour Tempering: 730 C for 3 hours	Ferrite and Tempered bainite
B	Normalising: 990 C for 1 hour Forced Air Cooling Temperating: 730 C for 3 hours	Fully Tempered Bainite
C	Same as above (Type B) + Thermal Ageing: 650 C for 190 hours	Ferrite and Carbide

Table - 6.6

Estimated 30,000 hr-Rupture Strength[MPa] of 2.25Cr-1Mo Steel Having Different Initial Microstructure Using Larson-Miller Parameter with C as 20

Microstructures		Temperature$^{\circ}$C			
Type	Feature	500	525	550	575
A	Ferrite-Bainite	170	131	95	60
B	Bainite	206	165	126	89
C	Ferrite-Carbide	140 (32)	110 (33)	83 (34)	55 (38)

NB :   The values reported within brackets indicate percentage loss of 30,000 hr-rupture strength due to thermal exposure.

Table -6.7

Estimated 100,000 hr-Rupture Strength[MPa] of 2.25Cr-1Mo Steel Having Different Initial Microstructure Using Larson-Miller Parameter with C as 20

Microstructures		Temperature$^{\circ}$C			
Type	Feature	500	525	550	575
A	Ferrite-Bainite	144	106	71	-
B	Bainite	179	138	100	57
C	Ferrite-Carbide	120 (33)	91 (34)	64 (36)	-

NB :   The values reported within brackets indicate percentage loss of 100,000 hr-rupture strength due to thermal exposure.

Table - 6.8

Reported Partial Regression Coefficients for Alloying Elements[139]

Alloying Element	C	Si	Mn	Ni	Cr	Cu	Mo
Partial Regression Coefficient (1/wt%)	3.228	-0.168	1.068	0.300	1.266	0.626	2.087

Table - 6.9

Steel Having Variation in Chemical Composition for Constant Section Thickness and Their Estimated Critical Cooling Time for Ferrite Transformation

Designation	C	Mn	Si	Element, wt% Cr	Mo	Critical Cooling Time, Sec.
St 68	0.13	0.53	0.23	2.21	0.87	4.3×10^3
St 69	0.10	0.45	0.25	2.27	0.98	5.7×10^3
St 70	0.12	0.51	0.21	2.23	0.96	6.3×10^3
St 71	0.11	0.44	0.28	2.13	0.96	3.6×10^3
St 72	0.12	0.49	0.16	2.35	0.95	8.3×10^3
St 73	0.12	0.42	0.24	2.26	0.96	5.4×10^3
St 74	0.13	0.44	0.38	2.32	0.97	7.3×10^3
St 75	0.17	0.46	0.29	2.24	0.90	6.0×10^3

NB : Sulphur and Phosphorus contents not reported; Product form and Section Thickness : 28.6 mm bar; Heat-Treatment:930°C, FC 33°C/hr.

Table - 6.10

Steels Having Variation in Chemical Composition for a Range of
Section Thickness and Their Estimated Critical Cooling Time for
Ferrite Transformation

Desig-nation	C	Mn	Si	Cr	Element, wt% Mo	Ni	S	P	Critical Cooling Time, Sec.
TH12.7	0.11	0.42	0.32	2.19	0.97	0.07	0.018	0.014	$4.4 \times 10^{+3}$
TH34.9	0.15	0.50	0.18	2.12	0.94	0.16	0.012	0.018	$5.7 \times 10^{+3}$
TH57.2	0.17	0.39	0.24	2.12	0.92	0.05	0.029	0.015	4.2×10^{3}
TH69.9	0.12	0.67	0.14	2.15	1.00	0.07	0.031	0.030	9.7×10^{3}

NB :   Heat - Treatment : N 940/960°C, T 690/700°C

Table - 6.11

Comparison of 100,000 hour-Rupture Strength[MPa]
of a Few Grades of Cr-Mo Steels[151-152]

Type of Steel	Temperature °C 600	650
2.25Cr-1Mo	44	29
9Cr-1Mo	41	17
Modified 9Cr-1Mo	102	54
AISI 304	102	71

Table - 6.12

Comparison of Assumed and Estimated Values of the Model Parameters a and b Representing the Effect of Particle Coarsening at Different Values of n and $\overset{o}{\varepsilon}_i$

Material	Parameter	Assumed	Estimated	
M1	a	1.82×10^{-5}	1.816×10^{-5}	$n = 7.9$
	b	8.4×10^{-1}	8.332×10^{-1}	$\overset{o}{\varepsilon}_i = 1.8 \times 10^{-6}$
M2	a	7.943×10^{-6}	7.934×10^{-6}	$n = 10.6$
	b	2.16	2.154	$\overset{o}{\varepsilon}_i = 1.38 \times 10^{-6}$
M3	a	5.4×10^{-4}	5.44×10^{-4}	$n = 3.2$
	b	0.51	0.492	$\overset{o}{\varepsilon}_i = 1 \times 10^{-6}$

Table - 6.13

Summary of Material Constants Estimated for a 2.25Cr-1Mo Steel

Parameter	Magnitude	Units
n	4.23	
Q	315	KJ mol^{-1}
ε_{io}	3.20×10^{-6}	h^{-1}
C	6.52×10^{-6}	MPa
Q_1	284.7	KJ mol^{-1}
Q_2	-107.03	KJ mol^{-1}
K_o	5.899×10^{-14}	$m^3 h^{-1}$
m	3.957	

Table - 6.14

Comparison of Parameter Representing Kinetics of Coarsening as Estimated in the Present work with those reported by Askins et al

Temperature °C	K, at different stress levels (m^3h^{-1})		K, Askins et al.[154] (m^3h^{-1})
	Minimum	Maximum	
500	9.223×10^{-9}	8.588×10^{-7}	1.124×10^{-8}
550	6.847×10^{-8}	1.382×10^{-5}	1.623×10^{-7}
600	1.62×10^{-6}	1.91×10^{-4}	2.344×10^{-6}

FIGURES

STRESS,MPa   2.25 Cr 1 Mo STEEL [44]

LMP = $A_1 + A_2 \log\sigma + A_3 (\log\sigma)^2 + A_4 (\log\sigma)^3$

Where A_1 = -14339, A_2 = 58397, A_3 = -30049, A_4 = 4632

□ 500 C   * 550 C   ◇ 600 C   × 650 C

T(19.3 + log tr)/1000
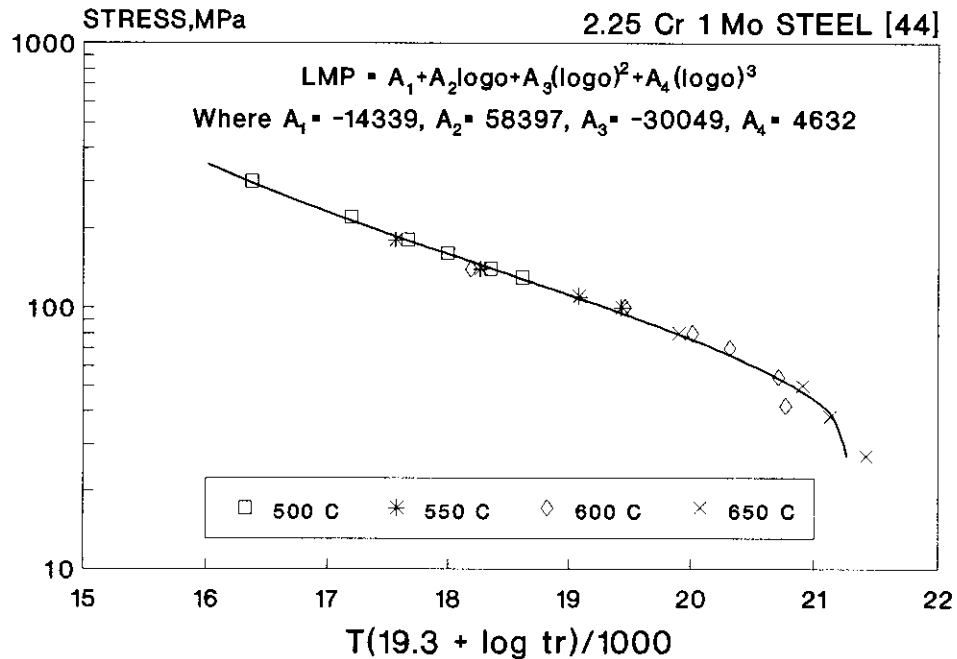
Fig.6.11 MASTER RUPTURE PLOT OF STRESS Vs. LARSON-MILLER
PARAMETER [LMP]

STRESS,MPa   2.25 Cr 1 Mo STEEL [44]

SDP = $A_1 + A_2 \log\sigma + A_3 (\log\sigma)^2 + A_4 (\log\sigma)^3$

Where A_1 = 0.00057, A_2 = -22.4, A_3 = 12.4, A_4 = -2.75

□ 500 C   * 550 C   ◇ 600 C   × 650 C

log tr - 17462.9/T
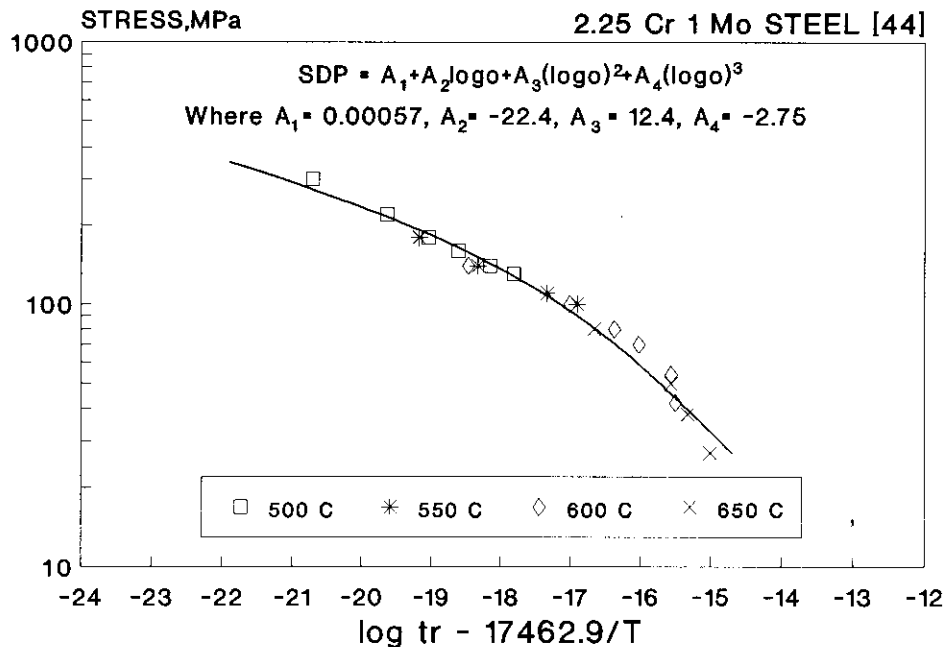
Fig.6.12 MASTER RUPTURE PLOT OF STRESS Vs. SHERBY-DORN
PARAMETER [SDP]

STRESS,MPa   2.25 Cr 1 Mo STEEL [44]

$MHP = A_1 + A_2 \log\sigma + A_3(\log\sigma)^2 + A_4(\log\sigma)^3$

Where $A_1 = -0.079$, $A_2 = 0.087$, $A_3 = -0.04$, $A_4 = 0.005$

□ 500 C   ✳ 550 C   ◇ 600 C   ✕ 650 C

(log tr − 15.8)/(T − 373)
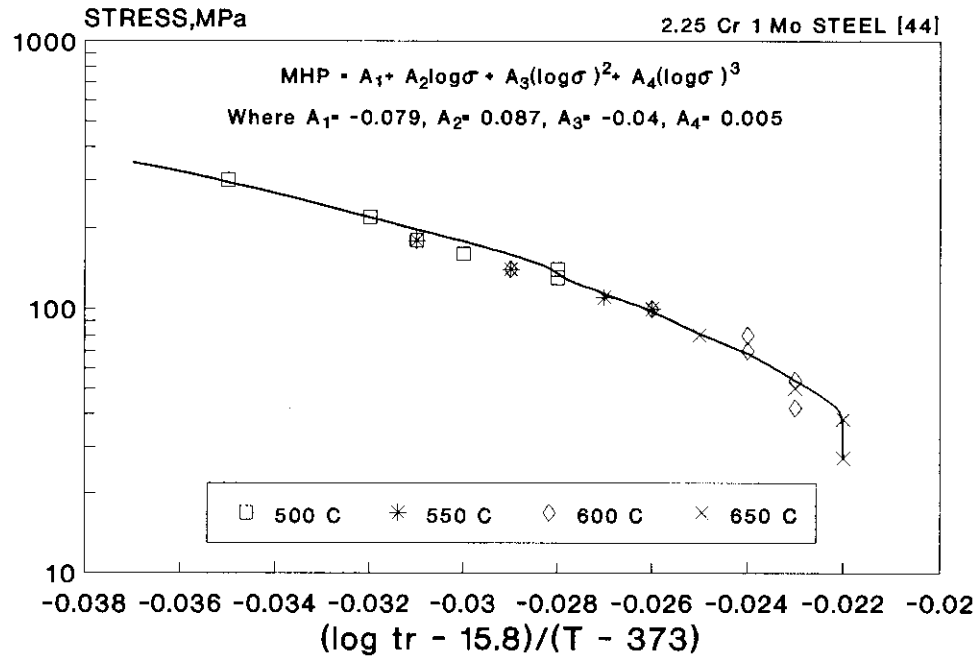
Fig.6.13 MASTER RUPTURE PLOT OF STRESS Vs. MANSON-HAFERD PARAMETER [MHP]

STRESS,MPa   2.25 Cr 1 Mo STEEL [44]

$LMP = A_1 + A_2 \log\sigma + A_3(\log\sigma)^2 + A_4(\log\sigma)^3$

Where $A_1 = -15417$, $A_2 = 61239.8$, $A_3 = -31557$, $A_4 = 4884$

□ 500 C   ✳ 550 C   ◇ 600 C   ✕ 650 C

T(20 + log tr)/1000
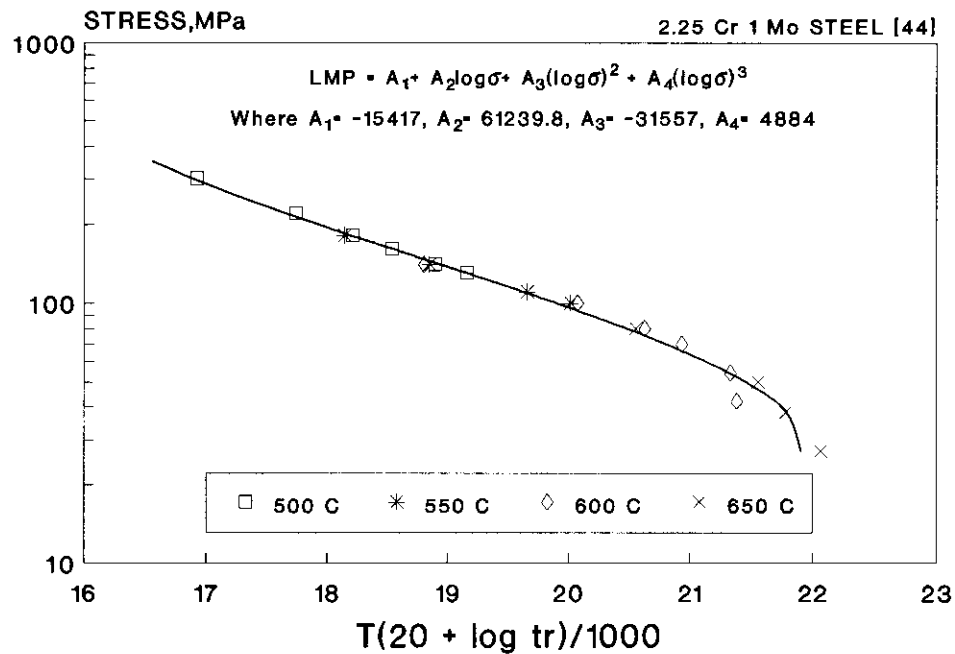
Fig.6.14 MASTER RUPTURE PLOT OF STRESS Vs. LARSON-MILLER PARAMETER [LMP] WITH C AS 20
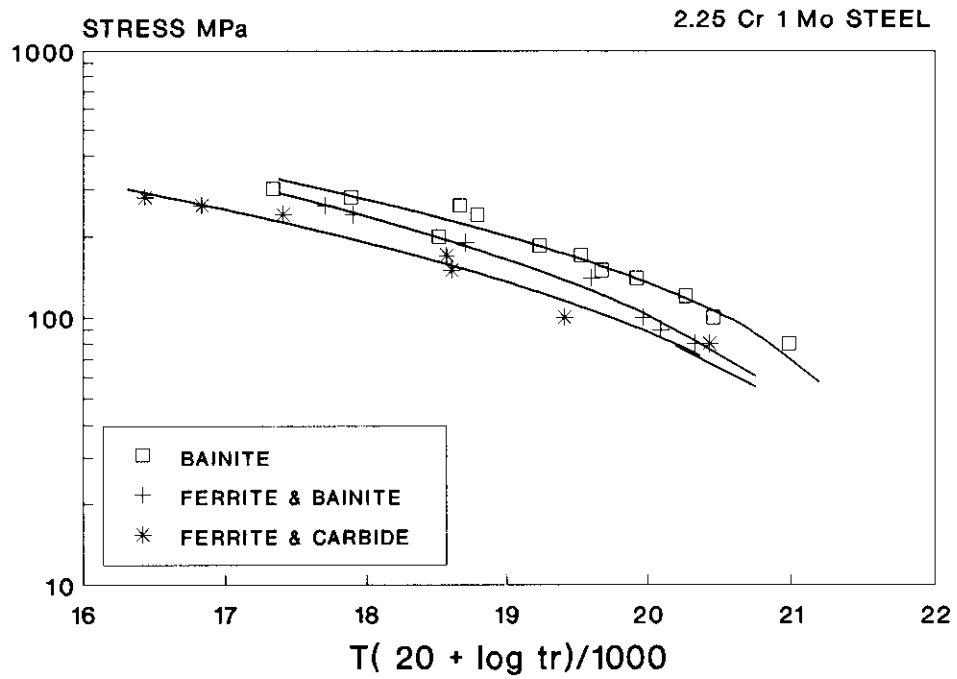
Fig. 4   MASTER RUPTURE PLOT OF STRESS Vs. LARSON-MILLER
PARAMETER OF 2.25 Cr 1 Mo STEEL HAVING DIFFERENT
INITIAL MICROSTRUCTURES
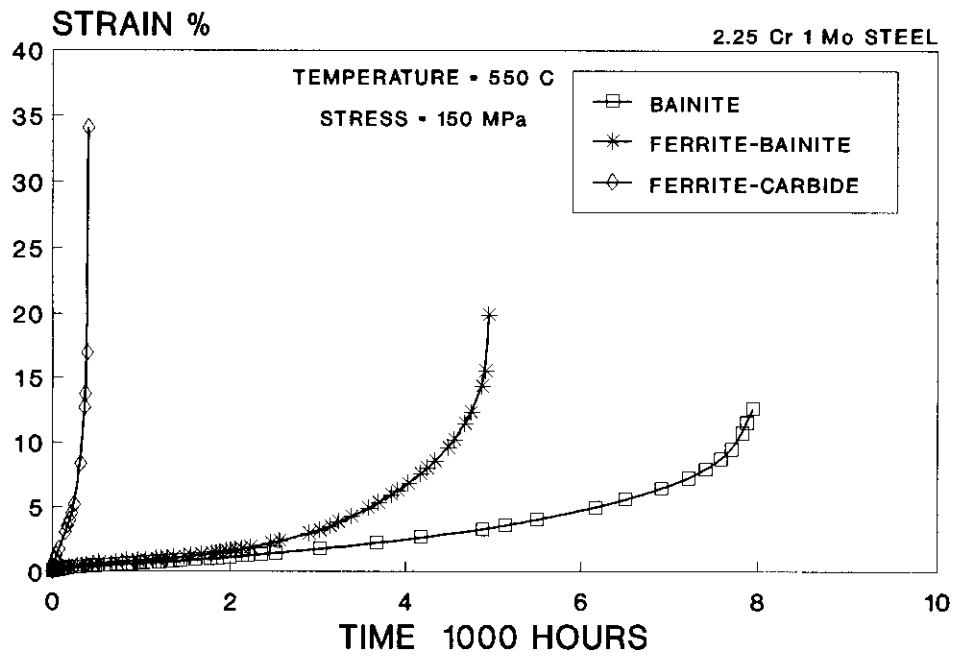
Fig.6.22(a) EXPERIMENTAL CREEP CURVES AT 550 C, 150 MPa
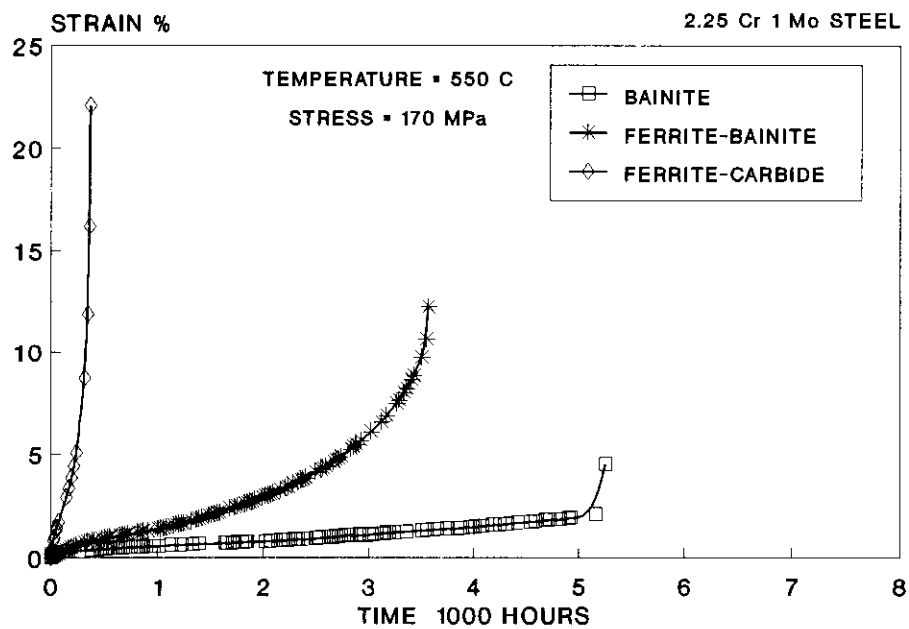
Fig.6.22(b) EXPERIMENTAL CREEP CURVES AT 550 C, 170 MPa

88
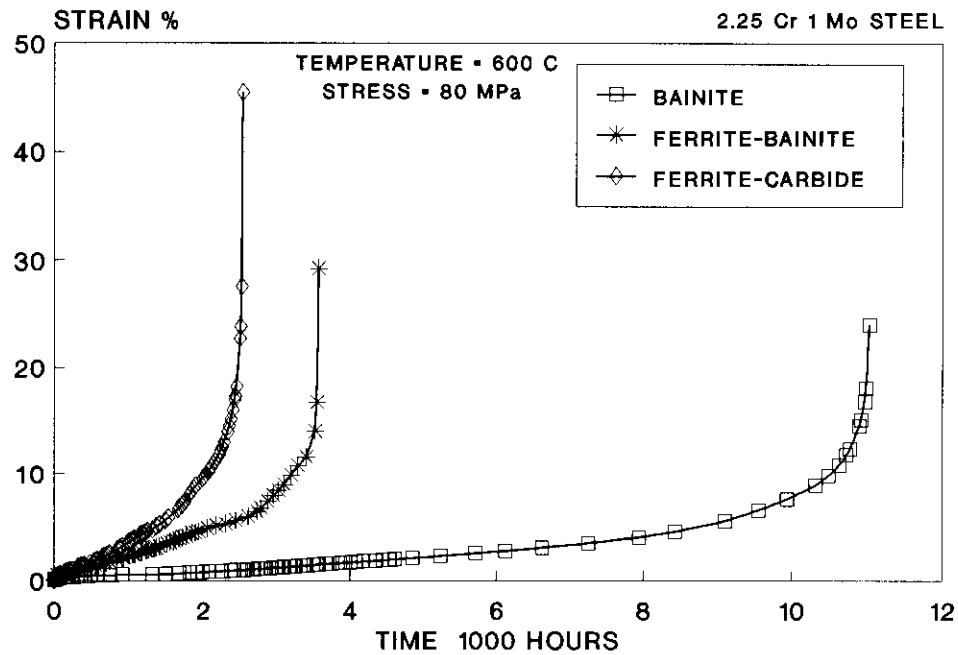
Fig.6.23(a) EXPERIMENTAL CREEP CURVES AT 600 C, 80 MPa
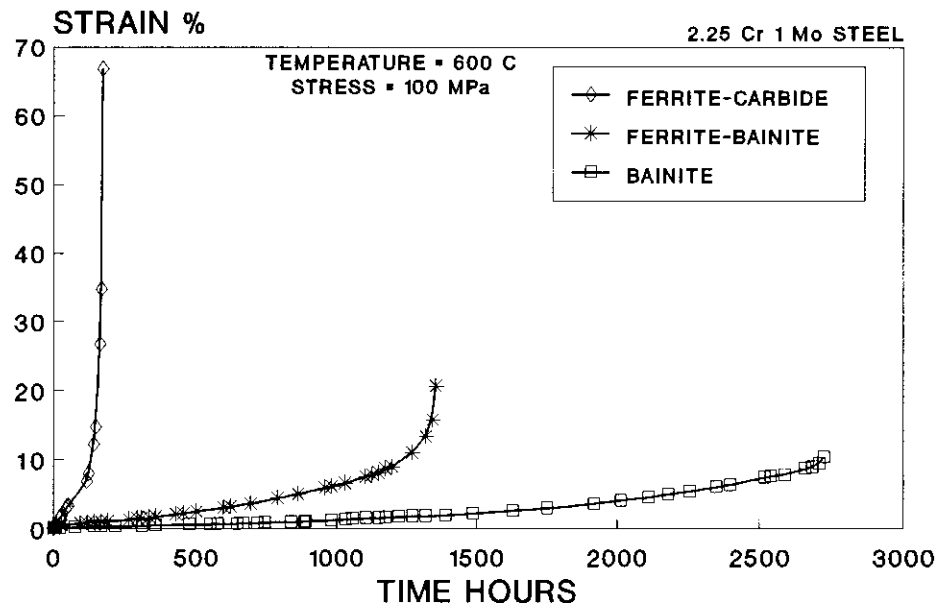
Fig.6.23(b) EXPERIMENTAL CREEP CURVES AT 600 C, 100 MPa

89
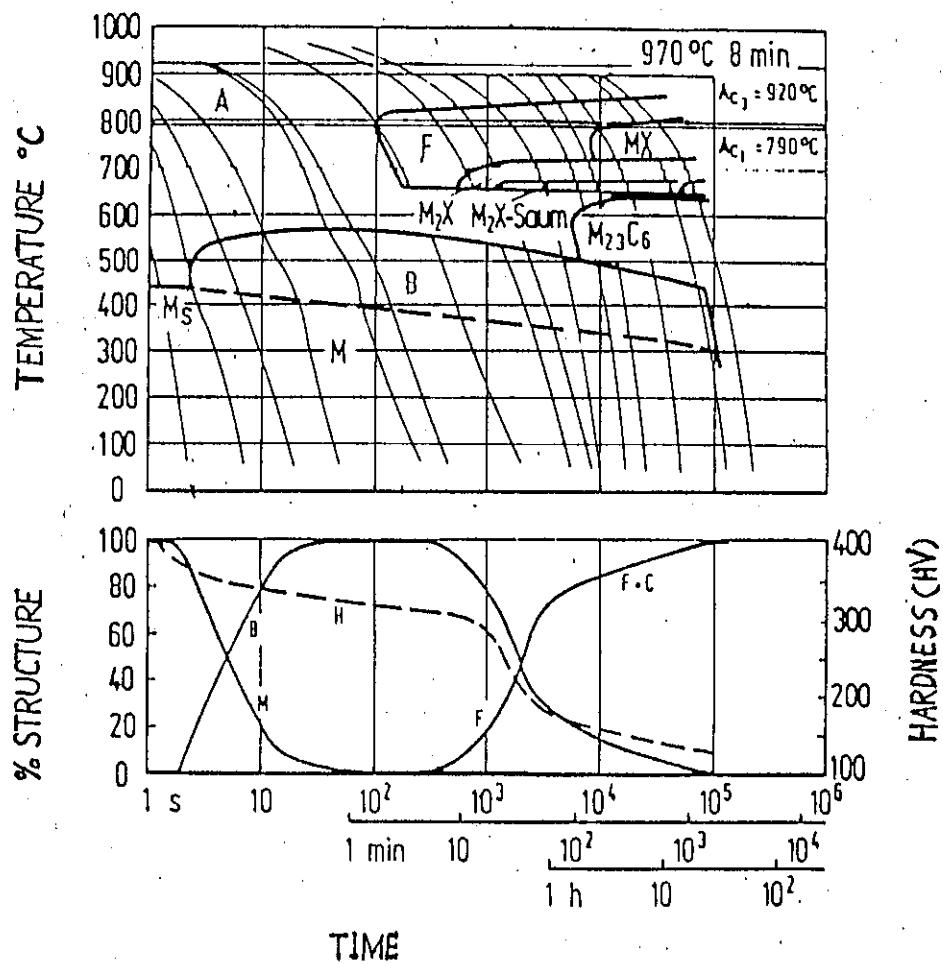
Fig.6.30(a) TYPICAL TIME TEMPERATURE TRANSFORMATION
DIAGRAM OF 2.25 Cr 1 Mo STEEL [136]
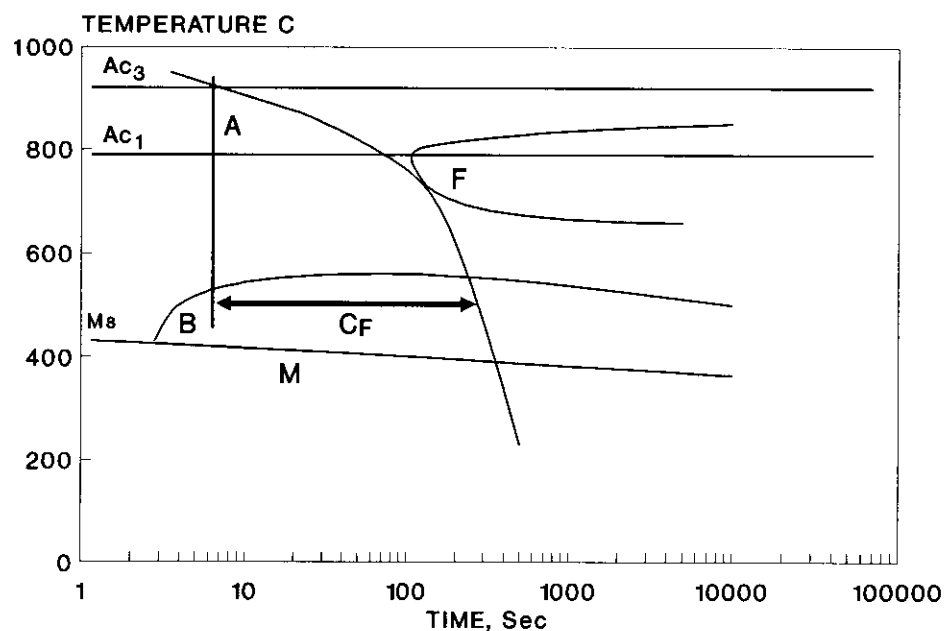
Fig.6.30(b) CRITICAL COOLING TIME (C_F) AT 500 C SHOWN ON
A SCHEMATIC T-T-T DIAGRAM OF 2.25 Cr 1 Mo STEEL

STRESS,MPa   2.25 Cr 1 Mo STEEL [15]
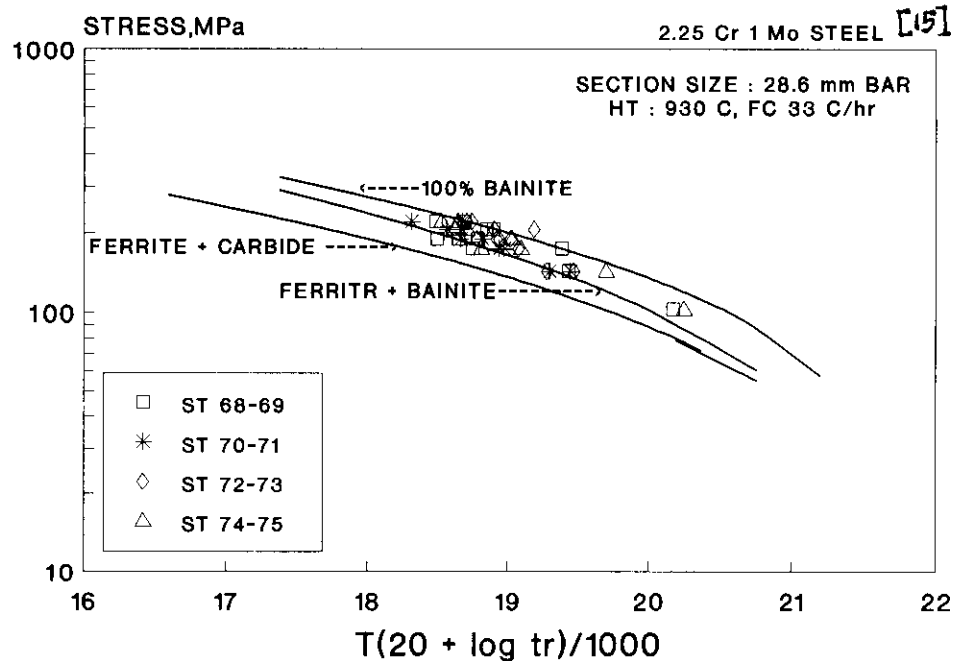
Fig. 5   PLOT OF STRESS Vs. LARSON-MILLER PARAMETER FOR
STEELS WITH MINOR VARIATION IN CHEMICAL COMPOSITION

STRESS,MPa   2.25 Cr 1 Mo STEEL [15]
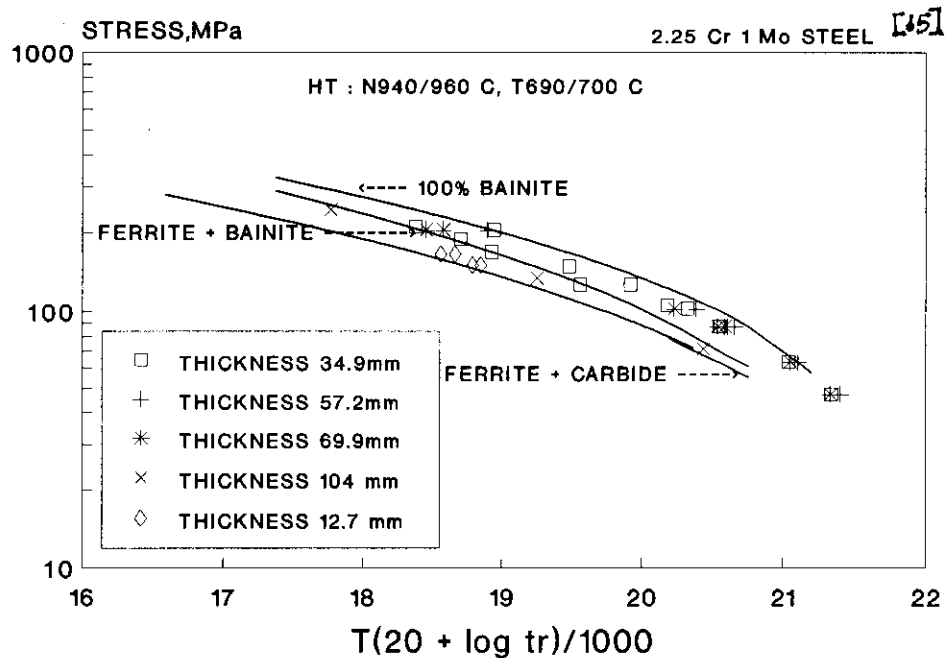
Fig. 6   PLOT OF STRESS Vs. LARSON-MILLER PARAMETER FOR
STEELS WITH DIFFERENT SECTION SIZE
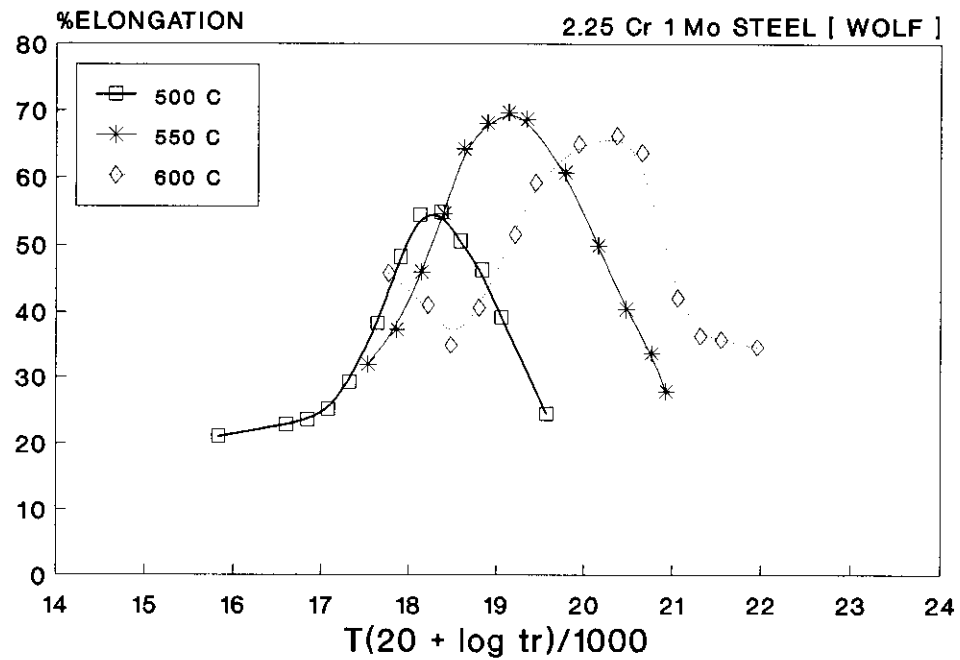
Fig.6.53 PLOT OF %ELONGATION AT RUPTURE Vs. LMP [34]
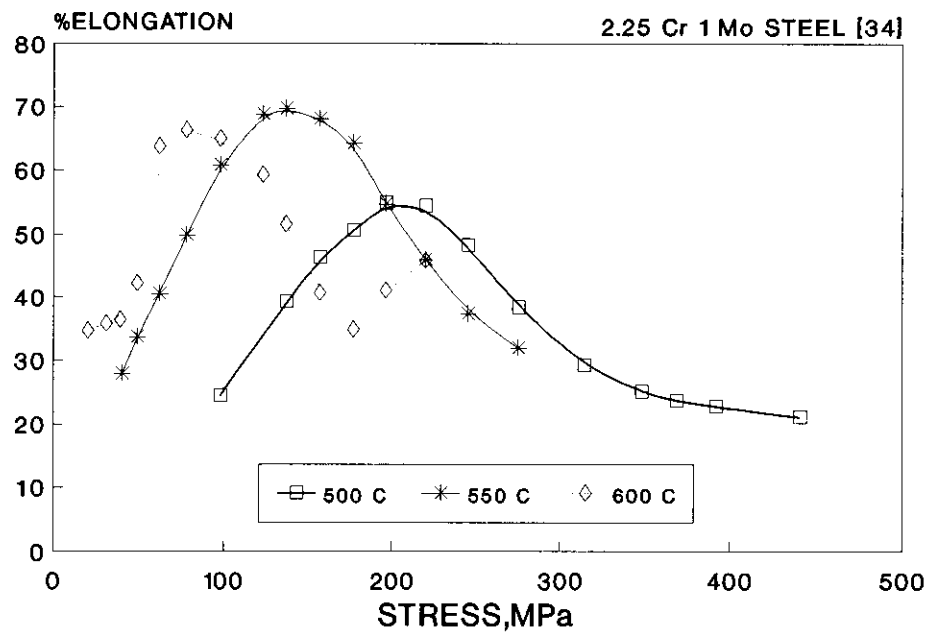
FiG.6.54 PLOT OF %ELONGATION AT RUPTURE Vs. STRESS

93
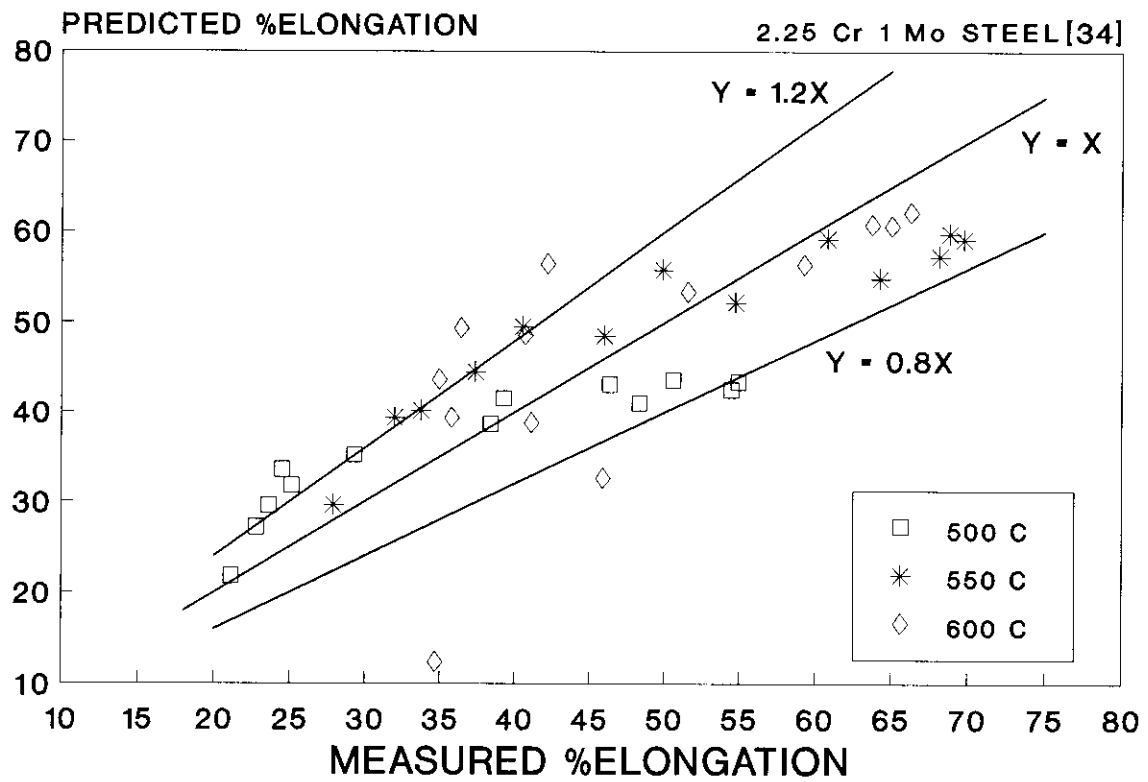
Fig.6.55 COMPARISON OF PREDICTED & ACTUAL ELONGATION
USING STRESS-TEMPERATURE FUNCTION
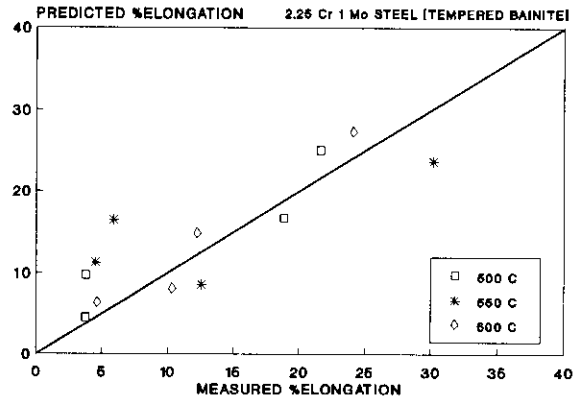
(a) INITIAL MICROSTRUCTURE : TEMPERED BAINITE
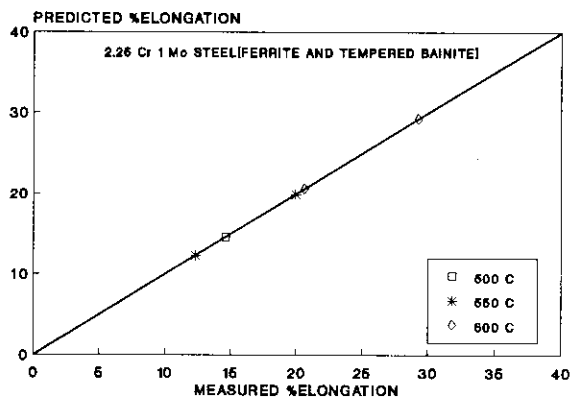
(b) INITIAL MICROSTRUCTURE : FERRITE AND BAINITE
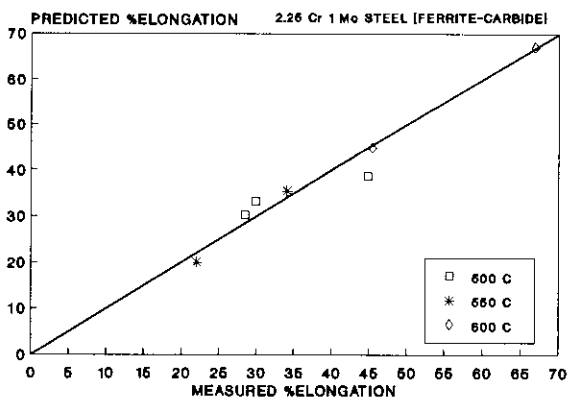
(c) INITIAL MICROSTRUCTURE : FERRITE AND CARBIDE

Fig.6.56(a-c) COMPARISON OF RUPTURE DUCTILITY PREDICTION
UNDER DIFFERENT MICROSTRUCTURAL CONDITIONS
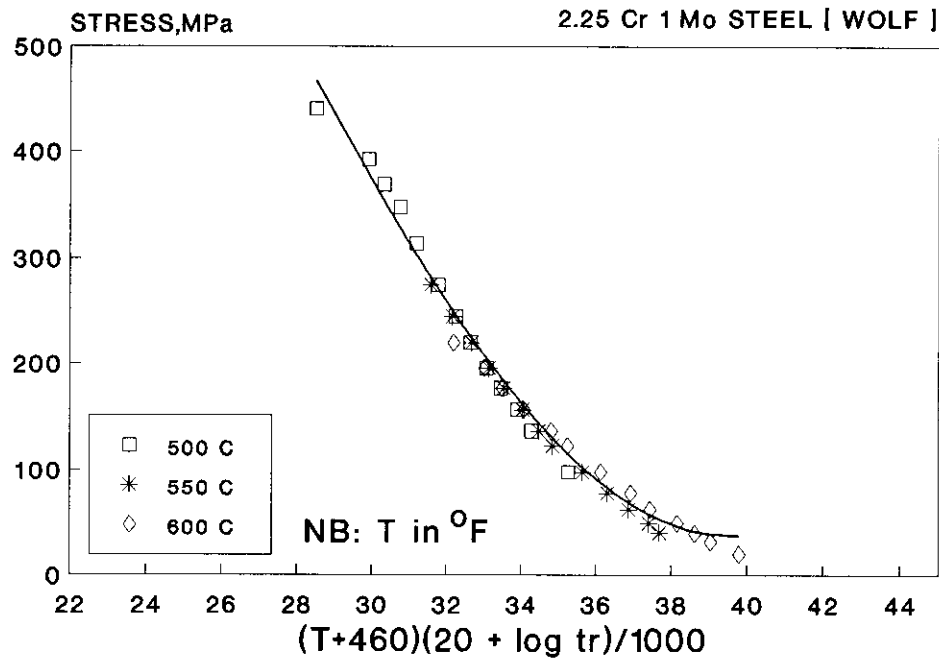
Fig.6.57(a) STRESS Vs. LMP PLOT OF PUBLISHED
STRESS RUPTURE DATA [34]
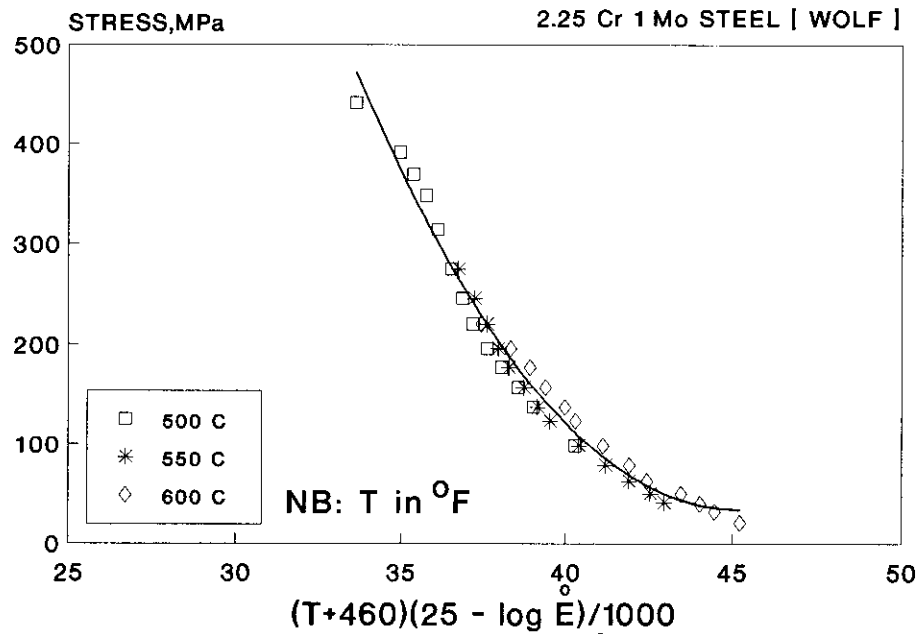
Fig.6.57(b) STRESS Vs. COMBINED T-Ė PLOT OF ABOVE DATA
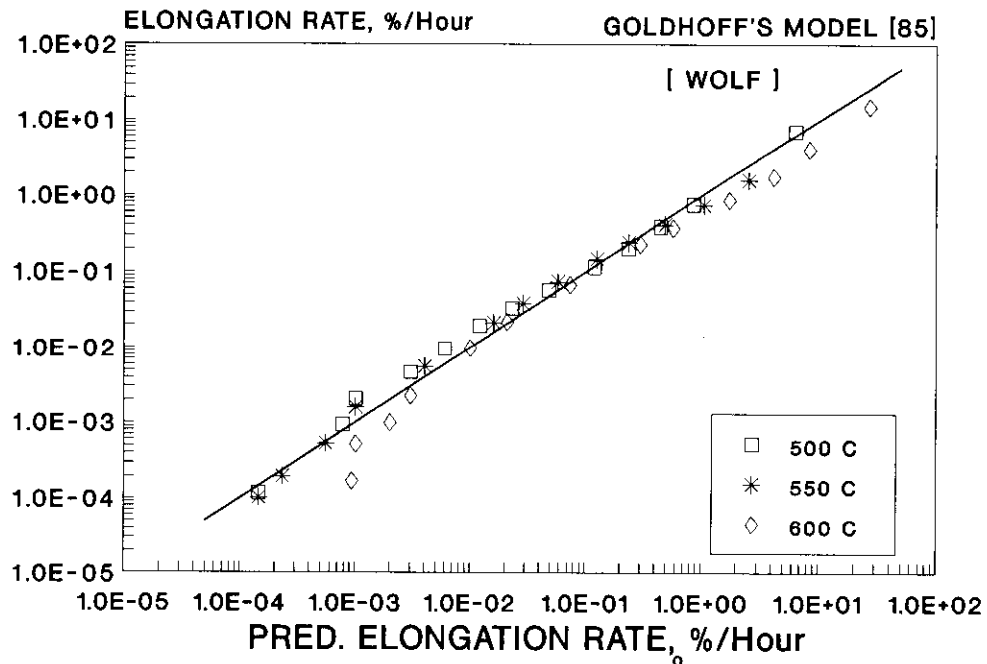
Fig.6.57(c) COMPARISON OF PREDICTED $\dot{E}$ WITH ACTUAL DATA
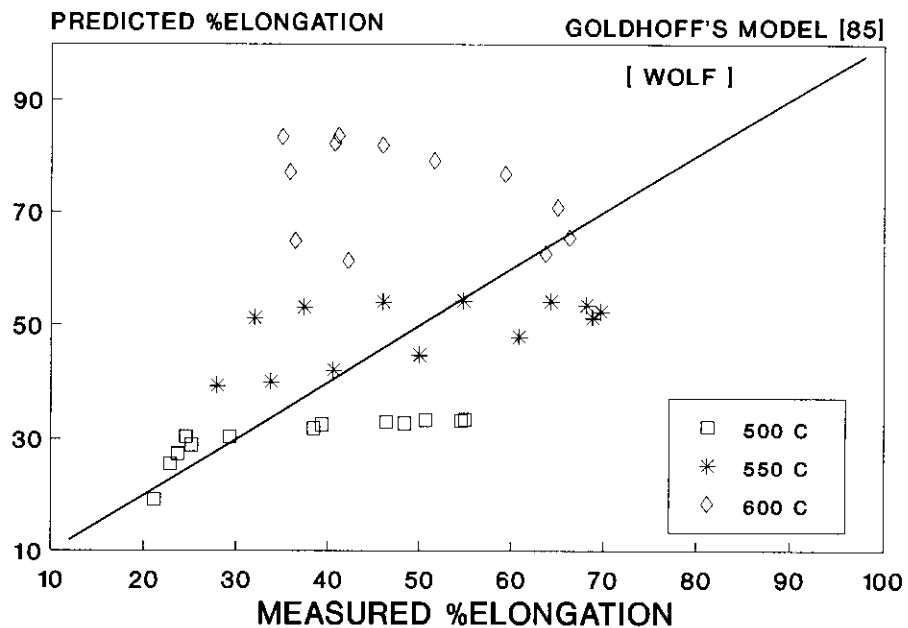
Fig.6.57(d) COMPARISON OF PREDICTED %EL WITH ACTUAL DATA

Fig.6.58(a) ELONGATION RATE Vs. RUPTURE TIME PLOT

Fig.6.58(b) COMPARISON OF PREDICTED %EL WITH ACTUAL DATA
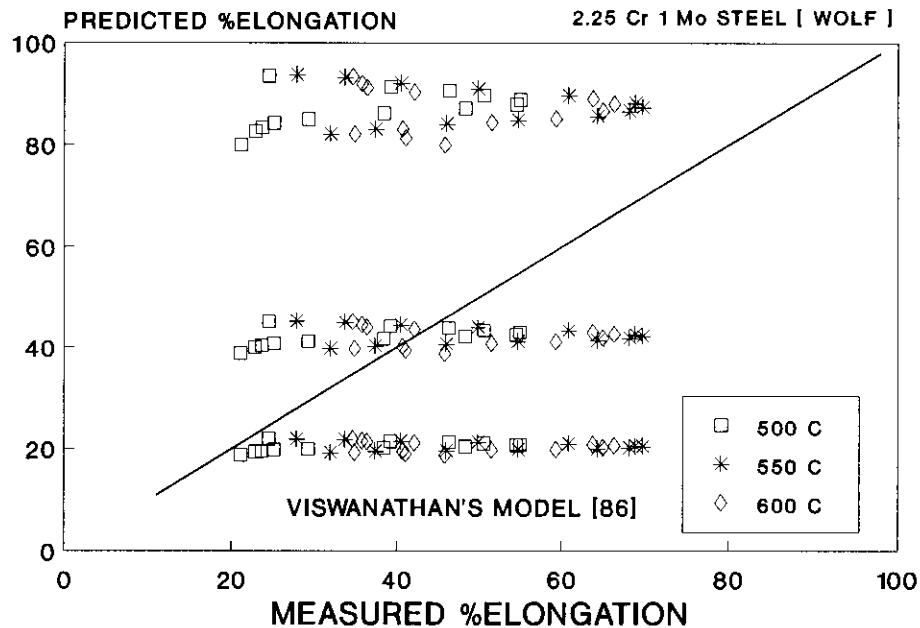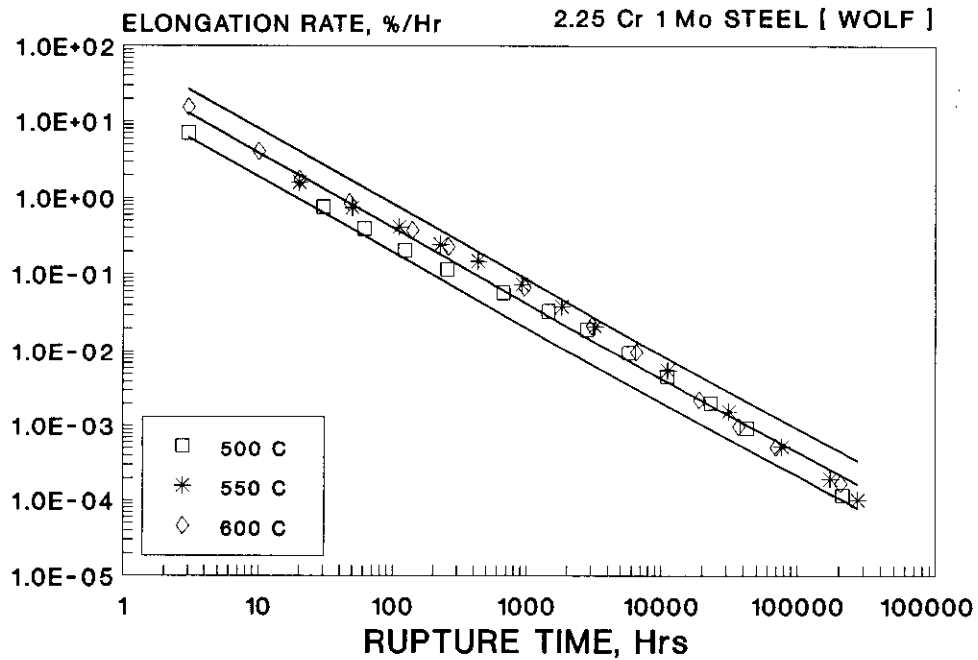
Fig.6.62 FRACTURED SURFACE OF CREEP EXPOSED 2.25Cr1Mo STEEL
EXHIBITING INTERGRANULAR MODE OF FRACTURE

Fig.6.63 FRACTURED SURFACE OF CREEP EXPOSED 2.25Cr1Mo STEEL
EXHIBITING TRANSGRANULAR MODE OF FRACTURE
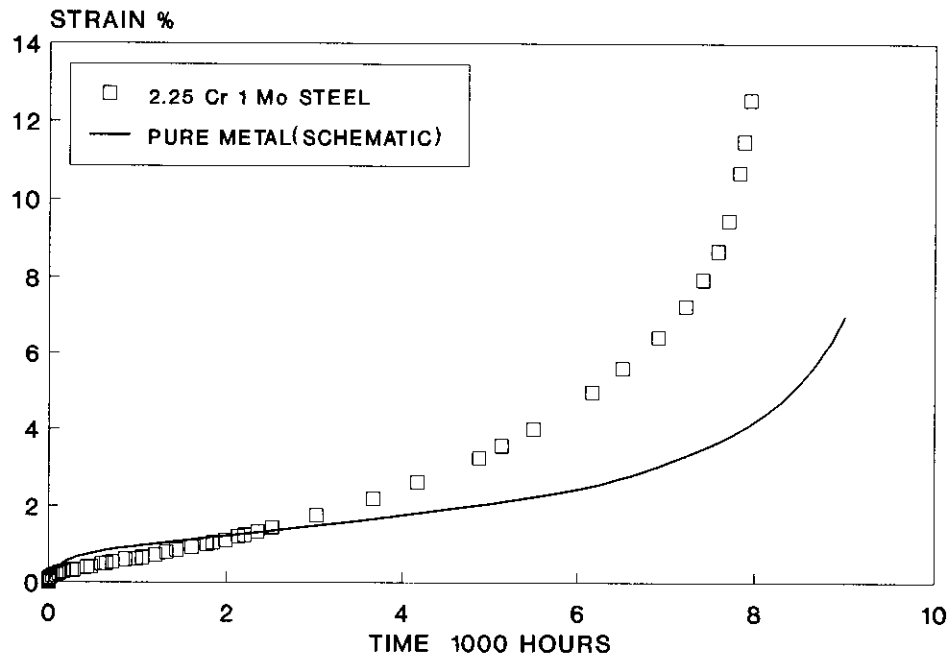
Fig.6.71 CREEP CURVES OF (a) PURE METAL (SCHEMATIC) AND (b) 2.25Cr1Mo STEEL (EXPERIMENTAL) AT 550 C, 150 MPa

(a) BEFORE CREEP EXPOSURE   (b) AFTER CREEP EXPOSURE
Fig.6.72(a,b) MICROSTRUCTURES BEFORE & AFTER CREEP EXPOSURE
EXHIBITING COARSENING OF CARBIDES IN 2.25Cr1Mo STEEL

STRAIN %   2.25 Cr 1Mo STEEL
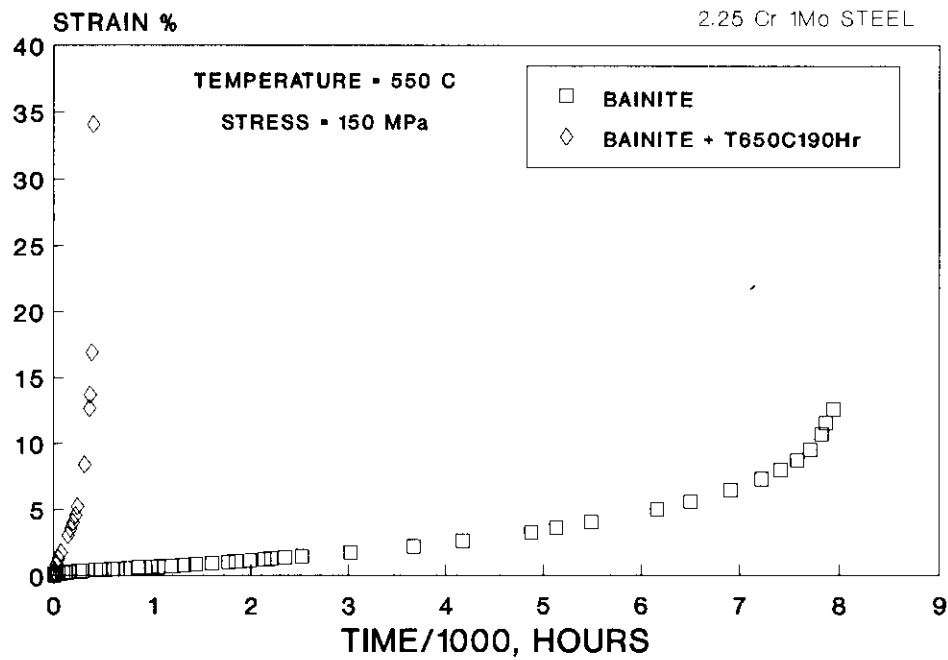
Fig.6.73 INFLUENCE OF THERMAL EXPOSURE ON CREEP CURVE

STRAIN %   2.25 Cr 1Mo STEEL
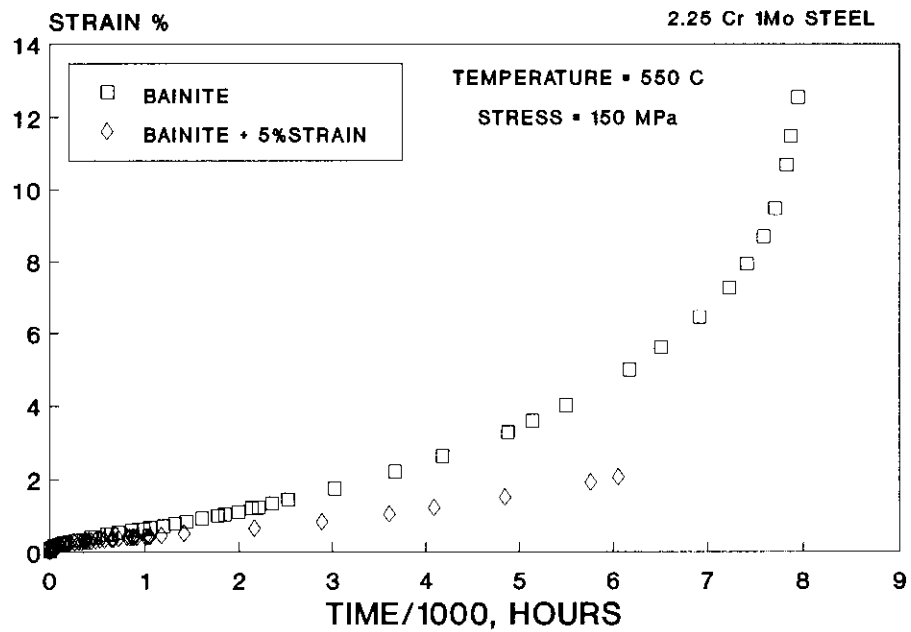
Fig.6.74 INFLUENCE OF PRE-STRAIN ON CREEP CURVE

104
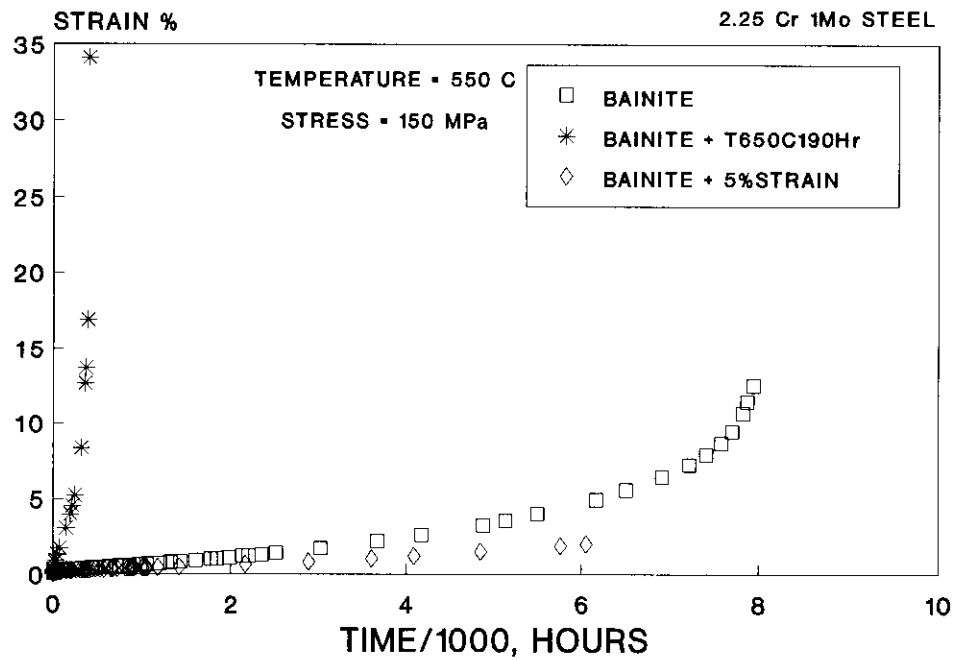
Fig.6.75 COMPARISON OF CREEP CURVES
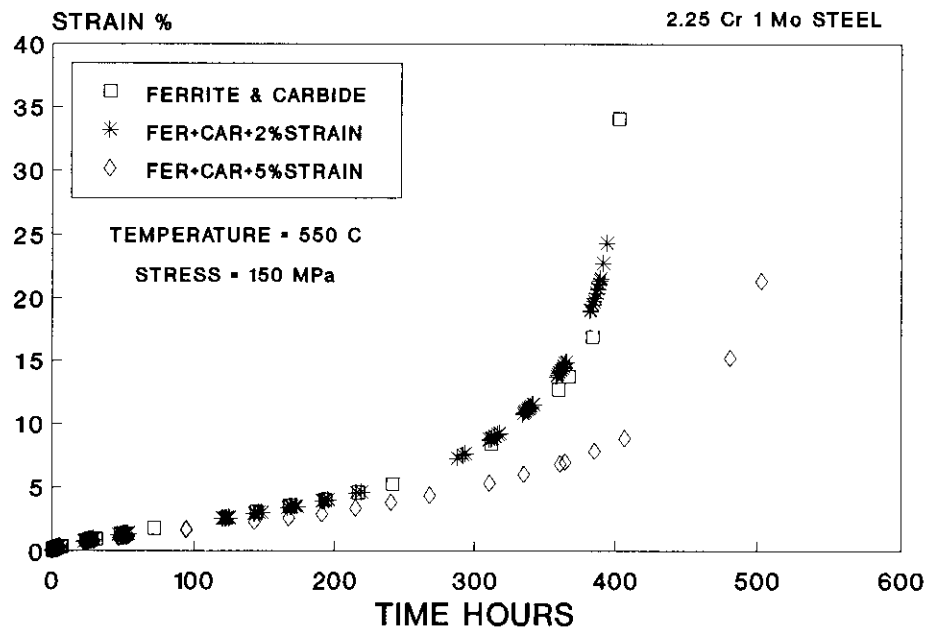
Fig.6.76 INFLUENCE OF PRE-STRAIN ON CREEP OF EXPOSED STEEL

105
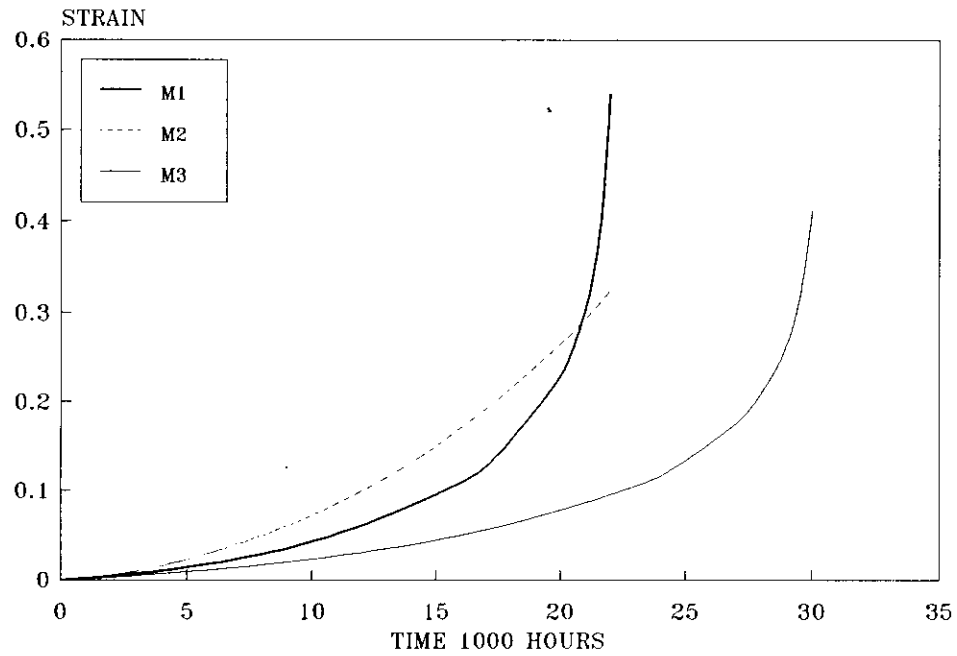
Fig.6.81 CREEP CURVES HAVING DIFFERENT PREDETERMINED SET OF MODEL PARAMETERS (a,b)
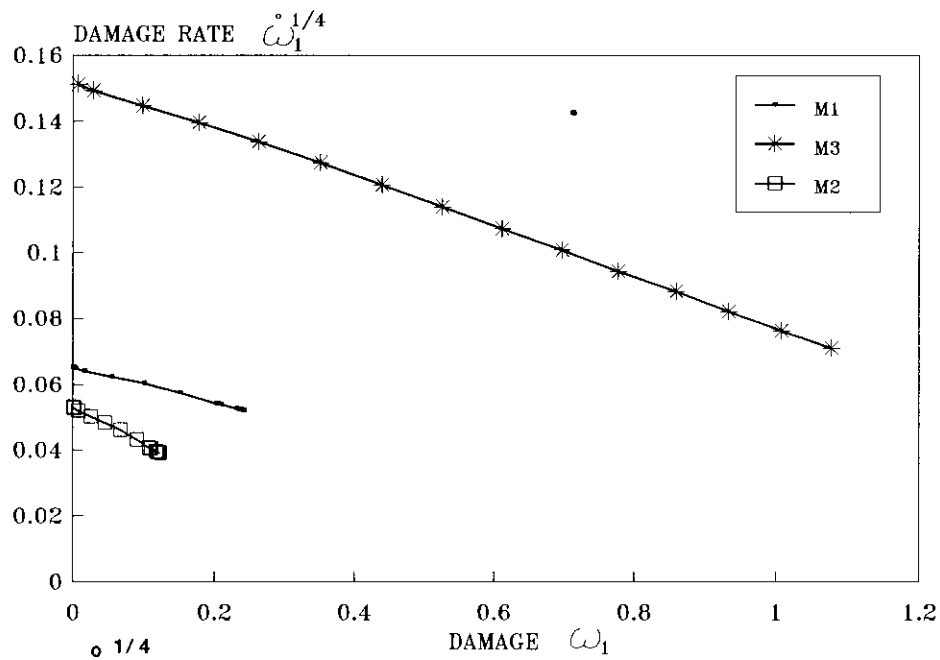
Fig.6.82 $\overset{\circ}{\omega}$ Vs. ω PLOT FOR SET OF CREEP CURVES IN Fig.6.81
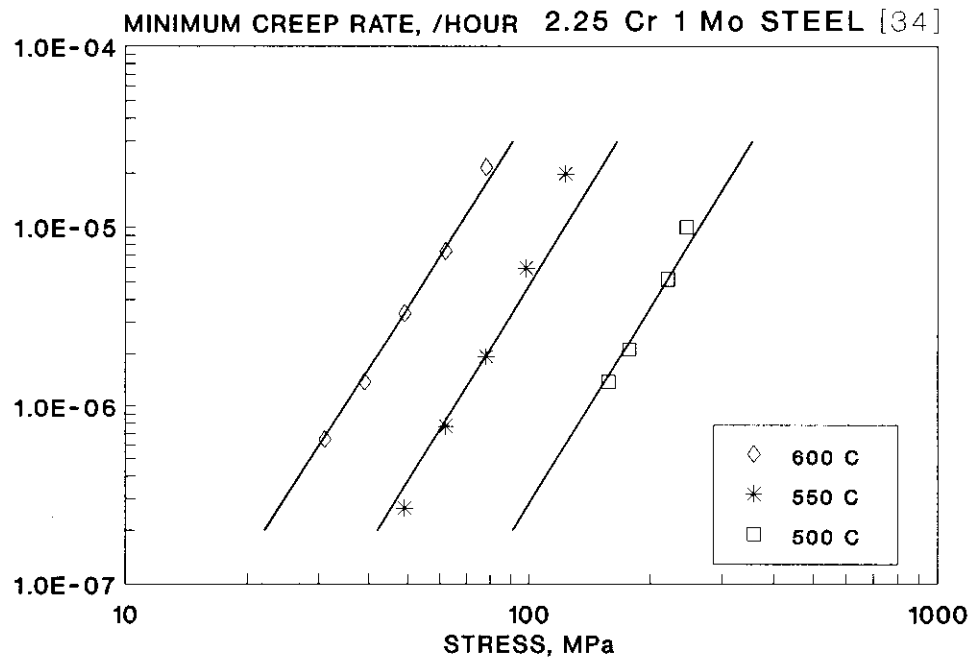
Fig.6.83 STRESS & TEMPERATURE DEPENDENCE OF MIN. CREEP RATE
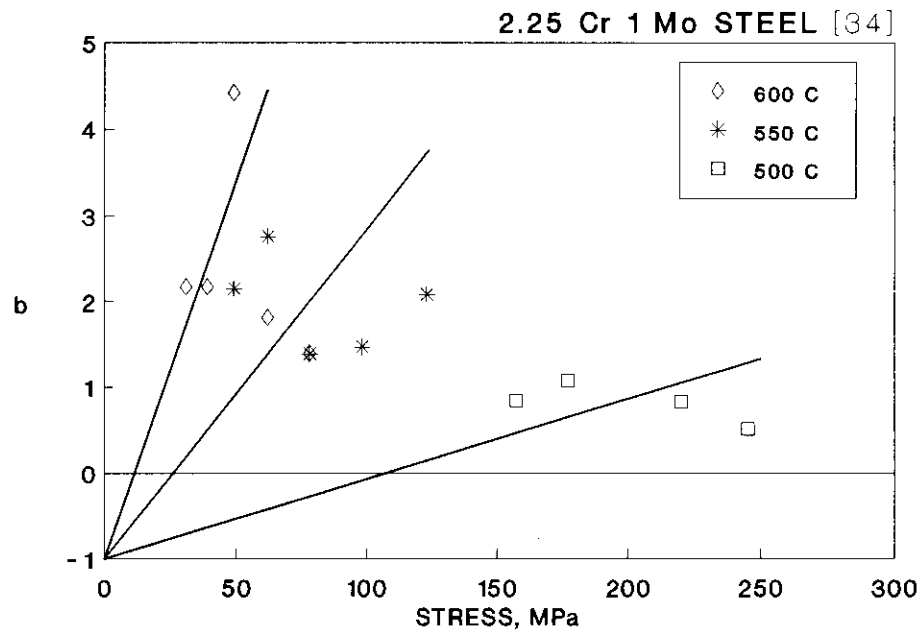
Fig.6.84 STRESS & TEMPERATURE DEPENDENCE OF " b "
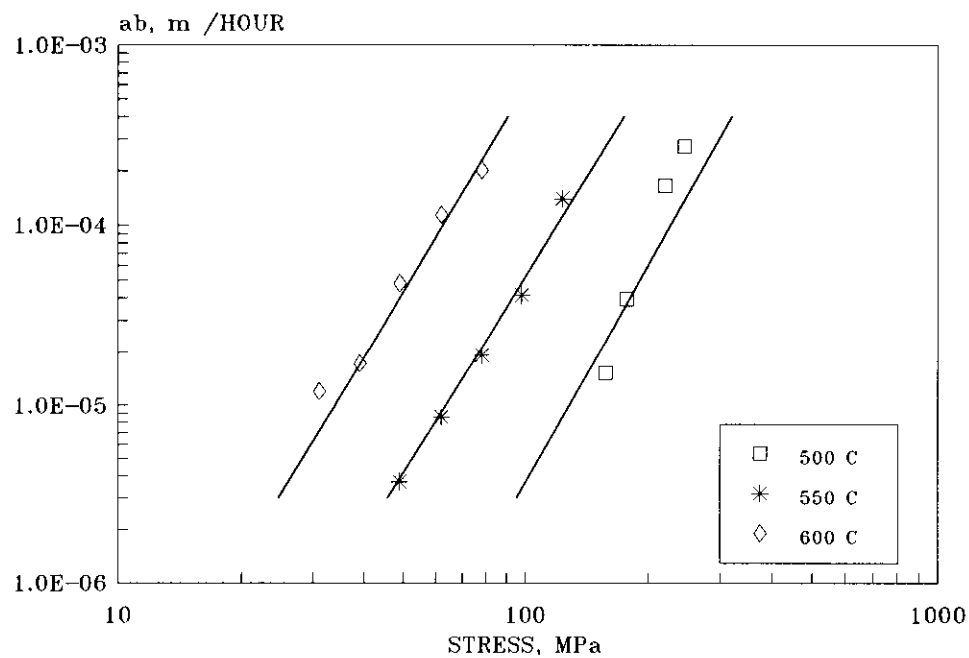
Fig.6.85 STRESS AND TEMPERATURE DEPENDENCE OF " ab "
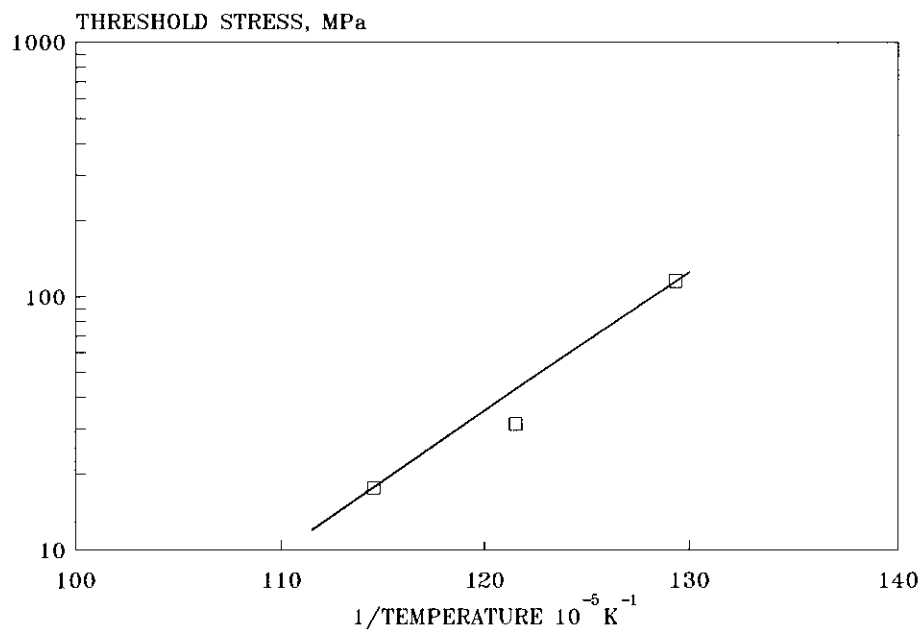
Fig.6.86 TEMPERATURE DEPENDENCE OF INITIAL THRESHOLD STRESS
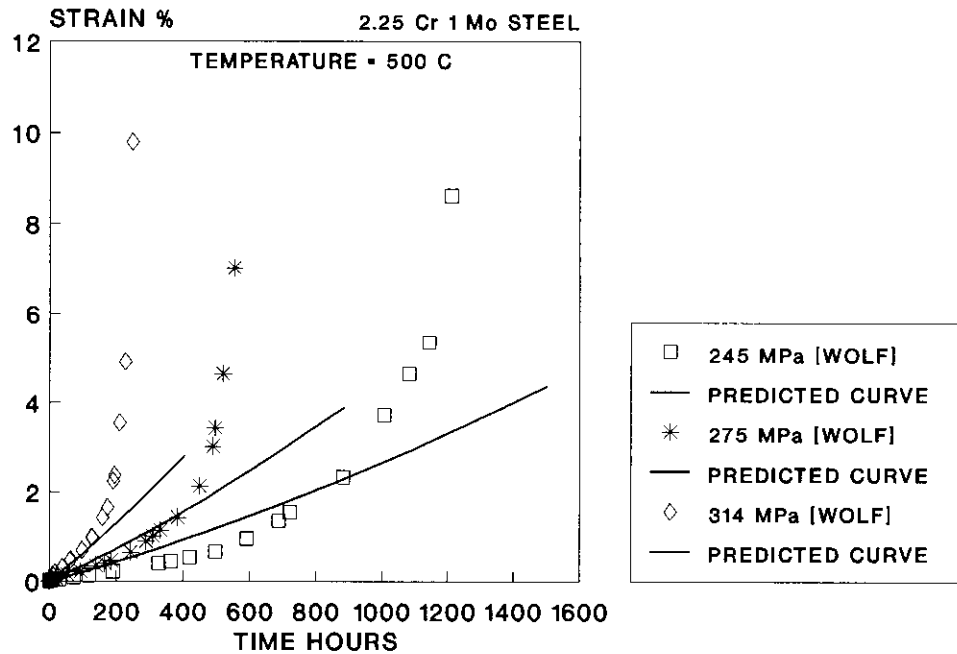
Fig.6.91(a) COMPARISON OF PREDICTED CREEP CURVES WITH
EXPERIMENTAL DATA AT 500 C [34]
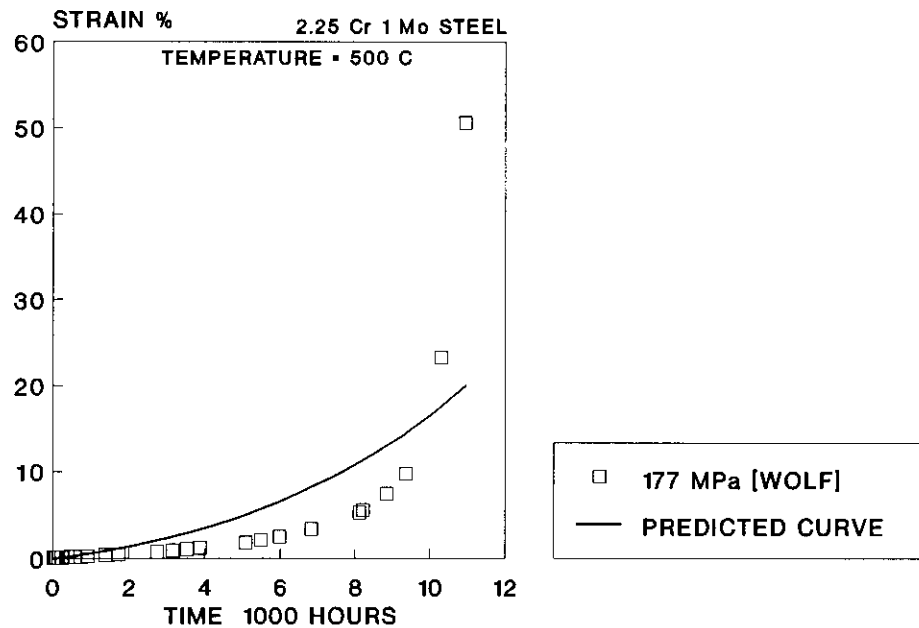
Fig.6.91(b) COMPARISON OF CREEP CURVE AT 500 C,177 MPa [34]
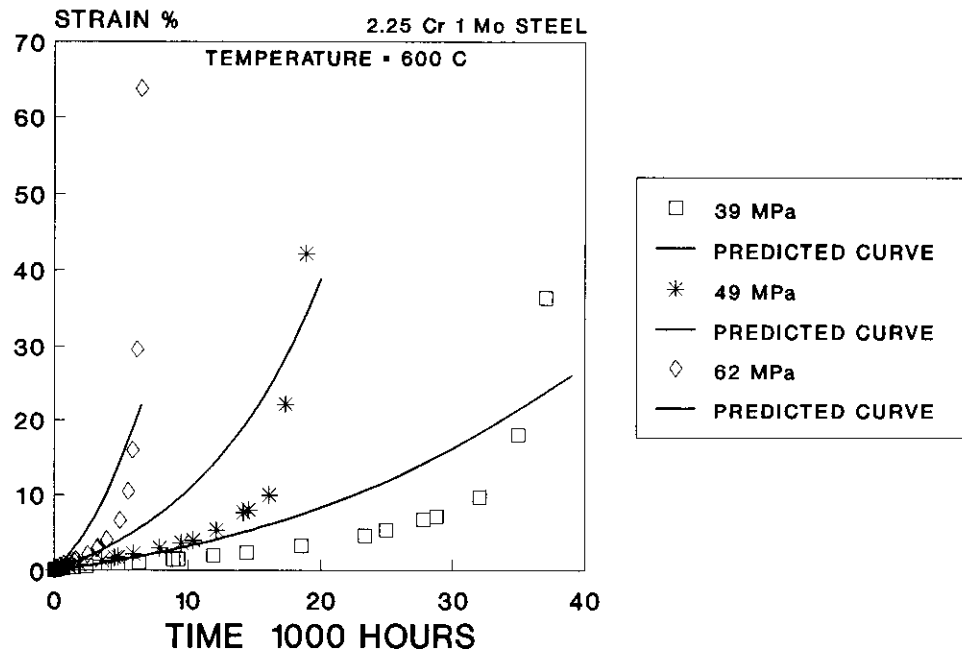
Fig.6.93(a) COMPARISON OF PREDICTED CREEP CURVES WITH EXPERIMENTAL DATA AT 600 C [34]
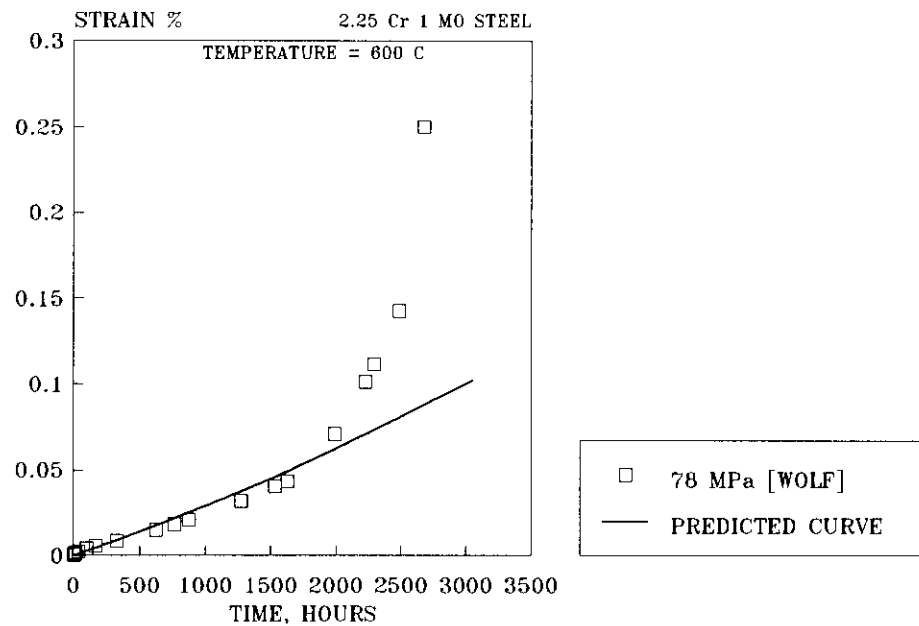
Fig.6.93(b) COMPARISON OF CREEP CURVE AT 600 C,78 MPa [34]

111
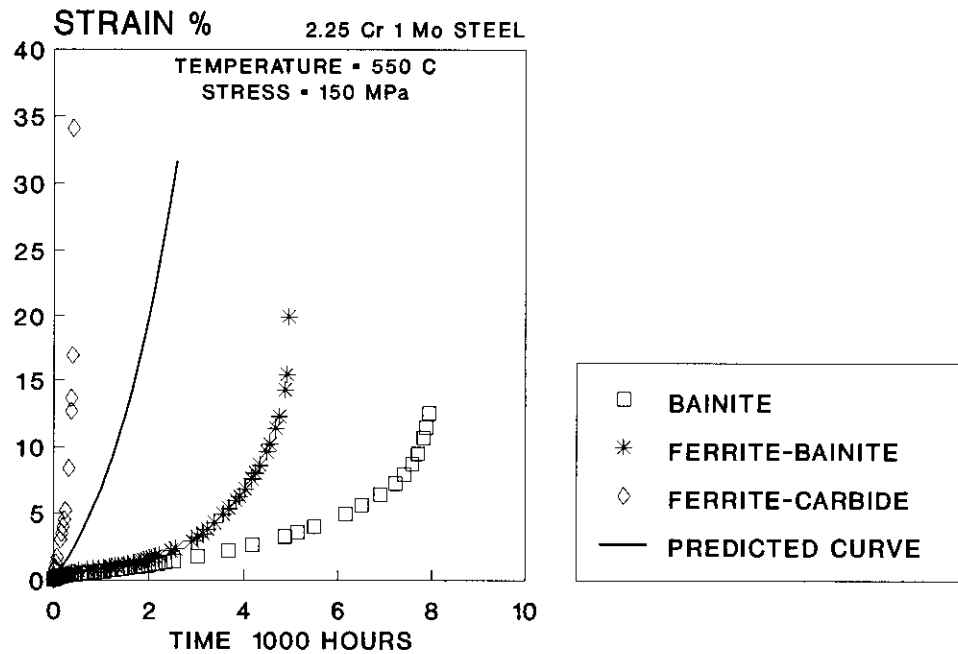
Fig.6.94(a) COMPARISON OF PREDICTED CREEP CURVE AT 550 C,
150 MPa WITH ACTUAL DATA FOR DIFFERENT MICROSTRUCTURES
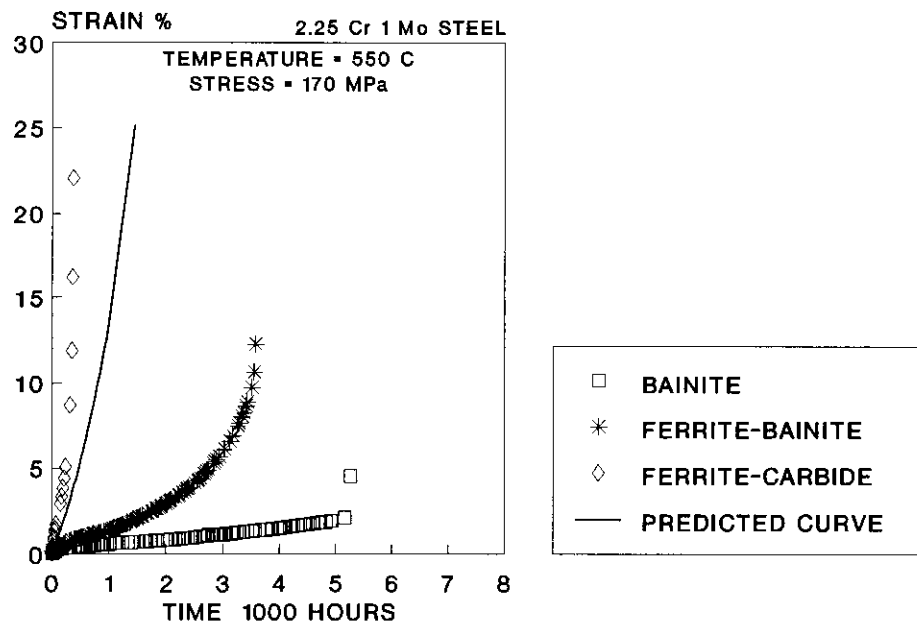
Fig.6.94(b) SIMILAR COMPARISON OF DATA AT 550 C, 170 MPa

ANNEXURES

Development of Computer Software for Stress Rupture Data Analysis
Using Sherby-Dorn Parameter (SDP)

The procedure followed for stress rupture data analysis using SDP is similar to the above mentioned procedure for LMP. However, the important equations involved in such a computation are as follows :

The relation between SDP and the applied stress(σ) is of the form:

$$\log tr = b/T + a_o + a_1(\log\sigma) + a_2(\log\sigma)^2 + a_3(\log\sigma)^3 + \cdots + a_m(\log\sigma)^M \quad (2a)$$

The variables and the constants in equation (2a) have the same meaning as defined previously. Substitution of $Xi = \log \sigma_i$, $Yi = \log tr_i$ and $Li = 1/Ti$ in equation (2a) leads to

$$Yi = bLi + a_o + a_1Xi + a_2Xi^2 + \cdots + a_mXi^M \quad (2b)$$

where i varies from 1 to N, N being the number of experimental points. The sum of the squares of the residuals, S, will be

$$S = \Sigma(Yi - bLi - a_o - a_1Xi - a_2Xi^2 \cdots a_mXi^M)^2 \quad (2c)$$

The summation term (Σ) is evaluated for all the experimental points (N). To minimise S, its first derivates are equated to zero.

$$dS/db = dS/da_o = dS/da_1 = dS/da_2 = \cdots = dS/da_m = 0 \quad (2d)$$

This leads to

$$\Sigma YiLi = b\Sigma Li^2 + a_o\Sigma Li + a_1\Sigma XiLi + a_2\Sigma LiXi^2 + \cdots + a_m\Sigma LiXi^M \quad (2.1)$$

$$\Sigma Yi = b\Sigma Li + Na_o + a_1\Sigma Xi + a_2\Sigma Xi^2 + a_3\Sigma Xi^3 + \cdots + a_m\Sigma Xi^M \quad (2.2)$$

$$\Sigma YiXi = b\Sigma LiXi + a_o\Sigma Xi + a_1\Sigma Xi^2 + a_2\Sigma Xi^3 + \cdots + a_m\Sigma Xi^{(M+1)} \quad (2.3)$$

$$\Sigma YiXi^M = b\Sigma LiXi^M + a_o\Sigma Xi^M + a_1\Sigma Xi^{(M+1)} + \cdots + a_m\Sigma Xi^{2M} \quad (2.m+2)$$

In the equations (2.1 to 2.m+2), the summation terms are easily evaluated once the degree of the polynomial is selected and then the simultaneous solution of equations (2.1 to 2.m+2) leads to the constants b, a_o, a_1, a_2, ---, a_m. A unique solution is thus obtained using all the experimental data simultaneously. The important stages of computation for obtaining the least square estimates of the unknowns are given in the flow diagram (Fig.A2). Based on this a computer programme is written in Fortran IV and tested. For life prediction and rupture strength estimation of service exposed and virgin materials, this programme has often been used.

START

READ N
READ σ(I), T(I), tr(I) FOR I=1,N

CALCULATE X(I)=LOG(σ(I))
          Y(I)=LOG(tr(I)
          L(I)=1/T(I) FOR I=1,N

READ M

IF M=0 — YES → STOP

NO

EVALUATE ALL SUM-TERMS IN EQNS.(2.1-2.m+2) TO FORM (M+2) NOS. OF SIMULTANEOUS EQNS IN (M+2) UNKNOWNS.

SOLVE EQNS. (2.1-2.M+2) FOR (M+2) UNKNOWNS USING GAUSS-JORDAN METHOD.

EVALUATE THE SUM SQUARE ERROR FROM EQN (2c) USING THE LEAST SQUARE ESTIMATES OF (M+2) UNKNOWNS.

WRITE (M+2) UNKNOWNS, SUM SQR ERROR, M

READ L (AS 0 OR 1)

IF L=0 — YES

NO

READ TEMP, TIME

EVALUATE RUPTURE STRENGTH FROM EQN. (2b) BY NEWTON RALPHSON METHOD

WRITE TEMP, TIME, RUPTURE STRENGTH

Fig. A2   FLOW DIAGRAM FOR EVALUATION OF (i) THE CONSTANTS IN EQUATION (2b), (ii) SUM OF THE SQUARES OF THE RESIDUALS, EQUATION (2c) AND (iii) RUPTURE STRENGTH AS A FUNCTION OF TEMPERATURE AND TIME.

Development of Computer Software for Stress Rupture Data Analysis
Using Manson-Haferd Parameter (MHP)

The relation of MHP with the applied stress(σ) is of the form :

$$(logtr-logto)/(T-To) = a_o+a_1(log\sigma)+a_2(log\sigma)^2+ --- +a_m(log\sigma)^M \qquad (3a)$$

The variables and the constants in the equation (3a) have the same meaning as defined previously. Substitution of $Xi=log\sigma_i$ and $Yi=logtr_i$ in equation (3a), leads to

$$Yi = logto+a_o(Ti-To)+a_1(Ti-To)Xi+a_2(Ti-To)Xi^2+----+a_m(Ti-To)Xi^M \qquad (3b)$$

where i varies from 1 to N, N being the number of experimental points. The sum of the squares of the residuals, S, is, therefore, given by

$$S = \Sigma[Yi-logto-a_o(Ti-To)-a_1(Ti-To)Xi --- -a_m(Ti-To)Xi^M]^2 \qquad (3c)$$

The summation term (Σ) is evaluated for all the experimental points (N).

To minimise the sum of the squares of the residuals, S, its first derivates are equated to zero.

$$dS/dlogto = dS/da_o = dS/da_1 = dS/da_2 =----= dS/da_m = 0 \qquad (3d)$$

This leads to

$$\Sigma Yi = Nlogto+a_o\Sigma(Ti-To)+a_1\Sigma(Ti-To)Xi+----+a_m\Sigma(Ti-To)Xi^M \qquad (3.1)$$

$$\Sigma Yi(Ti-To) = logto\Sigma(Ti-To)+a_o\Sigma(Ti-To)^2+----+a_m\Sigma(Ti-To)^2(Xi^M) \qquad (3.2)$$

$$\Sigma Yi(Ti-To)Xi = logto\Sigma(Ti-to)Xi+----+a_m\Sigma(Ti-To)^2(Xi)^{(M+1)} \qquad (3.3)$$

$$\Sigma Yi(Ti-To)Xi^M = logto\Sigma(Ti-To)Xi^M+----+a_m\Sigma(Ti-To)^2(Xi)^{(2M)} \qquad (3.m+2)$$

In the equations (3.1 to 3.m+2), the summation terms are easily evaluated once degree of the polynomial and the parametric constant T_o are selected and then the simultaneous solution of the equations (3.1 to 3.m+2) leads to the constants $\log t_o$, a_o, a_1, a_2, ---a_m. A unique solution is thus obtained using all the experimental data simultaneously. The important stages of computation for obtaining the least square estimates of the unknowns are given in the flow diagram (Fig.A3). Based on this a computer programme is written in Fortran IV and tested. For life prediction and rupture strength estimation of the service exposed and virgin materials, this programme has also often been used.
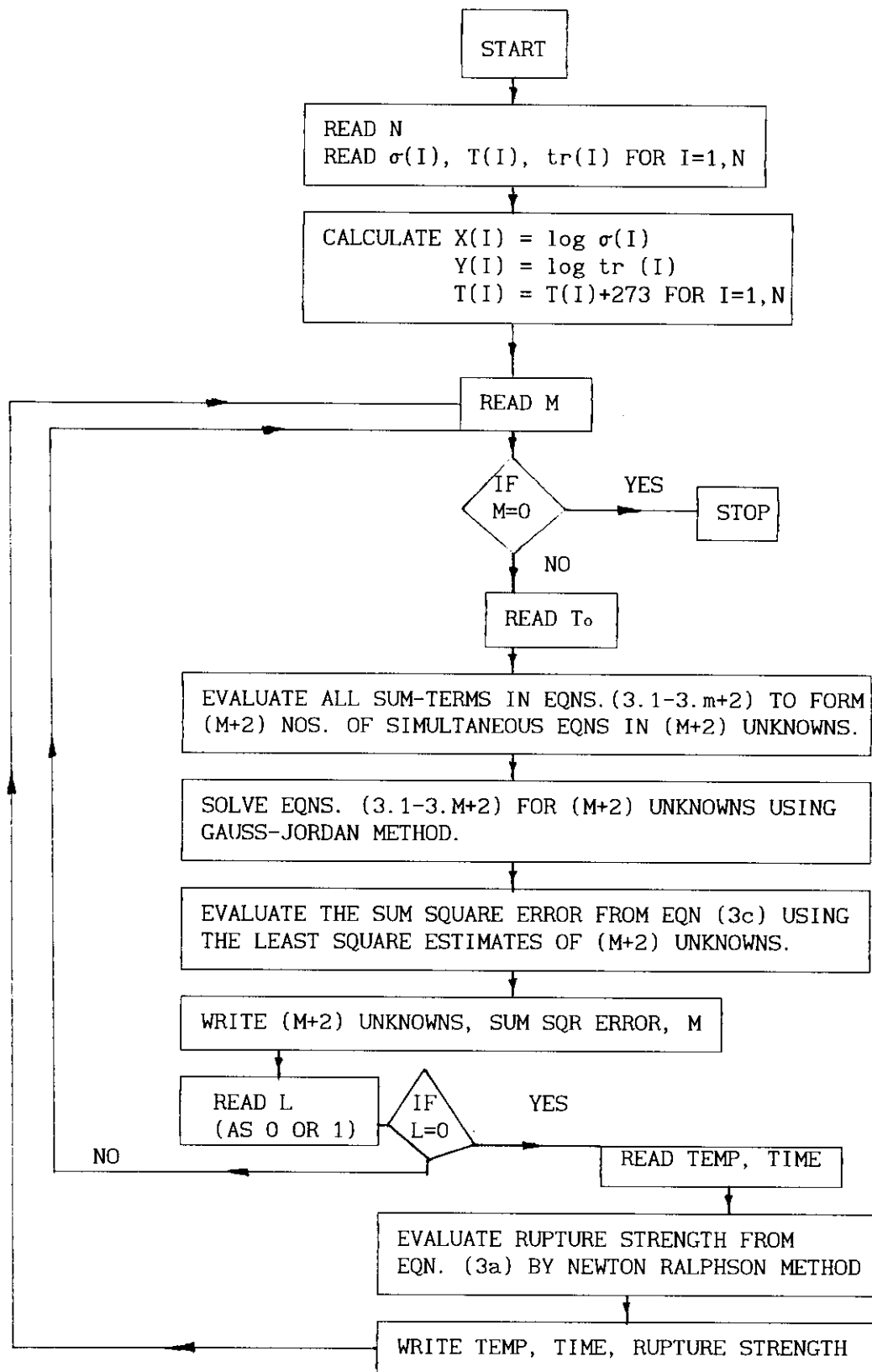
Fig. A3   FLOW DIAGRAM FOR EVALUATION OF (i) THE CONSTANTS IN EQUATION (3a), (ii) SUM OF THE SQUARES OF THE RESIDUALS, EQUATION (3c) AND (iii) RUPTURE STRENGTH AS A FUNCTION OF TEMPERATURE AND TIME.

Development of computer software for Estimation of Model Parameters and their Stress-Temperature Dependence

The creep behaviour of Cr-Mo steel based on particle coarsening kinetics is represented by the following set of coupled differential equations :

$$\overset{o}{\varepsilon} = \overset{o}{\varepsilon}_i \ (1 + \omega_1)^n \exp(\omega_2) \tag{4a}$$

$$\overset{o}{\omega}_1 = a \ (1 - b\omega_1)^4 \tag{4b}$$

$$\overset{o}{\omega}_2 = n\overset{o}{\varepsilon} \tag{4c}$$

The variables ε, ω_1, ω_2 and the parameters $\overset{o}{\varepsilon}_i$, a, b, n have the same meaning as defined previously.

The stress and temperature dependence of these parameters can be described by the following equations :

$$\overset{o}{\varepsilon}_i = \overset{o}{\varepsilon}_{io} \sigma^n \exp(-Q/RT) \tag{4d}$$

$$b = (\sigma - \sigma_{oi})/\sigma_{oi} \tag{4e}$$

$$ab = K/(3d_o^3) \tag{4f}$$

where K which represents kinetics of particle coarsening has been shown to follow the following stress-temperature dependence.

$$K = K_o \sigma^m \exp \ (-Q_1/RT) \tag{4g}$$

The temperature dependence of initial threshold stress (σ_{oi}) was also shown to be governed by

$$\sigma_{oi} = C \ \exp(-Q_2/RT) \tag{4h}$$

The estimation of eight material constants such as $\overset{o}{\varepsilon}_{io}$, n, Q, K_o, m, Q_1, C and Q_2 can thus be used to represent the complete creep behaviour over a range of stress and temperature where particle coarsening kinetics is primarily the rate controlling mechanism for creep deformation.

The important steps of computation to obtain these constants are as follows :

1. Numerically differentiate strain-time plots to generate strain rate-time (strain) plots. From these obtain minimum (initial) creep rate ($\overset{o}{\varepsilon}_i$) over a range of stress and temperature.

2. Establish stress-temperature dependence of initial creep rate ($\overset{o}{\varepsilon}_i$) by multiple linear regression analysis of a set of ($\log\sigma$, I/T and $\log \overset{o}{\varepsilon}_i$) data using equation (4d) and thus obtain ε_{io}, n, Q.

3. Compute damage (ω_1) accumulation resulting from particle coarsening over a range of stress and temperature using the following expression

$$\omega_1 = (\overset{o}{\varepsilon}/\overset{o}{\varepsilon}_i)^{1/n}\exp(-\varepsilon)-1 \qquad (4i)$$

4. Numerically differentiate these values (damage-time data) to generate $\overset{o}{\omega}_1^{1/4}$ vs. ω_1 plot. Compute the parameters 'a' and 'b' representing the extent of softening from the intercept and slope of such plots over a range of stress and temperature.

5. Compute initial threshold stress (σ_{oi}) at different temperature from the slope of b vs. σ plot using equation (4e).

6. Establish temperature dependence of initial threshold stress (σ_{oi}) by linear regression analysis of a set of (I/T, $\log \sigma_{oi}$) data using equation (4h) and thus obtain C and Q_2.

7. Compute stress-temperature dependence of 'ab' by multiple linear regression analysis of a set of $(\log \sigma, \ I/T, \ \log ab)$ data and thus obtain $K_o/(3d_o^3)$. Compute subsequently to estimate K_o using the value of d_o, initial inter particle spacing.

Based on the above steps a suitable computer software has been developed. This has the following features : (a) creating/updating strain-time data file as a function of stress and temperature; (b) Analysis of data to estimate the parameters $(\overset{o}{\varepsilon}_i, \ a, \ b, \ n)$; (c) creating/updating parametric database as a function of stress and temperature; (d) Estimation of material constants from parametric database; (e) creep strain prediction as a function of time under arbitrary stress temperature conditions using these estimated constants.

ANNEXURE - V

Time Softening Model

The high temperature creep strength of many engineering materials results from the presence of dispersed particles of precipitates in the matrix. These particles can be regarded as providing a resistance to creep deformation through the introduction of a threshold stress σ_o which is inversely proportional to the interparticle spacing d. Accordingly, threshold stress can be expressed as

$$\sigma_o = B/d \qquad (A1)$$

where B is a constant.

With continuous thermal exposure during creep tests interparticle spacing increases, resulting in a decreasing threshold stress. Since the creep rate $(\overset{o}{\varepsilon})$ is determined by the effective stress defined as $(\sigma - \sigma_o)$, instead of the applied stress(σ), the usual power law creep equation $\overset{o}{\varepsilon}$ should, therefore, be modified as

$$\overset{o}{\varepsilon} = A \ (\sigma - \sigma_o)^n \qquad (A2)$$

where A and n are the material constants. Since σ_o decreases with increasing creep exposure $\overset{o}{\varepsilon}$ will continue to rise during the creep test.

At high temperatures the dispersed particles may coarsen by a diffusional process resulting in an increased inter particle spacing. Kinetics of such a coarsening is often represented as

$$d^3 = d_o^{\ 3} + Kt \qquad (A3)$$

where K is a rate constant and d_o is the initial interparticle spacing.

Rearrangement of equation (A2) yields

$$\overset{o}{\varepsilon} = A \ [(\sigma - \sigma_{oi}) + (\sigma_{oi} - \sigma_o)]^n$$

$$= \overset{o}{\varepsilon}_i [1 + (\sigma_{oi} - \sigma_o)/(\sigma - \sigma_{oi})]^n \qquad (A4)$$

where $\overset{o}{\varepsilon}_i \ [=A(\sigma-\sigma_{oi})^n]$ and σ_{oi} are the initial creep rate and initial threshold stress respectively.

Differentiation and combination of equations (A1) and (A3) yield

$$\overset{o}{\sigma}_o = - K\sigma_o^4 / (3B^3) \qquad (A5)$$

The damage parameter ω_1 due to particle coarsening can be defined as

$$\omega_1 = (\sigma_{oi} - \sigma_o)/(\sigma - \sigma_{oi}) \qquad (A6)$$

Under constant stress creep test the damage accumulation rate $\overset{o}{\omega}_1$ due to coarsening of particles can be obtained by differentiation of equation (A6)

$$\overset{o}{\omega}_1 = -\overset{o}{\sigma}_o / (\sigma - \sigma_{oi}) \qquad (A7)$$

combination of equations (A5) and (A7) yield

$$\overset{o}{\omega}_1 = K\sigma_o^4/[3B^3(\sigma-\sigma_{oi})] = K\sigma_{oi}^4(\sigma_o/\sigma_{oi})^4/[3B^3(\sigma-\sigma_{oi})] \qquad (A8)$$

Williams and Cane[75] considered the situation where tertiary creep is due to progressive weakening of the material by coarsening of dispersed particles that impart high strength to engineering materials. Dyson and McLean[76] formulated the constitutive laws representing the evolution of creep strain and damage in the form of coupled diferential equations. A set of such equations can be obtained by combining equation (A6) with equation (A4) and (A8)

$$\overset{o}{\varepsilon} = \overset{o}{\varepsilon}_i \, (1 + \omega_1)^n \tag{A9}$$

$$\overset{o}{\omega}_1 = a \, (1 - b\omega_1)^4 \tag{A10}$$

where $a = (K\sigma_{oi}^{\;4})/\{3B^3 \, (\sigma - \sigma_{oi})\}$ and $b = (\sigma - \sigma_{oi})/\sigma_{oi}$

The material parameters $\overset{o}{\varepsilon}_i$, n, a and b are required to be evaluated for complete evolution of time dependent strain and damage. Based on the assumption that n = 4 which is widely accepted for creep studies of simple metals, equations (A9) and (A10) can be integrated to derive an expression for creep strain as a function of time.

$$\varepsilon = (\overset{o}{\varepsilon}_i t)/(b^4)\{(1+b)^4 - 2(1+b)^3/(abt)[(1+3abt)^{2/3} - 1]$$

$$+6(1+b)^2/(abt)[(1+3abt)^{1/3} - 1]$$

$$-4(1+b)/(3abt)\ln(1+3abt) + 1/(abt)[1 - (1+3abt)^{-1/3}]\} \tag{A11}$$

The constants $\overset{o}{\varepsilon}_i$, a and b of the equation (A11) can be estimated by least square analysis of experimental creep strain – time data.

In contrast to constant stress creep behaviour, loss of external section due to geometrical changes that occur during constant load creep test also contribute additional creep strain. Considering the effects of damages ω_1 due to coarsening of precipitates and ω_2 due to loss of external section, a set of coupled differential equations to represent the entire creep behaviour, following Dyson and McLean[36], can be formulated as follows :

$$\overset{o}{\varepsilon} = \overset{o}{\varepsilon}_i \, (1 + \omega_1)^n \exp (\omega_2) \tag{A12}$$

$$\overset{o}{\omega}_1 = a \, (1 - b\omega_1)^4 \tag{A13}$$

$$\overset{o}{\omega}_2 = n\overset{o}{\varepsilon} \tag{A14}$$

The damage parameter ω_1 due to particle coarsening during constant load creep would be same as that defined for constant stress creep and represented by equation (A6). The damage parameter ω_2 due to loss of external section is related to the change in cross-section of the test specimen A for uniaxial creep test with constant load. Accordingly it can be defined as

$$\omega_2 = n \, \ln(A_o/A) = n\varepsilon \qquad\qquad (A15)$$

where A_o is original cross section of the test specimen.

If tests are conducted under constant stress condition then $\omega_2 = 0$ signifying that only two of the above coupled differential equations (A12 and A13) are sufficient to describe the process. The set of coupled differential equations (A9) and (A10) for constant stress creep can thus be derived by substituting $\omega_2 = 0$ in the equations (A12) and (A14).

CREEP AND RUPTURE DATA USED IN THE THESIS

Table - A1

Stress Rupture Data for 2.25Cr-1Mo Steel(Tube) [44]

Temp. C	Stress MPa	Rupture time,Hrs	%Elonga-tion	%Red. in area
500	300	76.3	30	80
500	220	877	42	84
500	180	3553.3	50	86
500	160	9478.9	49	87
500	140	27329.8	37	86
500	130	59481.3	38	83
550	180	110.2	51	86
550	140	783	53	88
550	110	7660.6	41	86
550	100	20586.3	29	84
600	140	34.4	55	90
600	100	993.9	46	84
600	80	4241.5	40	86
600	70	9496.7	29	87
600	54	27094.7	25	89
600	42	31347.2	27	93
650	80	183.6	42	91
650	50	2254	33	93
650	38	3932.1	24	92
650	27	8025.2	33	96

Table - A2

Experimental Stress Rupture Data for 2.25Cr-1Mo Steel having
Different Initial Microstructures

(a) Initial Microstructure : Bainite

Temp. C	Stress MPa	Rupture time,Hrs	%Elonga-tion	%Red. in area
500	300	266	21.6	83.6
500	280	1372	18.8	75.4
500	260	13860	3.7	6.3
500	240	20115	3.7	9.3
550	200	312	30	82
550	185	2327	5.8	12.7
550	170	5250	4.4	4.5
550	150	7940	12.6	27
600	140	658	12.2	22
600	120	1623	4.6	23.2
600	100	2722	10.3	27.4
600	80	11026	24	64

(b) Initial Microstrucrture : Ferrite and Bainite

Temp. C	Stress MPa	Rupture time,Hrs	%Elonga-tion	%Red. in area
500	260	800	47	79
500	240	1460	46	79
500	190	15680	39	75
550	140	6528	15	34
550	100	18288	45	48
600	90	1035	71	89
600	80	1935	64	87

(c) Initial Microstructure : Ferrite and Carbide

Temp. C	Stress MPa	Rupture time,Hrs	%Elonga-tion	%Red. in area
500	280	18	29.8	76.4
500	260	59	44.8	56.7
500	240	324	28.4	82.8
550	170	367	22	73.5
550	150	402	34.1	80.9
600	100	171	66.8	86.4
600	80	2535	45.5	84.9

Table - A3

Experimental Creep Strain Data at 550 C, 150 MPa for 2.25Cr-1Mo Steel
having Different Initial Microstructures

Bainite		Ferrite & Bainite		Ferrite & Carbide	
Time,Hrs	%Strain	Time,Hrs	%Strain	Time,Hrs	%Strain
0.03	0.005	0.01	0.014	0.033	0.033
0.07	0.01	0.783	0.028	0.083	0.04
0.1	0.017	1.533	0.04	0.167	0.055
0.27	0.033	18.033	0.078	0.417	0.084
0.6	0.036	42.033	0.099	0.667	0.106
1.1	0.046	114.033	0.226	1.667	0.132
2.1	0.076	138.533	0.245	2.167	0.182
19.1	0.113	186.033	0.311	3.667	0.248
44.1	0.165	282.033	0.396	5.667	0.309
91.1	0.188	330.033	0.445	6.667	0.338
119.1	0.228	378.033	0.491	23.667	0.795
164.35	0.264	450.033	0.537	27.667	0.849
259.1	0.309	521.867	0.658	30.667	0.906
283.1	0.318	714.033	0.733	47.917	1.276
427.1	0.393	834.033	0.794	71.667	1.724
475.1	0.404	954.533	0.837	144.167	3.032
595.6	0.464	1051.533	0.877	167.667	3.508
643.1	0.478	1170.033	0.956	192.917	3.988
716.1	0.527	1290.033	1.015	216.833	4.539
859.1	0.586	1363.283	1.058	241.167	5.201
979.1	0.609	1482.033	1.125	311.667	8.367
1051.1	0.644	1554.033	1.186	359.667	12.671
1195.1	0.704	1674.033	1.285	366.667	13.678
1315.1	0.767	1794.533	1.364	383.667	16.901
1435.1	0.831	1890.033	1.461	402	34.1
1603.1	0.907	1962.033	1.546		
1772.1	0.984	2058.033	1.651		
1843.35	1.024	2130.033	1.739		
1987.1	1.082	2226.033	1.837		
2131.1	1.191	2466.033	2.203		
2203.35	1.222	2562.033	2.342		
2347.6	1.315	2898.033	2.917		
2515.1	1.423	3018.033	3.187		
3019.1	1.736	3234.033	3.801		
3667.1	2.185	3379.533	4.27		
4171.35	2.616	3570.033	4.888		
4872.1	3.249	3690.033	5.331		
5131.1	3.565	3834.033	5.959		
5491.6	4.004	3906.033	6.269		
6163.35	4.969	4026.033	6.827		
6501.35	5.589	4170.033	7.587		
6907.1	6.439	4242.033	8.004		
7219.1	7.249	4338.033	8.586		
7411.1	7.935	4482.033	9.61		
7579.1	8.687	4554.033	10.2		
7702.6	9.463	4674.033	11.431		
7819.35	10.688	4746.533	12.284		
7867.1	11.475	4866.033	14.266		
7940	12.6	4914.033	15.458		
		4950	20		

Table - A4

Experimental Creep Strain Data at 550 C, 170 MPa for 2.25Cr-1Mo Steel having Different Initial Microstructures

Bainite		Ferrite & Bainite		Ferrite & Carbide	
Time,Hrs	%Strain	Time,Hrs	%Strain	Time,Hrs	%Strain
0.1	0.02	0.033	0.001	0.017	0.03
0.533	0.037	0.15	0.01	0.05	0.043
1.033	0.045	0.65	0.019	0.083	0.053
2.033	0.065	1.15	0.021	0.167	0.074
19.867	0.124	2.15	0.028	0.25	0.085
26.033	0.152	4.4	0.029	0.433	0.102
50.533	0.195	22.15	0.073	0.5	0.113
115.533	0.255	29.15	0.103	1.25	0.155
163.333	0.289	46.15	0.133	2	0.208
381.033	0.364	70.15	0.175	2.75	0.244
477.533	0.411	142.15	0.354	3.75	0.288
547.533	0.441	166.15	0.419	4.75	0.328
650.283	0.469	190.15	0.484	6	0.372
717.533	0.485	214.15	0.542	6.75	0.396
839.533	0.521	238.15	0.589	23.75	0.818
959.533	0.552	312.65	0.7	30.75	0.964
1128.533	0.603	341.15	0.761	47.75	1.306
1321.533	0.644	407.15	0.846	71.75	1.72
1633.533	0.705	503.15	0.922	143.75	2.914
1704.533	0.721	550.15	0.975	167.75	3.346
1826.033	0.757	670.15	1.086	191.75	3.84
2065.533	0.805	718.15	1.132	215.75	4.406
2232.533	0.851	814.15	1.204	239.75	5.065
2375.783	0.895	862.15	1.263	314.25	8.704
2519.533	0.946	910.15	1.279	342.75	11.893
2664.533	0.998	1006.15	1.39	359.75	16.196
2711.533	1.011	1030.15	1.41	367	22
2808.533	1.077	1078.15	1.467		
2905.283	1.102	1174.65	1.585		
3048.533	1.153	1222.15	1.643		
3169.533	1.199	1318.15	1.772		
3241.533	1.222	1366.15	1.835		
3359.533	1.256	1414.15	1.926		
3505.53	1.305	1510.15	2.073		
3650.033	1.357	1557.98	2.154		
3744.033	1.384	1678.15	2.364		
3865.533	1.441	1750.15	2.469		
3985.533	1.47	1846.15	2.637		
4057.533	1.512	1918.15	2.768		
4176.533	1.571	2014.15	2.956		
4321.533	1.625	2063.32	3.055		
4418.033	1.673	2158.15	3.265		
4537.533	1.725	2230.15	3.42		
4682.283	1.8	2326.15	3.653		
4721.533	1.827	2399.4	3.852		
4825.533	1.841	2494.15	4.126		
4898.533	1.908	2566.15	4.329		
4921.533	1.918	2662.15	4.643		
5157.533	2.077	2710.15	4.803		
5250	4.4	2830.65	5.268		
		2926.15	5.665		
		3022.15	6.101		
		3166.15	6.889		
		3262.15	7.48		
		3334.15	8.025		
		3406.15	8.645		
		3430.15	8.857		
		3502.15	9.759		
		3550.15	10.65		
		3565	12		

Table - A5

Experimental Creep Strain Data at 600 C, 80 MPa for 2.25Cr-1Mo Steel having Different Initial Microstructures

Bainite		Ferrite & Bainite		Ferrite & Carbide	
Time,Hrs	%Strain	Time,Hrs	%Strain	Time,Hrs	%Strain
0.033	0.014	0.033	0.005	0.017	0.017
0.2	0.027	0.167	0.011	0.067	0.029
0.367	0.034	1.417	0.023	0.1	0.034
0.95	0.047	2.417	0.051	1.7	0.067
2.95	0.064	3.417	0.077	3.45	0.112
4.95	0.082	4.417	0.091	5.2	0.174
21.95	0.14	45.417	0.475	6.2	0.184
45.95	0.175	69.417	0.547	23.2	0.303
69.95	0.201	93.417	0.608	27.7	0.347
142.95	0.271	165.417	0.744	47.2	0.47
169.95	0.269	213.417	0.822	71.2	0.543
192.45	0.306	261.417	0.899	142.95	0.781
241.95	0.313	357.417	1.083	167.2	0.833
313.95	0.372	415.667	1.159	215.2	0.91
360.45	0.388	501.417	1.312	239.2	0.962
411.95	0.412	597.417	1.463	311.2	1.242
484.45	0.44	669.917	1.576	335.7	1.322
573.95	0.46	693.417	1.632	383.2	1.414
746.95	0.491	742.583	1.715	479.2	1.648
912.45	0.531	837.417	1.938	527.2	1.751
1319.95	0.546	909.417	2.072	551.2	1.862
1491.95	0.59	1005.417	2.287	575.2	1.943
1679.95	0.654	1078.667	2.422	647.2	2.194
1822.95	0.705	1173.417	2.644	695.2	2.34
1990.95	0.754	1225.417	2.75	743.2	2.503
2253.95	0.859	1269.417	2.86	864.2	2.98
2379.95	0.916	1341.417	3.018	911.2	3.201
2541.95	0.969	1413.417	3.19	1007.2	3.612
2661.95	1.03	1509.917	3.422	1055.45	3.829
2735.95	1.077	1605.417	3.683	1151.7	4.252
2853.95	1.108	1726.083	4.015	1200.45	4.412
2997.95	1.183	1893.417	4.472	1321.2	4.761
3069.95	1.216	1941.417	4.588	1415.2	5.231
3165.95	1.275	2061.417	4.843	1535.2	5.86
3237.95	1.308	2302.417	5.298	1655.2	6.625
3357.95	1.369	2613.417	5.949	1707.2	6.944
3405.95	1.397	2783.167	6.715	1751.2	7.321
3501.25	1.455	2949.417	7.905	1823.2	8.107
3573.95	1.528	3094.917	8.951	1871.2	8.598
3717.95	1.583	3189.417	9.819	1895.2	8.831
3865.95	1.637	3285.417	10.742	1991.7	9.503
4005.95	1.698	3405.417	11.504	2039.2	9.932
4173.95	1.795	3525.417	13.993	2087.2	10.371
4437.95	1.894	3549.417	16.708	2112.2	10.646
4605.95	1.989	3565	29	2159.2	11.174
5229.95	2.298			2207.86	11.793
6118.95	2.769			2231.2	12.126
7246.95	3.506			2279.2	12.955
7941.95	4.047			2327.2	13.925
8421.95	4.56			2351.2	14.454
9096.95	5.502			2375.2	15.137
9549.95	6.573			2399.2	15.954
9933.95	7.575			2423.2	16.959
10317.95	8.866			2430.533	17.277
10487.45	9.767			2447.2	18.191
10629.95	10.824			2495.2	22.747
10725.95	11.778			2502.45	23.875
10773.95	12.29			2519.2	27.622
10893.95	14.441			2535	45.5
10917.95	15.043				
10965.95	16.766				
10989.95	18.092				
11026	24				

Table - A6

Experimental Creep Strain Data at 600 C, 100 MPa for 2.25Cr-1Mo Steel having Different Initial Microstructures

Bainite		Ferrite & Bainite		Ferrite & Carbide	
Time,Hrs	%Strain	Time,Hrs	%Strain	Time,Hrs	%Strain
0.133	0.025	0.017	0.0006	0.0001	0.015
0.3	0.039	0.2	0.023	0.017	0.029
0.8	0.048	1.033	0.057	0.05	0.048
1.3	0.053	2.033	0.09	0.083	0.061
2.05	0.059	5.033	0.2	0.25	0.1
2.55	0.075	22.033	0.5	0.75	0.2
20.55	0.1	29.033	0.5	1.25	0.2
72.55	0.2	94.033	0.8	2.25	0.3
139.55	0.3	118.033	0.9	19.25	1.4
309.55	0.4	142.033	1	21.25	1.5
355.55	0.5	166.033	1	23.25	1.6
475.55	0.6	190.033	1.1	24.25	1.7
575.55	0.7	264.533	1.3	26.25	1.8
667.55	0.8	293.033	1.5	43.25	2.8
743.55	0.9	310.033	1.5	47.25	3.1
835.55	1	336.533	1.6	50.5	3.3
888.55	1.1	359.033	1.7	116.75	6.9
979.55	1.2	430.033	2.1	122	8
1028.55	1.3	455.033	2.2	139.25	12.2
1055.55	1.4	502.033	2.5	146.25	14.7
1102.55	1.5	598.033	3	163.25	26.7
1173.55	1.6	622.033	3.2	167.25	34.7
1219.55	1.7	694.033	3.6	170.6	66.8
1268.55	1.8	790.033	4.4		
1387.55	1.9	862.033	5		
1485.8	2.2	958.033	5.9		
1627.55	2.6	982.033	6.1		
1749.55	2.9	1030.033	6.6		
1915.55	3.6	1102.033	7.5		
2011.55	4.1	1126.533	7.8		
2108.55	4.5	1174.033	8.6		
2179.55	5	1198.033	8.9		
2253.55	5.4	1270.033	11		
2347.55	6	1318.033	13.3		
2395.55	6.3	1342.033	15.7		
2515.55	7.4	1354.033	20.6		
2539.55	7.6				
2587.55	7.8				
2659.55	8.7				
2683.55	8.9				
2707.55	9.4				
2722.55	10.3				

Table - A7

Stress Rupture Data for 2.25Cr-1Mo Steel(28.6mm Bar) with Minor Variation in Chemical Composition [39]

Steel	Temp. C	Stress MPa	Rupture time,Hrs	%Elonga- tion	%Red. in area
St 68	565	220	200	22.5	76.9
St 68	565	205	351	20.6	74
St 68	565	189	177	18.3	81.2
St 68	565	173	1339	12	62.5
St 68	565	142	1527	19.7	61.9
St 69	565	220	115	23.8	86.5
St 69	565	205	307	27.2	81.4
St 69	565	189	117	30.6	87
St 69	565	189	259	23.3	81.4
St 69	565	173	234	27.9	85
St 69	565	102	11640	12.7	59.5
St 70	565	220	71	25.6	80.4
St 70	565	205	188	25.6	82.4
St 70	565	189	186	28.2	82.5
St 70	565	173	399	20.1	82.5
St 70	565	142	1070	25	71.2
St 71	565	220	193	23	81.4
St 71	565	205	143	25.3	82.3
St 71	565	189	285	26.6	64
St 71	565	173	440	25	87
St 71	565	142	1597	24.2	80
St 72	565	220	233	18.7	59.4
St 72	565	205	783	14.3	74.5
St 72	565	189	376	25.7	76.3
St 72	565	189	493	22	76.1
St 72	565	142	1019	16.6	59.2
St 73	565	220	212	25	80
St 73	565	205	360	28.3	80.6
St 73	565	189	397	28.1	81
St 73	565	173	582	26.5	81.2
St 73	565	142	1720	23.4	76.8
St 74	565	220	127	27.3	77.4
St 74	565	205	168	29.6	79
St 74	565	189	255	29.7	77.6
St 74	565	173	278	34.4	78.5
St 74	565	102	14530	12.2	54
St 75	565	220	177	24.4	89.2
St 75	565	205	212	26.6	83
St 75	565	189	512	24	80
St 75	565	173	610	28.2	75
St 75	565	142	3179	20.2	64.5

Table - A8

Stress Rupture Data for 2.25Cr-1Mo Steel with Different Section Size [39]

Thickness mm	Temp. C	Stress MPa	Rupture time,Hrs	%Elonga-tion	%Red. in area
104	500	244	968	28.7	82.7
104	550	134	2445	31.7	77.4
104	600	71	2562	32.7	79
69.9	566	205	139	40	79
69.9	566	205	98	59	83
69.9	566	102	12951	36	80
69.9	566	87	30081	37	77
69.9	593	87	5957	46	83
69.9	593	63	20283	46	86
69.9	593	47	43086	37	89
57.2	566	205	331	47	73
57.2	566	102	19845	43	81
57.2	566	87	36710	34	80
57.2	593	87	7157	46	84
57.2	593	63	23726	63	90
57.2	593	47	52108	38	89
34.9	566	205	377	38	76
34.9	566	102	16859	43	84
34.9	566	87	31169	48	84
34.9	593	87	5485	52	86
34.9	593	63	19509	57	88
34.9	593	47	43573	39	84
34.9	538	211	457	28	85.4
34.9	538	189	1138	26.7	80.6
34.9	565	168	378	36.3	87.5
34.9	565	148	1743	29	77.5
34.9	565	126	5864	24.1	63.2
34.9	593	126	384	21.3	87.5
34.9	593	105	2016	21.5	79.7
12.7	565	165	141	31	83
12.7	565	165	186	27.8	83.8
12.7	565	150	264	25.2	87.3
12.7	565	150	307	34.6	87.7

Table - A9

Creep and Rupture Data for 2.25Cr-1Mo Steel [34]

Temp. C	Stress MPa	Min.Creep Rate(/hr)	Rupture time,Hrs	%Elonga- tion
500	98	2.00E-07	210296	24.47
500	137	7.18E-07	42213	39.23
500	157	1.37E-06	22892	46.29
500	177	2.11E-06	10931	50.57
500	196	2.58E-06	5736	54.89
500	220	5.16E-06	2784	54.44
500	245	1.00E-05	1443	48.3
500	275	1.62E-05	661	38.34
500	314	5.25E-05	253	29.25
500	348	1.21E-04	123	25.08
500	369	2.74E-04	61	23.6
500	392	7.81E-04	30	22.77
500	441	1.49E-02	3	21.08
550	40	1.09E-07	272134	27.875
550	49	2.65E-07	172197	33.713
550	62	7.73E-06	76050	40.509
550	78	1.91E-06	31462	49.877
550	98	9.59E-06	11053	60.815
550	123	1.99E-05	3218	68.811
550	137	2.63E-05	1809	69.711
550	157	5.89E-05	918	68.143
550	177	9.63E-05	431	64.27
550	196	1.62E-04	226	54.718
550	220	2.77E-04	111	45.984
550	245	4.63E-04	50	37.347
550	275	9.23E-04	20	31.952
600	20	1.54E-07	204147	34.68
600	31	6.48E-07	68986	35.78
600	39	1.38E-06	37002	36.37
600	49	3.35E-06	18889	42.18
600	62	7.35E-06	6489	63.73
600	78	2.16E-05	3050	66.29
600	98	5.70E-05	957	65
600	123	2.09E-04	258	59.28
600	137	3.60E-04	139	51.55
600	157	6.61E-04	47	40.68
600	177	1.69E-03	20	34.91
600	196	4.72E-03	10	41.08
600	220	1.00E-02	3	45.87

Table - A10

Experimental Creep Strain Data at 550 C, 150 MPa for Prestrained
2.25Cr-1Mo Steel having Different Initial Microstructures

Bainite 5% Prestrain		Ferrite & Carbide 2% Prestrain		Ferrite & Carbide 5% Prestrain	
Time,Hrs	%Strain	Time,Hrs	%Strain	Time,Hrs	%Strain
0.017	0.009	0	0.002	0	0.003
0.033	0.012	0.017	0.016	0.017	0.009
0.05	0.014	0.033	0.024	0.033	0.011
0.067	0.015	0.117	0.042	0.05	0.013
0.083	0.017	0.2	0.056	0.067	0.015
0.1	0.019	0.283	0.064	0.083	0.016
0.117	0.02	0.367	0.074	0.1	0.021
0.133	0.021	0.45	0.082	0.117	0.022
0.15	0.022	0.533	0.09	0.133	0.025
0.167	0.022	0.7	0.101	0.15	0.026
0.183	0.023	0.783	0.109	0.167	0.029
0.2	0.023	0.867	0.113	0.183	0.032
0.3	0.028	0.95	0.12	0.2	0.035
0.383	0.032	1.033	0.123	0.217	0.039
0.467	0.033	1.117	0.13	0.233	0.042
0.717	0.037	1.533	0.152	0.25	0.045
0.967	0.04	2.283	0.19	0.267	0.048
1.467	0.042	2.533	0.199	0.35	0.061
2.467	0.052	2.867	0.216	0.433	0.068
3.467	0.057	3.033	0.225	0.517	0.076
4.467	0.061	3.283	0.233	0.6	0.081
5.467	0.063	3.533	0.244	0.683	0.09
22.467	0.129	4.033	0.266	0.767	0.093
23.467	0.123	4.283	0.272	0.85	0.097
24.467	0.124	4.533	0.281	0.933	0.105
46.467	0.156	4.783	0.287	1.017	0.112
47.467	0.158	5.283	0.305	1.1	0.116
70.467	0.176	22.283	0.759	1.183	0.118
95.467	0.197	23.033	0.772	1.267	0.122
148.467	0.215	23.533	0.778	1.35	0.126
167.967	0.22	24.033	0.786	1.433	0.13
191.467	0.221	24.533	0.795	1.517	0.134
214.467	0.25	25.033	0.807	1.6	0.139
262.467	0.261	26.033	0.829	1.683	0.143
310.467	0.281	26.783	0.849	1.767	0.147
335.05	0.28	27.783	0.863	2.017	0.159
358.467	0.288	29.033	0.883	2.267	0.169
382.717	0.287	29.533	0.902	2.517	0.178
407.967	0.292	46.45	1.225	2.767	0.187
435.467	0.298	48.033	1.248	3.017	0.201
478.467	0.316	48.783	1.258	3.267	0.207
528.467	0.322	49.283	1.266	3.517	0.222
574.467	0.333	49.783	1.274	3.767	0.233
648.717	0.34	50.283	1.285	4.017	0.238
670.217	0.354	50.783	1.288	4.267	0.243
724.133	0.366	51.283	1.296	4.6	0.255
816.467	0.393	51.783	1.304	4.767	0.262
843.467	0.393	52.283	1.31	5.017	0.267
866.967	0.399	52.783	1.317	5.267	0.273
890.217	0.401	53.283	1.326	5.517	0.277
914.967	0.404	119.783	2.483	5.767	0.288
1008.967	0.415	120.783	2.495	22.767	0.654
1037.217	0.417	121.783	2.511	23.267	0.657
1058.717	0.425	122.283	2.515	23.767	0.679
1176.217	0.449	123.283	2.562	24.267	0.684
1418.633	0.5	124.783	2.564	24.767	0.687
2165.467	0.655	125.283	2.572	25.767	0.741
2882.967	0.831	142.283	2.891	26.267	0.775
3604.467	1.041	143.283	2.906	27.767	0.762
4083.967	1.211	145.783	2.946	28.767	0.823
4847.467	1.499	148.033	2.984	29.767	0.809
5759.967	1.908	166.283	3.35	46.767	1.031
6051.467	2.039	168.283	3.398	47.767	1.059
		169.283	3.418	49.267	1.064
		190.783	3.886	50.767	1.08
		195.283	3.99	52.767	1.109
		215.533	4.517	53.767	1.122
		287.283	7.277	94.267	1.642
		310.283	8.719	94.767	1.647
		314.283	9.004	142.767	2.241
		334.117	10.773	167.35	2.541
		341.617	11.536	190.767	2.886
		358.117	13.743	215.017	3.292
		365.117	14.896	240.267	3.792
		381.867	18.943	267.767	4.303
		385.117	19.999	310.767	5.303
		387.117	20.746	335.017	5.979
		388.117	21.145	360.767	6.822
		391.117	22.741	364.267	6.952
		393.617	24.342	385.267	7.827
				406.767	8.83
				480.767	15.211
				502.517	21.336

Table - A11

Creep Strain Data at 500 C for 2.25Cr-1Mo Steel [34]

Stress = 245 MPa		Stress = 275 MPa		Stress = 314 MPa	
Time,Hrs	%Strain	Time,Hrs	%Strain	Time,Hrs	%Strain
0	0	0	0	0	0
1.722	0.01	0.325	0.01	0.103	0.024
4.41	0.016	1.022	0.016	0.294	0.033
9.864	0.025	2.716	0.024	0.796	0.046
29.652	0.049	9.124	0.046	2.005	0.063
71.997	0.091	20.406	0.074	9.584	0.126
117.854	0.132	53.347	0.141	18.339	0.189
189.776	0.212	93.256	0.217	38.725	0.304
325.005	0.397	139.467	0.338	61.847	0.46
360.807	0.45	165.345	0.406	63.246	0.469
417.532	0.533	183.642	0.453	96.768	0.688
496.136	0.663	242.804	0.65	125.858	0.974
589.537	0.952	287.331	0.889	126.491	0.983
686.285	1.354	308.109	1.007	157.753	1.415
721.615	1.53	330.69	1.13	172.67	1.657
881.664	2.326	383.031	1.415	189.737	2.234
1005.49	3.722	447.724	2.118	193.713	2.368
1082.422	4.643	488.052	3.023	208.575	3.55
1142.01	5.356	496.036	3.438	224.578	4.918
1209.59	8.615	519.063	4.637	246.825	9.789
		552.044	7.03		

Table - A12

Creep Strain Data at 500 C, 177 MPa for 2.25Cr-1Mo Steel [34]

Time,Hrs	%Strain
0	0
18.414	0.01
48.939	0.019
81.772	0.028
131.135	0.04
212.03	0.057
383.031	0.089
589.537	0.132
896.267	0.202
1362.59	0.306
1714.92	0.394
2732.65	0.728
3136.41	0.86
3504.21	0.998
3867.19	1.174
5071.23	1.743
5465.3	2.056
5976.63	2.463
6816.03	3.341
8099.2	5.2
8197.949	5.496
8828.72	7.385
9351.22	9.725
10277.6	23.257
10930.6	50.572

Table – A13

Creep Strain Data at 550 C for 2.25Cr-1Mo Steel [34]

Stress = 78 MPa		Stress = 98 MPa		Stress = 123 MPa	
Time,Hrs	%Strain	Time,Hrs	%Strain	Time,Hrs	%Strain
0	0	0	0	0	0
2.971	0.01	1.424	0.01	0.771	0.01
6.728	0.017	5.855	0.025	1.857	0.017
11.632	0.023	13.366	0.041	3.675	0.027
24.47	0.038	23.976	0.059	10.546	0.053
50.851	0.058	74.057	0.116	20.36	0.084
124.435	0.1	115.611	0.152	61.87	0.182
268.27	0.158	194.257	0.217	166.999	0.391
408.656	0.201	364.475	0.354	379.677	0.802
600.029	0.262	509.55	0.453	590.301	1.216
1450.41	0.459	695.118	0.567	804.417	1.67
3435.07	0.818	1158.47	0.875	959.961	2
6136.67	1.285	1764.71	1.197	1149.05	2.443
7746.15	1.627	2467.13	1.64	1331.14	3.137
7865.425	1.651	2763.25	1.805	1608.835	4.17
9234.1	1.924	3088.84	1.987	1619.59	4.21
11703.7	2.38	3338.21	2.205	1838.31	5.076
14773.3	3.153	3804.54	2.507	1978.62	5.809
15730.85	3.367	4822.03	3.107	2155.9	6.867
18122.1	3.901	5526.5	3.805	2292.18	7.595
19989.3	4.679	5655.1	3.933	2413.252	8.454
22504.1	6.04	6418.79	5.051	2487.37	8.979
23596.27	7.467	6936.99	6.129	2633.82	11.439
24024.6	8.027	7651.77	7.77	2905.2	13.458
26826.9	10.461	8135.45	9.261	3014.03	30.83
28756.8	13.926	8289.75	9.835	3217.67	68.811
29111.5	15.911	8756.38	11.57		
29712.4	19.118	9271.92	13.284		
29800	28.239	9737.89	15.178		
29956.2	37.713	9858	19.056		
31461.7	49.877	10311.2	24.636		
		10444	34.154		
		10610.4	49.554		
		11053	60.815		

Table - A14

Creep Strain Data at 550 C, 108 MPa for 2.25Cr-1Mo Steel [18]

Time,Hrs	%Strain
0	0
469.167	1.1
852.222	1.8
1197.222	2.2
2001.667	3.3
2805.555	4
3821.667	5.5
4779.444	6.6
5795	8.2
6503.611	10
7097.5	12.3
7614.722	16.1
7739.444	18.4
7863.889	20.4
7923.333	22.1

Table - A15

Creep Strain Data at 600 C for 2.25Cr-1Mo Steel [34]

Stress = 39 MPa		Stress = 49 MPa		Stress = 62 MPa	
Time,Hrs	%Strain	Time,Hrs	%Strain	Time,Hrs	%Strain
0	0	0	0	0	0
1.145	0.01	0.602	0.01	0.245	0.01
3.964	0.019	2.656	0.023	0.901	0.02
10.027	0.03	7.359	0.04	2.518	0.034
38.481	0.061	17.865	0.063	8.608	0.065
96.554	0.097	50.108	0.105	25.791	0.115
273.055	0.168	165.073	0.198	81.53	0.215
652.038	0.262	470.693	0.348	181.503	0.334
1451.57	0.413	1060.91	0.566	421.081	0.547
2391.22	0.556	1851.58	0.806	740.989	0.779
4742.67	0.877	3567.83	1.337	1123.99	1.031
6304.37	1.085	4513.61	1.658	1463.6	1.252
8842.02	1.418	4722.175	1.74	1622.267	1.384
9250.574	1.48	5877.39	2.193	2451.15	2.077
11899.9	1.882	7877.48	2.948	3165.54	2.876
14386.6	2.33	9444.35	3.591	3244.535	3.006
18501.15	3.185	10385.4	3.977	3874.68	4.043
18503.1	3.185	12097.9	5.312	4866.802	6.572
23311.6	4.588	14166.52	7.587	4881.62	6.61
24902.2	5.294	14505.8	7.96	5501.99	10.424
27751.73	6.646	16081.6	9.906	5805.11	15.959
28770.2	7.13	17321.2	22.173	6175.67	29.567
32027.6	9.633	18888.7	42.176	6489.07	63.727
34925.9	18.024				
37002.3	36.374				

Table - A16

Creep Strain Data at 600 C, 78 MPa for 2.25Cr-1Mo Steel [34]

Time,Hrs	%Strain
0	0
0.098	0.01
0.947	0.032
2.318	0.052
5.225	0.079
12.023	0.1
29.92	0.2
96.554	0.4
162.372	0.5
324.71	0.9
623.111	1.5
762.542	1.8
870.329	2.1
1266.83	3.2
1525.085	4
1622.6	4.3
1986.09	7
2220.1	10.1
2287.627	11.1
2481.67	14.2
2672.96	25